Volume 13 | Number 1 | January-December 2024

JCB | Journal of Circulating Biomarkers

ABOUTSCIENCE

JCB | GENERAL INFORMATION

Aims and Scope
Journal of Circulating Biomarkers is an international, peer-reviewed, open access, scientific, online only journal, published continually. It focuses on all aspects of the rapidly growing field of circulating blood-based biomarkers and diagnostics using circulating protein and lipid markers, circulating tumor cells (CTC), circulating cell-free DNA (cfDNA) and extracellular vesicles, including exosomes, microvesicles, microparticles, ectosomes and apoptotic bodies. The journal publishes high-impact articles related to circulating biomarkers and diagnostics, ranging from basic science to translational and clinical applications, circulation protein and lipid markers, CTC, cfDNA and extracellular vesicle.

Included within the scope are a broad array of specialties:
Oncology
Immunology
Neurology
Metabolic diseases
Cardiovascular medicine
Diagnostics and therapeutics
Infectious diseases

Abstracting and Indexing
CNKI Scholar
CrossRef
DOAJ
Ebsco Discovery Service
Embase
Google Scholar
J-Gate
OCLC WorldCat
Opac-ACNP (Catalogo Italiano dei Periodici)
Opac-SBN (Catalogo del servizio bibliotecario nazionale)
PubMed Central
ROAD (Directory of Open Access Scholarly Resources)
ScienceOpen Scilit
Scimago
Scopus
Sherpa Romeo
Transpose

Publication process
Peer review
Papers submitted to JCB are subject to a rigorous peer review process, to ensure that the research published is valuable for its readership. JCB applies a single-blind review process and does not disclose the identity of its reviewers.

Lead times
Submission to final decision: 6-8 weeks
Acceptance to publication: 2 weeks

Publication fees
All manuscripts are submitted under Open Access terms. Article processing fees cover any other costs, that is no fee will be applied for supplementary material or for colour illustrations. Where applicable, article processing fees are subject to VAT.

Open access and copyright

Author information and manuscript submission
For full author guidelines and online submission visit
www.aboutscience.eu

ABOUTSCIENCE

Aboutscience Srl
Piazza Duca d'Aosta, 12 - 20124 Milano (Italy)

Editorial and production enquiries
jcb@aboutscience.eu

Supplements, reprints and commercial enquiries
Lucia Steele - email: lucia.steele@aboutscience.eu

Publication data
eISSN: 1849-4544
Continuous publication
Vol. 13 is published in 2024

JCB Journal of Circulating Biomarkers

Contents

Volume 13 Number 1 January-December 2024

JCB
J Circ Biomark 2024; 13: 1-6
ISSN 1849-4544 | DOI: 10.33393/jcb.2024.2636
ORIGINAL RESEARCH ARTICLE

Detection of PSMA expression on circulating tumor cells by blood-based liquid biopsy in prostate cancer

Santosh Gupta[1], Luisa Fernandez[1], David Bourdon[1], Anis A. Hamid[2], Anupama Pasam[3], Ernest Lam[1], Richard Wenstrup[1], Shahneen Sandhu[2,3]

[1]Translational Research and Assay Development, Epic Sciences, San Diego, California - USA
[2]Department of Medical Oncology, University of Melbourne, Melbourne, Victoria - Australia
[3]Department of Medical Oncology, Peter MacCallum Cancer Centre, Melbourne, Victoria - Australia

ABSTRACT

Background: For patients with mCRPC, PSMA-targeted radioligand treatment has significantly improved the clinical outcome. A blood-based liquid biopsy assay for recognizing PSMA protein expression on circulating tumor cells may be beneficial for better informing therapeutic decision-making and identifying the patients most likely to benefit from PSMA-targeted radioligand therapy.

Methods: Using high-throughput imaging and digital AI pathology algorithms, a four-color immunofluorescence assay has been developed to find PSMA protein expression on CTCs on a glass slide. Cell line cells (LNCaP/PC3s/22Rv1) spiked into healthy donor blood were used to study the precision, specificity, sensitivity, limit of detection, and overall accuracy of the assay. Clinical validation and low-pass whole-genome sequencing were performed in PSMA-PET-positive patients with high-risk mCRPC (N = 24) utilizing 3 mL of blood.

Results: The PSMA CTC IF assay achieved analytical specificity, sensitivity, and overall accuracy above 99% with high precision. In the clinical validation, 76% (16/21) of the cases were PSMA positive with CTC heterogeneity, and 88% (21/24) of the patients contained at least one conventional CTC per milliliter of blood. Thirty-six low-pass-sequenced CTCs from 11 individuals with mCRPC frequently exhibited copy number increases in *AR* and *MYC* and losses in *RB1, PTEN, TP53*, and *BRCA2* locus.

Conclusions: The analytical validation utilizing Epic Sciences' liquid biopsy CTC platform demonstrated the potential to detect PSMA protein expression in CTCs from patients with mCRPC. This assay is positioned as an effective research tool to evaluate PSMA expression, heterogeneity, and therapeutic response in many ongoing clinical studies to target tumors that express PSMA.

Keywords: Circulating tumor cells, Liquid biopsy, mCRPC, Prostate-specific membrane antigen (PSMA)

Introduction

A type II transmembrane glycoprotein receptor called prostate-specific membrane antigen (PSMA) is increased in metastatic prostate malignancies and may increase tumor dedifferentiation and treatment resistance (1). The biological basis for PSMA expression in prostate cancer is still unknown; however, research suggests that it plays a role in PI3K-Akt signaling through glutamate signaling (2). Conventional imaging techniques, including magnetic resonance imaging (MRI), computerized tomography (CT), and bone scans, have poor sensitivity and specificity for detecting tumor lesions, especially when prostate-specific antigen (PSA) levels are low. Therefore, PSMA can be used as a target for imaging with radioligands like ^{68}Ga-PSMA-11 and ^{18}F-DCFPyL, which the Food and Drug Administration (FDA) recently approved for PSMA-targeted positron emission tomography (PET) imaging in prostate cancer (3). PSMA is also an established therapeutic target for advanced prostate cancer based on the prospective, phase III VISION trial (NCT03511664) of ^{177}Lu-PSMA-617 radioligand therapy (RLT) that demonstrated improved overall survival (OS) and progression-free survival (PFS) compared to standard of care (SoC) in PSMA-positive advanced metastatic castration-resistant prostate cancer (mCRPC) (4). However, a variety of biological factors, including the stage of

Received: July 18, 2023
Accepted: January 8, 2024
Published online: February 21, 2024

Corresponding author:
Santosh Gupta, PhD
email: santosh.gupta@epicsciences.com

David Bourdon, PhD
email: david.bourdon@epicsciences.com

Santosh Gupta and Luisa Fernandez contributed equally.

the illness (sensitive vs. therapy resistant), the type of treatment, the timing, and geography, may have an impact on PSMA expression in prostate cancer (5).

Analysis of circulating tumor cells is one of the liquid biopsy approaches. Cancer cells known as circulating tumor cells (CTCs) escape from tumors and travel to other organs such as the bones, liver, and lungs via the blood circulation or lymphatic system (6). CTCs are trustworthy, constant, independent predictors and prognostic biomarkers of disease response, PFA, and OS because they directly correlate with systemic tumor burden (7,8). Therefore, it would be advantageous to have a meaningful CTC-based diagnostic and predictive biomarker test that can assist clinical decision-making regarding the management of men with prostate cancer. Furthermore, CTC detection holds enormous potential in numerous clinical applications including cancer screening, monitoring treatment response, diagnosis and prognosis evaluation, target identification, and understanding cancer metastasis and emergence of drug resistance (6,9).

Monitoring the level of PSMA protein expression on CTCs as part of a liquid biopsy offers a noninvasive approach that could be used in conjunction with or in lieu of standard PSMA-PET imaging, which itself presents challenges due to variable access and high cost. Clinically, PSMA CTC profiling is being investigated as a potential prognostic and pharmacodynamic biomarker in patients with mCRPC.

Clinical results in men with mCRPC have been markedly improved by PSMA-targeted radioligand treatment (10,11). Detecting PSMA protein expression on CTCs using a liquid biopsy approach may help to improve therapeutic choices and pinpoint the individuals most likely to benefit from PSMA-targeted RLT in prostate cancer (7-13). In this article, we describe the development and validation of a PSMA CTC assay, as well as the application of single-cell CTC sequencing technology to evaluate deoxyribonucleic acid (DNA) copy number changes and CTC heterogeneity in late-stage high-risk men with mCRPC.

Materials and methods

Cell line and culture

To produce lab-derived (LD) slides, multiple distinct cell line cells (CLCs; LNCaP, PC3, 22Rv1, MDA-MB-231, MDA-MB-453, and DU145) with various PSMA expression levels were spiked into healthy blood. Using sterile procedures and RPMI cell line culture media, all CLCs were grown at Epic Sciences. CLCs were then trypsinized, suspended at single-cell levels, numbered, and spiked into healthy donor (HD) blood samples obtained in a Streck BCT container at the proper CLC concentrations in order to give the CLC for assay development and later assay validation (18).

Epic immunofluorescence PSMA assay

The PSMA tyramide signal amplification (TSA) CTC assay was developed utilizing three different prostate cancer cell lines, including LNCaP (high PSMA expression), 22Rv1 (low PSMA expression), and PC3 (no PSMA expression). These CLCs were spiked into healthy blood samples (1:10,000 CLC/white blood cell [WBC] dilutions) to create LD CLC slides for the PSMA assay development and clinical validation. Subsequently, on a proprietary glass slide, three million intact nucleated blood cells were deposited and frozen at −80°C. In order to identify intact nucleated, biomarker-positive, and negative CTC cells, these frozen slides were defrosted and utilized for immunofluorescent staining with a range of antibodies against cytokeratins, CD45, PSMA, and DAPI. Then, CTCs were detected on immunostained glass slides from patient blood samples using a high-throughput Pyxis imaging system with digital pathology artificial intelligence algorithms. In this four-color PSMA CTC assay, PSMA expression was measured on individual CLC, and CTCs recognized as traditional CTCs (CK+, CD45−, and intact DAPI nuclei) with typical CTC morphological characteristics utilizing an anti-PSMA (Abcam, ERP6253) rabbit monoclonal antibody, as illustrated in Figure 1 (14,18). cRatio, which is the ratio of a cell's intensity on a specific channel divided by the median cell intensities over all frames in that channel, was applied to determine the CK expression and PSMA protein expression cutoffs (>3 and >6, respectively).

Analytical validation

We computed the PSMA protein biomarker expression's subcellular localization and assessed the PSMA CTC assay's limit of detection (LOD), specificity, sensitivity, precision, and overall accuracy. For the accuracy and precision experiments, three independent stain runs for different LD slide lots were examined. To evaluate the specificity of the PSMA TSA assay, three technical replicates each of the PSMA expression negative cell lines, including MDA-MB-231, MDA-MB-453, and DU145, plus HD slides were evaluated, together with two process controls (one positive and one negative). The analytical sensitivity of the PSMA TSA assay was assessed using 14 technical replicates of the LNCaP slide, each with a different number of spike-in CLCs. Additionally, a design of experiments technique was utilized with eight stain repetitions to evaluate the accuracy of the PSMA TSA assay. Furthermore, eight technical replicates and two process control slides were stained to evaluate the PSMA TSA assay's accuracy. Finally, to evaluate the PSMA TSA assay's analytical LOD, 24 LD slides containing four different CLC/WBC dilution ratios (1, 10, 30, and 300 CLCs/3E6; six slides each) were evaluated by immunofluorescence (IF) utilizing the optimized PSMA TSA assay. The LOD was determined by analyzing the linearity between the expected and observed numbers of CLCs for each group of slides as well as the lowest number of CLCs identified. The CTC candidates were manually checked by two independent, qualified individuals from Epic Sciences. "CTC per mL" of blood was used to represent the concentration of all CTCs and PSMA-expressing CTCs for each patient (Fig. 1).

Clinical validation and low-pass whole-genome sequencing

A cohort of 24 men with mCRPC and avid PSMA expression confirmed by PSMA-PET/CT scans underwent CTC sampling for clinical validation of the PSMA CTC assay using 3 mL blood samples. Additionally, 36 CTCs from 11 of these men were selected to undergo single-cell low-pass whole-genome sequencing for copy number alteration analysis, as shown

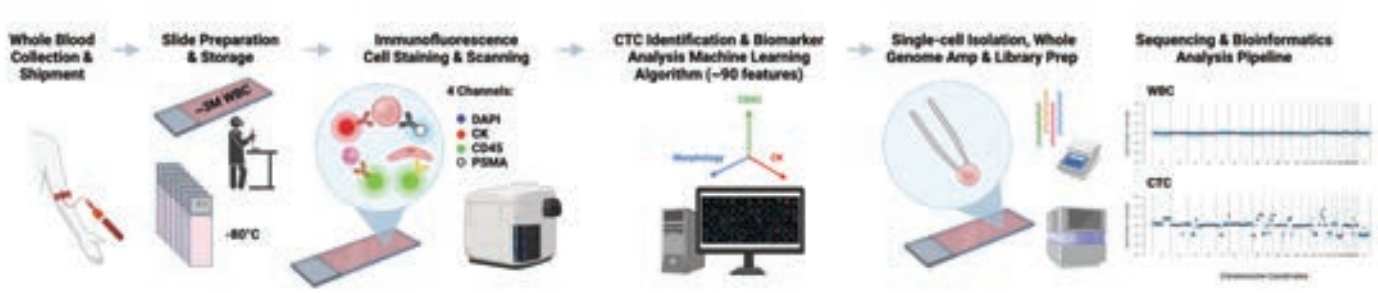

FIGURE 1 - CTC enumeration, biomarker detection, cell picking, and single-cell genomic analysis workflow. CTC = circulating tumor cell.

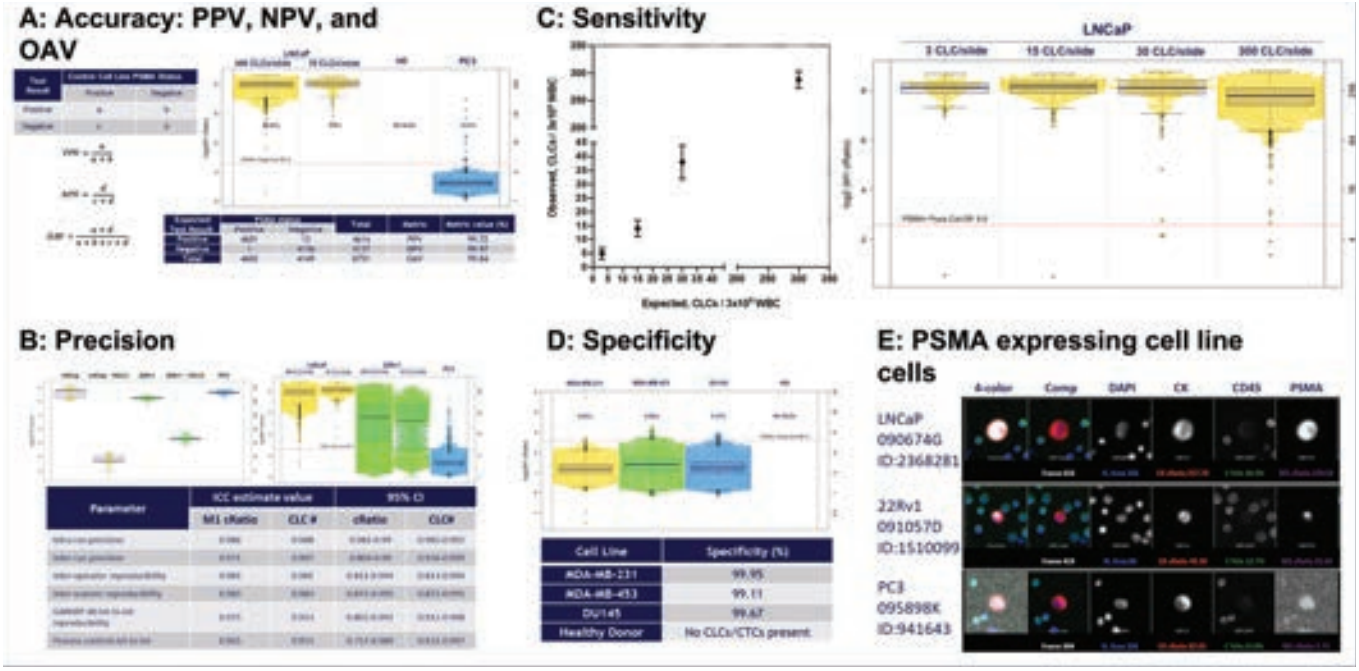

FIGURE 2 - PSMA assay development. A) Denoting the accuracy (PPV, NPV, and OAV) during PSMA assay development. The PSMA assay achieved PPV, NPV, and OAV of over 99%. **B)** The overall precision of the PSMA assay was ICC 0.98. **C)** Sensitivity: the lower spike-in concentration in which 1 PSMA+ CLC was detected 90% of the time and the LOD was 1 CLC when 3 CLCs were spiked into the blood sample prior to slide deposition. **D)** Specificity for the PSMA TSA assay was >99%. **E)** Gallery of PSMA-expressing CLCs (LNCaP, 22Rv1, and PC3). CLC = cell line cell; ICC = intra-class correlation; LOD = limit of detection; NPV = negative predictive value; OAV = overall accuracy value; PPV = positive predictive value; PSMA = prostate-specific membrane antigen; TSA = tyramide signal amplification.

in Figure 1 (15). The single CTCs were manually isolated using microcapillaries. They were whole-genome amplified using the SeqPlex™ Enhanced DNA Amplification Kit (SeqXE) from Sigma-Aldrich. The amplified products were made into sequencing libraries and sequenced on an Illumina NextSeq 500 to generate paired-end 150-bp reads. The sequencing data was analyzed using a copy number analysis pipeline that Epic developed (16). Briefly, the sequencing reads were aligned to the hg38 human reference; the low-quality alignments were excluded. The remaining reads were binned, scaled, and corrected for known biases (such as GC bias). The bin counts were then used for copy number variation (CNV) calling using a z-score statistic, which quantifies the amount of deviation in the bin counts of a given cell relative to a population of normal cells.

Results

PSMA assay development utilizing Epic Sciences' CTC platform

As part of technical feasibility, the development of the PSMA assay was conducted using a multistep approach that included antibody discovery, cell line screening, and the creation of LD slides. Based on a total of 4,614 PSMA-positive and 4,137 PSMA-negative cells, the assay had over 99% positive predictive value, negative predictive value, and overall accuracy value (Fig. 2A). Furthermore, precision was assessed across a variety of metrics, including lot-to-lot reproducibility and process control lot-to-lot repeatability, and it demonstrated high precision (>0.97). To further assess the precision

across all intra-run, inter-run, operator, scanner, lot-to-lot repeatability, and process control lots, intra-class correlation (ICC) was calculated; the average result was 0.976 (Fig. 2B). The lower LOD was defined to be the lowest spike-in concentration in which at least one PSMA+ CLC was detected 90% of the time, and the LOD at where 1 CLC/million was spiked into the blood sample prior to slide deposition (Fig. 2C). The specificity for the PSMA TSA assay was calculated based on PSMA-negative, including MDA-MB-231, MDA-MB-453, and DU145, CLCs, which was over 99% (Fig. 2D). A gallery of PSMA-expressing CLCs from LNCaP, 22Rv1, and PC3 are shown in Figure 2E.

PSMA CTC protein expression detection in mCRPC patients

In a cohort of 24 patients with PSMA-PET positive high-risk mCRPC progressed on androgen receptor signaling inhibitor such as enzalutamide or abiraterone, using 3 mL of blood samples, CTC enumeration and PSMA protein expression were demonstrated with the PSMA CTC assay developed in cancer CLCs. Staining, classification of the slides, and analysis of the 24 mCRPC samples revealed that 21/24 (88%) had at least one traditional CTC [CK(+), CD45(−), and intact DAPI] per milliliter of blood (ranging from 0 to 30 CTCs/mL across the cohort). Of these, 76% (16/21) cases had PSMA protein expression positive CTCs (CK+, CD45−, and DAPI), ranging from 0 to 27 CTCs/mL of blood, suggesting there might be tumor heterogeneity (PSMA-positive and PSMA-negative CTCs; Fig. 3A). Example CTCs in mCRPC patients with PSMA staining are shown in Figure 3B.

Low-pass whole-genome sequencing at single CTC level

To identify the CNV, 36 single CTCs from 11 patients were picked, amplified, and low-pass whole-genome sequenced. The sequencing data was analyzed using a copy number analysis pipeline, where read counts were binned and corrected for known biases. The resulting bin counts were used for CNV calling. The CTCs from 11 patients that underwent low-pass whole-genome sequencing revealed genomic heterogeneity; frequent genomic amplification of the genes *AR* (27%), *MYC* (64%), and *MYCN* (45%); and copy loss of *PTEN* (36%), *TP53* (64%), *BRCA2* (45%), *CHD1* (55%), and *RB1* (45%) (Fig. 4A). Genomic variation at the chromosomal level and at the single CTC level is shown in Figure 4B.

Discussion and conclusion

In this article, we detailed the development of a PSMA blood-based CTC assay utilizing Epic Sciences' PSMA CTC assay platform. We performed analytical validation on LD slides and clinical validation on CTC samples from men with mCRPC with documented PSMA expression on PET scans. The analytical validation demonstrated high performance, which firmly supported its capability to identify the PSMA protein expression in CTCs from high-risk patients with mCRPC. Further, Epic Sciences' PSMA CTC assay platform can be coupled with single-cell CTC sequencing to evaluate CNV and genomic heterogeneity in late-stage disease.

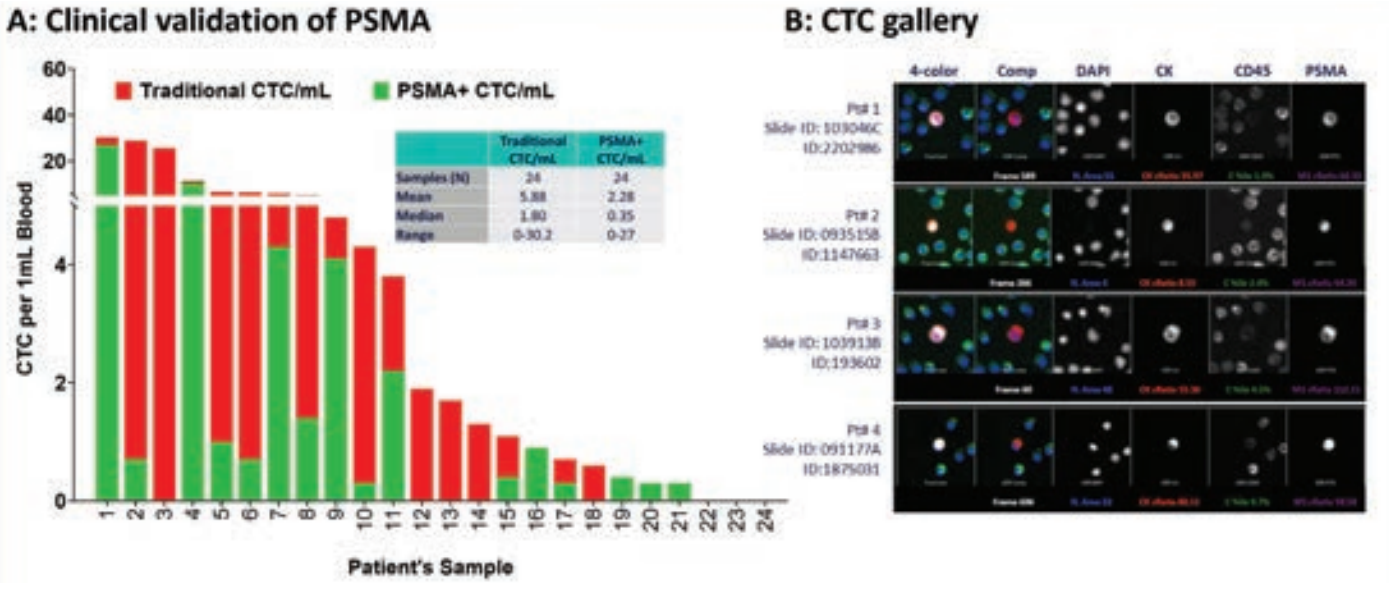

FIGURE 3 - Clinical validation of PSMA protein expression in CTCs of men with mCRPC. A) Analysis of 24 mCRPC samples revealed that 21/24 (88%) had at least one conventional CTC/mL (range: 0-30 CTCs/mL), of which 16/21 (76%) were PSMA positive (range: 0-27 CTCs/mL) with considerable tumor heterogeneity. **B)** A representative gallery of CTCs with PSMA expression in four unique CTCs in mCRPC patients. CTC = circulating tumor cell; mCRPC = metastatic castration-resistant prostate cancer; PSMA = prostate-specific membrane antigen.

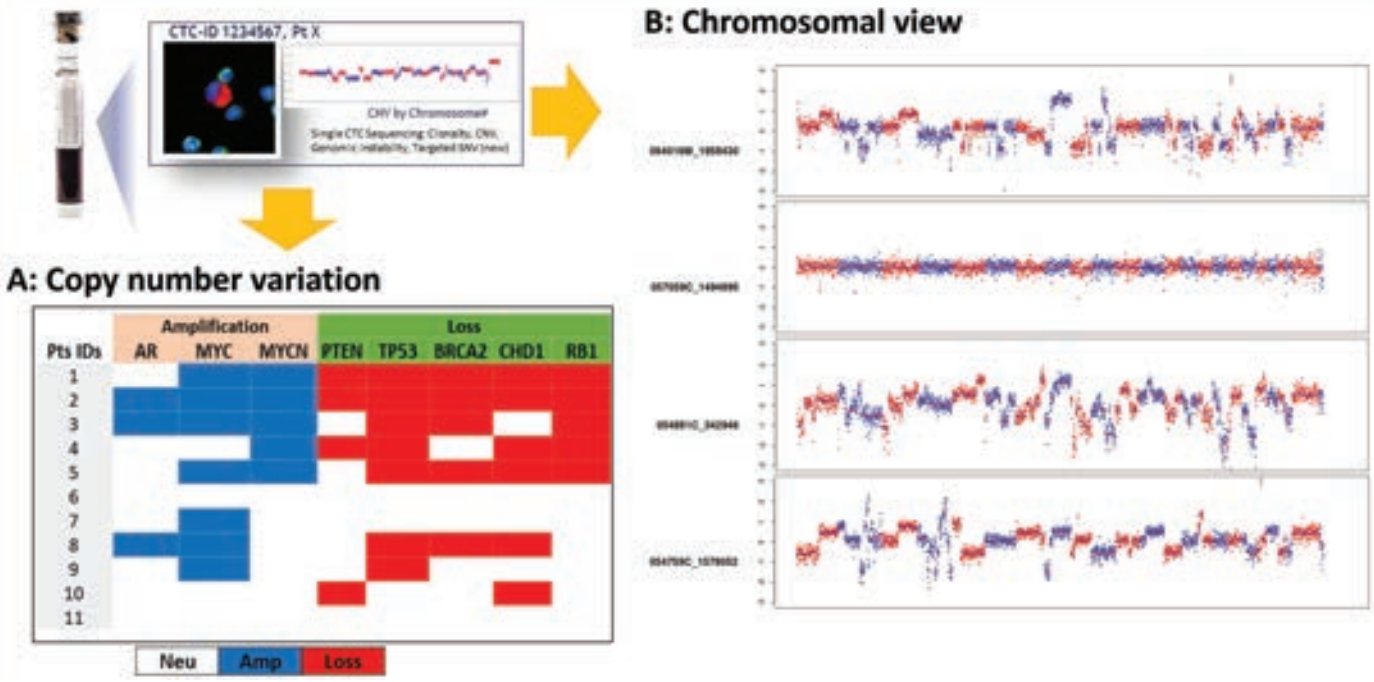

FIGURE 4 - Individual CTCs can be identified and collected for next-generation sequencing to identify CNVs. A) 36 CTCs sequenced from 11 patients exhibited genomic heterogeneity and frequent *AR* (3/11), *MYC* (7/11), and *MYCN* (5/11) amplification and loss of *PTEN* (4/11), *TP53* (7/11), *BRCA2* (5/11), *CHD1* (6/11), and *RB1* (5/11). **B)** Genome-wide chromosomal view images showing CNV at the single CTC level in mCRPC patients. CNV = copy number variation; CTC = circulating tumor cell; mCRPC = metastatic castration-resistant prostate cancer.

Expression of PSMA in mCRPC makes PSMA an attractive drug target. PSMA-targeted therapies are used in the management of metastatic prostate cancer and may have potential for wider usage in personalized management of metastatic prostate cancer (4). The PSMA protein, which is present on the plasma membrane of cells, is overexpressed in over 90% of individuals with mCRPC, and independently linked to shorter PFS and OS (4). Novartis recently received FDA approval for the PSMA RLT, ^{177}Lu-PSMA-617, based on the improvement in PFS and OS from ^{177}Lu-PSMA-617 in conjunction with best SoC compared with SoC alone in men with mCRPC who had previously received potent androgen receptor pathway inhibitors and chemotherapy in the phase III VISION trial (4). In numerous research studies, PET imaging has been utilized to validate that patients have a curable PSMA-specific condition and track response to treatment. When compared to traditional imaging (CT, MRI), PSMA-PET is far more sensitive and specific to PSMA for detecting micro-metastatic illness at both initial staging and biochemical recurrence (NCCN 2021). Although PSMA-negative tumor cells might not be visible by PSMA-PET imaging, they might nevertheless contribute to the development of progressive disease, particularly in heavily treated mCRPC. The correlation between PSMA-PET imaging parameters and PSMA-positive and PSMA-negative CTC enumeration is an area of active investigation. Additionally, serial CTC profiling to monitor response to PSMA-targeted therapy (traditionally based on PSA and conventional imaging and/or PET) and associations with clinical outcomes require further research and validation in large trial datasets. This research effort could help to identify the 25%-30% of men with mCRPC who exhibit primary resistance to PSMA RLT, thereby mitigating additional exposure and allowing early transition to alternate therapies (17). The analytical results of the Epic Sciences' PSMA CTC assay clearly confirm its viability for detecting PSMA expression and for single-cell whole-genome sequencing in CTCs from patients with mCRPC to identify genomic abnormalities known to be recurrent in this disease phase (*AR, PTEN, TP53, CHD1*, and *BRCA1/2*). High levels of sensitivity, specificity, and overall accuracy were shown by the PSMA CTC test.

Finally, we discussed the development of a PSMA blood-based assay for CTC identification and the implementation of the low-pass whole-genome single-cell sequencing workflow to detect variations in copy number at the genome level and to further define CTC tumor heterogeneity in late-stage high-risk mCRPC. This test is positioned as a potent research tool to detect and prospectively monitor PSMA-positive CTC expression and examine tumor heterogeneity, therapeutic response, and resistance in these mCRPC patients. The PSMA-avid disease is the focus of numerous ongoing clinical trials, including PRINCE (NCT03658447) and the LuPARP study (NCT03874884), which utilize this powerful assay for early disease identification, disease monitoring, and understanding drug resistance in patients with mCRPC.

Abbreviations: CLC = cell line cell; CNV = copy number variation; CT = computerized tomography; CTC = circulating tumor cell; DNA = deoxyribonucleic acid; FDA = Food and Drug Administration; HD = healthy donor; ICC = intra-class correlation; IF = immunofluorescence; LD = lab derived; LOD = limit

of detection; mCRPC = metastatic castration-resistant prostate cancer; MRI = magnetic resonance imaging; NPV = negative predictive value; OS = overall survival; PET = positron emission tomography; PFS = progression-free survival; PPV = positive predictive value; PSA = prostate-specific antigen; PSMA = prostate-specific membrane antigen; RLT = radioligand therapy; SoC = standard of care; TSA = tyramide signal amplification; WBC = white blood cell

Disclosures

Conflict of Interest: The authors declare no conflict of interest.

Financial support: This research was supported by Epic Sciences, Victorian Cancer Agency, Australia and Prostate Cancer Foundation.

References

1. Bakht MK, Derecichei I, Li Y, et al. Neuroendocrine differentiation of prostate cancer leads to PSMA suppression. Endocr Relat Cancer. 2018;26(2):131-146. CrossRef PubMed
2. Kaittanis C, Andreou C, Hieronymus H, et al. Prostate-specific membrane antigen cleavage of vitamin B9 stimulates oncogenic signaling through metabotropic glutamate receptors. J Exp Med. 2018;215(1):159-175. CrossRef PubMed
3. Zaman MU, Fatima N, Zaman A, Sajid M, Zaman U, Zaman S. Diagnostic challenges in prostate cancer and 68Ga-PSMA PET imaging: a game changer? Asian Pac J Cancer Prev. 2017;18(10):2625-2628. PubMed
4. Sartor O, de Bono J, Chi KN, et al; VISION Investigators. Lutetium-177-PSMA-617 for metastatic castration-resistant prostate cancer. N Engl J Med. 2021;385(12):1091-1103. CrossRef PubMed
5. Lapidus RG, Tiffany CW, Isaacs JT, Slusher BS. Prostate-specific membrane antigen (PSMA) enzyme activity is elevated in prostate cancer cells. Prostate. 2000;45(4):350-354. CrossRef PubMed
6. Ashworth TR. A case of cancer in which cells similar to those in the tumors were seen in the blood after death. Australas Med J. 1869;14:146-149.
7. Armstrong AJ, Luo J, Nanus DM, et al. Prospective multicenter study of circulating tumor cell AR-V7 and taxane versus hormonal treatment outcomes in metastatic castration-resistant prostate cancer. JCO Precis Oncol. 2020;4:PO.20.00200. CrossRef PubMed
8. Deng Z, Wu S, Wang Y, Shi D. Circulating tumor cell isolation for cancer diagnosis and prognosis. EBioMedicine. 2022;83:104237. CrossRef PubMed
9. Alix-Panabières C, Pantel K. Challenges in circulating tumour cell research. Nat Rev Cancer. 2014;14(9):623-631. CrossRef PubMed
10. Cohen SJ, Punt CJ, Iannotti N, et al. Relationship of circulating tumor cells to tumor response, progression-free survival, and overall survival in patients with metastatic colorectal cancer. J Clin Oncol. 2008;26(19):3213-3221. CrossRef PubMed
11. de Bono JS, Scher HI, Montgomery RB, et al. Circulating tumor cells predict survival benefit from treatment in metastatic castration-resistant prostate cancer. Clin Cancer Res. 2008;14(19):6302-6309. CrossRef PubMed
12. Boudadi K, Suzman DL, Anagnostou V, et al. Ipilimumab plus nivolumab and DNA-repair defects in AR-V7-expressing metastatic prostate cancer. Oncotarget. 2018;9(47):28561-28571. CrossRef PubMed
13. De Bono JS, Pantel K, Efstathiou E, et al. CTC counts as a biomarker of prognosis and response in metastatic castration-resistant prostate cancer (mCRPC) from the CARD trial. J Clin Oncol. 2021;39(6_suppl):161. CrossRef
14. Armstrong AJ, Halabi S, Luo J, et al. Prospective multicenter validation of androgen receptor splice variant 7 and hormone therapy resistance in high-risk castration-resistant prostate cancer: the PROPHECY Study. J Clin Oncol. 2019;37(13):1120-1129. CrossRef PubMed
15. Greene SB, Dago AE, Leitz LJ, et al. Chromosomal instability estimation based on next generation sequencing and single cell genome wide copy number variation analysis. PLoS One. 2016;11(11):e0165089. CrossRef PubMed
16. Armstrong AJ, Gupta S, Healy P, et al. Pharmacodynamic study of radium-223 in men with bone metastatic castration resistant prostate cancer. PLoS One. 2019;14(5):e0216934. CrossRef PubMed
17. Hamid A, Hofman MS, Bressel M, et al. Circulating tumour cells (CTCs) and PSMA PET correlates in the phase I PRINCE trial of 177Lu-PSMA-617 plus pembrolizumab for metastatic castration resistant prostate cancer (mCRPC). J Clin Oncol 2022;40(16_suppl):5027. CrossRef
18. Lu D, Krupa R, Harvey M, et al. Development of an immunofluorescent AR-V7 circulating tumor cell assay – A blood-based test for men with metastatic prostate cancer. J Circ Biomark. 2020 Oct 23;9:13-19. PubMed

JCB
J Circ Biomark 2024; 13: 7-13
ISSN 1849-4544 | DOI: 10.33393/jcb.2024.2689
ORIGINAL RESEARCH ARTICLE
Open Access

Relation between interleukin-13 and annexin-V levels and carotid intima-media thickness in nephrotic syndrome

Asmaa A. Elsehmawy[1], Rasha M. Gouda[1], Fatma Elzhraa A.E. Diab[2], Ola I. Saleh[3], Heba M. Galal[3], Mona G. Al Anany[4,5], Salwa S. Abd Elgawad[1], Marwa M. Hassan[6], Mohamed A. M. Kamal[2], Ahmed Y. Elamir[7]

[1]Pediatric Department, Al-Azhar University, Cairo - Egypt
[2]Clinical Pathology Department, Al-Azhar University, Cairo - Egypt
[3]Radiology Department, Al-Azhar University, Cairo - Egypt
[4]Physiology Department, Al-Azhar University, Cairo - Egypt
[5]Armed Forces College of Medicine, Cairo - Egypt
[6]Community Medicine Department, Al-Azhar University, Cairo - Egypt
[7]Radiology Department, Cairo University, Cairo - Egypt

ABSTRACT

Background and aim: The aim of the current study is to assess the relation between carotid intima-media thickness (CIMT) measurements, renal Doppler resistive index (RI) and serum levels of interleukin-13 (IL-13) and annexin-V (An-V) in children with idiopathic nephrotic syndrome (INS).

Materials and methods: The present case-control study was conducted on 60 children with INS and 60 age- and sex-matched healthy children. All participants were subjected to evaluation of serum levels of IL-13 and An-V and ultrasound Doppler measurement of CIMT and renal RI.

Results: Patients expressed significantly higher An-V (5.9 ± 2.6 vs. 2.1 ± 0.8 ng/mL, p<0.001) and IL-13 (19.2 ± 7.6 vs. 3.4 ± 1.4 ng/L) levels when compared with healthy counterparts. Moreover, it was shown that patients had significantly higher CIMT (0.49 ± 0.06 vs. 0.35 ± 0.03, p<0.001) as compared to controls. No significant differences were noted between the studied groups regarding right or left RIs. Correlation analysis identified significant direct correlation between serum An-V levels and albumin/creatinine ratio (ACR) (r = 0.55), cholesterol (r = 0.48), triglycerides (r = 0.36), IL-13 (r = 0.92) and CIMT (r = 0.53). Similar correlations could be found between serum IL-13 levels and CIMT measurements and the corresponding parameters.

Conclusions: The present study suggests an association between higher early atherosclerosis expressed as elevated CIMT measurements in children with INS and elevated serum levels of An-V and IL-13.

Keywords: Annexin-V, Carotid intima-media thickness, Idiopathic nephrotic syndrome, Interleukin-13

Introduction

Idiopathic nephrotic syndrome (INS) is a common childhood disease with average global incidence of 4.7 per 100,000 persons (1). According to one report, most affected children in African countries including Egypt are steroid sensitive (2). Fortunately, the condition has generally favorable prognosis with the majority of patients achieving complete remission (3). However, about 1% of patients may develop end-stage renal disease by the age of 18 (4). INS is characterized by significant proteinuria as well as other pathological alterations. It results from enhanced plasma protein permeability of the glomerular filtration membrane. Although most patients benefit from steroid treatment, 10%-20% of affected children have steroid-resistant nephrotic syndrome (SRNS) (5,6).

While the exact cause of INS is unknown, an imbalance between T helper (Th)1 and Th2 cells is most likely to blame. It is suggested that activation of Th2 cells is a key factor in the pathophysiology of minimal change disease (MCD). Th2-released cytokines interleukin-4 (IL-4), IL-10 and especially IL-13 may play a part in the induction of proteinuria (7). IL-13 is a pleiotropic type 2 cytokine involved in the pathogenesis of many allergic (8), inflammatory (9) and malignant

Received: October 22, 2023
Accepted: May 16, 2024
Published online: June 18, 2024

Corresponding author:
Asmaa A. Elsehmawy
email: asmaawakeel@yahoo.com

conditions (10). In MCD patients, IL-13 may change glomerular permeability and cause proteinuria (7). Annexin-V (An-V) is a cytoplasmic calcium-binding protein with pleotropic functions (11,12). The cells of the distal tubules and the glomerular epithelium contain considerable levels of An-V. It is frequently used as an apoptotic marker in many pathological conditions including systemic sclerosis (13), diabetes (14) and atherosclerosis (15). It helped to explain a variety of kidney-related events, such as acute kidney damage and diabetic nephropathy. It has also been utilized as a biochemical indicator of atherosclerosis in patients with chronic kidney disease (16).

The carotid intima-media thickness (CIMT) measured by ultrasound is used as a marker of atherosclerotic changes (17). In children with INS, atherosclerotic changes may accelerate progression to chronic kidney disease and are mainly related to dyslipidemia (18,19). Intrarenal hemodynamics was found to be a potential indicator of systemic vascular injury and a helpful tool for better stratifying short- and long-term cardiovascular risk in various clinical subgroups. Particularly, renal Doppler resistive index (RI) and renal pulsatility index (PI) are closely associated with well-known markers of subclinical organ damage, such as CIMT, arterial stiffness, and left ventricular mass (20).

Renal RI has been shown as a noninvasive prognostic marker for assessing the renal disease progression, especially in hypertension, as well as proteinuria (21-24). Additionally, numerous studies have shown that intrarenal hemodynamic dysfunction directly contributes to unfavorable cardiovascular events and even death across a variety of populations, particularly in those with chronic kidney disease (12). The present study hypothesized that there is a relation between subclinical atherosclerosis and inflammatory markers in children with INS. The aim of the current study is to assess the relation between CIMT, renal Doppler RI and serum levels of IL-13 and An-V in children with INS.

Materials and methods

Study design

The present cross-sectional case-control study was conducted during the period from August 2021 to May 2022. The study protocol was approved by the ethical committee and the legal guardians of included children proved written informed consent before participation.

Participants

The study included 60 children with INS diagnosed on the basis of the International Study of Kidney Disease in Children criteria (25). In addition, there were 60 age- and sex-matched healthy children who served as the control group. Children with acquired or congenital heart disease, active systemic vasculitis, chronic kidney disease and severe edema at the time of examination or taking lipid-lowering drugs were excluded from the study.

Variables

All participants underwent thorough clinical evaluations, including measurements of weight, height, body mass index (BMI), arterial blood pressure (BP), examination for edema and cardiac examination to exclude congenital or acquired heart disease. All patients completed a thorough clinical history that included past medical history, age at diagnosis, disease duration, responsiveness to steroid treatment, frequency of relapses and use of immunosuppressive drugs. Steroid sensitivity was defined as complete remission at the standard dose of prednisone or prednisolone (PDN) (60 mg/m^2/day or 2 mg/kg/day, maximum 60 mg/day) within 4 weeks, while steroid resistance was defined as failure to achieve remission after 4-8 weeks of daily oral PDN therapy at a dose of 2 mg/kg/day (26). In SRNS patients, 19 patients received calcineurin inhibitors, while 3 patients received mycophenolate mofetil.

For measurement of BP, the patient was seated correctly; BP readings for the systolic and diastolic phases were taken using a mercury sphygmomanometer with an appropriate cuff size. At 2-minute intervals, three measurements were collected from each participant, and the average of the last two measurements was recorded. Values >95th percentile are regarded as elevated by the American Academy of Pediatrics for systolic BP and diastolic BP in the pediatrics population (27).

For laboratory assessment, 6 mL of venous blood was withdrawn after 10 hours of fasting and divided into three aliquots; 2 mL was evacuated in ethylenediaminetetraacetic acid (EDTA) tube for complete blood count (Sysmex KX21N, Kobe, Japan). The remaining 4 mL was evacuated in two serum separator tubes, centrifuged at 3,500 rpm for 10 minutes; two mL serum was used for measurement of kidney function tests (urea and creatinine), lipid profile (total cholesterol, triglycerides) and serum albumin; and the other 2 mL was separated and frozen at −20°C for later analysis of IL-13 and An-V. An early morning urine sample was used for albumin/creatinine ratio (ACR) measurement. Measurement of serum IL-13 and An-V was done using the commercial enzyme-linked immunosorbent assay (ELISA) kits (Bioassay Technology Laboratory, China; Cat. No. 202208016). The assay ranges of IL-13 and An-V were from 0.5 to 100 ng L and 0.1 to 35 ng mL, respectively.

Measurement of CIMT was done using the ultrasound machine (Philips 50G ultrasound machine) with high-frequency linear probe (7.5 MHz) (Fig. 1). The examination was done in supine position; the neck is extended and slightly turned to the contralateral side. Prior to measurement, the patients had rest for 10 minutes. The arterial wall of the common carotid artery was assessed bilaterally in a longitudinal view; both walls were clearly visualized to obtain proper measurements. Zoomed frozen images were taken clearly demonstrating the intima-media thickness. Measurements were taken from the far wall of each common carotid artery 1 cm proximal to bifurcation. The measurements were made three times on each side and the average of the measurements was taken. The mean of measurements of the left and right common carotid arteries was calculated.

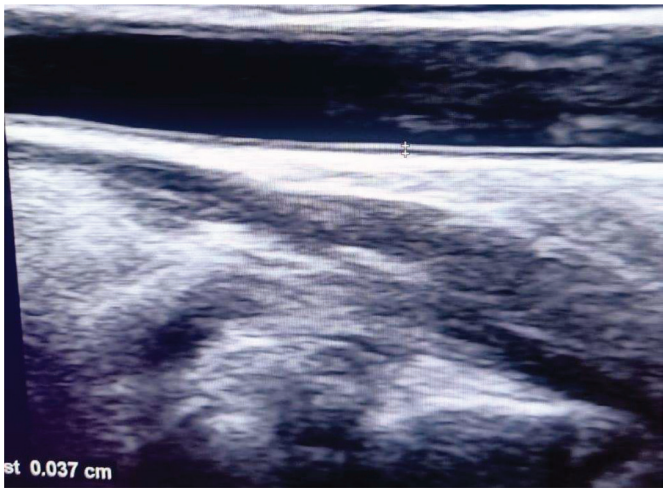

FIGURE 1 - B mode ultrasound of carotid intima-media thickness measurement.

Renal Doppler ultrasound evaluation was done in the lateral oblique position or oblique position; however, the left kidney was better examined in a right lateral decubitus. The examination was done using Philips 50G ultrasound machine with low-frequency convex probe (5 MHz) (Fig. 2). Firstly, both kidneys were scanned using B mode for detection of any gross abnormalities such as stones, backpressure changes, echogenicity, cortical thickness or focal lesions. Color Doppler was applied to see interlobar arteries, and then the sample volume was applied to cover only the arterial diameter of interest. Optimum waveform was obtained by adjustment of both the pulse repetition frequency (PRF) and the wall filter to avoid aliasing. Measurement of Doppler parameters was taken at breath holds in cooperative children and in younger children at quiet respiration. For each kidney, RIs of renal interlobar arteries at the upper, middle and lower poles were assessed three times, then the average of the measurements was taken. The arterial RI was calculated by the equation (peak systolic velocity − end diastolic velocity) divided by (peak systolic velocity), and its value is derived via the computer algorithm in the ultrasound machine.

Statistical methods

Results were reviewed, given codes and enrolled into the Statistical Package for Social Sciences (IBM SPSS) version 23. Normality of data distribution was assessed using Kolmogorov-Smirnov test. Quantitative data were displayed as means and standard deviation (SD) or median and interquartile range (IQR). Qualitative data were displayed as numbers and percentages. Comparison of non-quantitative data was done by Chi-square test. Comparison of quantitative data with the parametric patterns was done by independent *t*-test, while non-parametric data were compared using Mann-Whitney U-test. Correlation between various variables was done using Pearson's correlation coefficient for parametric data and Spearman's correlation coefficient for non-parametric data. A p-value was considered to be significant if less than 0.05.

Results

The present study included 60 children with INS and 60 age- and sex-matched healthy controls. Patients had disease duration of 2.9 ± 2.6 years. Comparison between the studied groups regarding clinical, laboratory and ultrasonic parameters revealed that patients had significantly lower serum albumin levels (1.7 ± 0.4 vs. 3.5 ± 0.3 g/dL, p<0.001) and significantly higher platelet count (381.4 ± 105.2 vs. 332.4 ± 94.2, p = 0.008), ACR (5,945.5 ± 2,866.6 vs. 75.4 ± 122.4 mg/g, p<0.001), cholesterol (456.3 ± 139.5 vs. 163.8 ± 126.3 mg/dL, p<0.001) and triglyceride (214.6 ± 112.0 vs. 123.6 ± 38.7 mg/dL, p<0.001) levels when compared with controls.

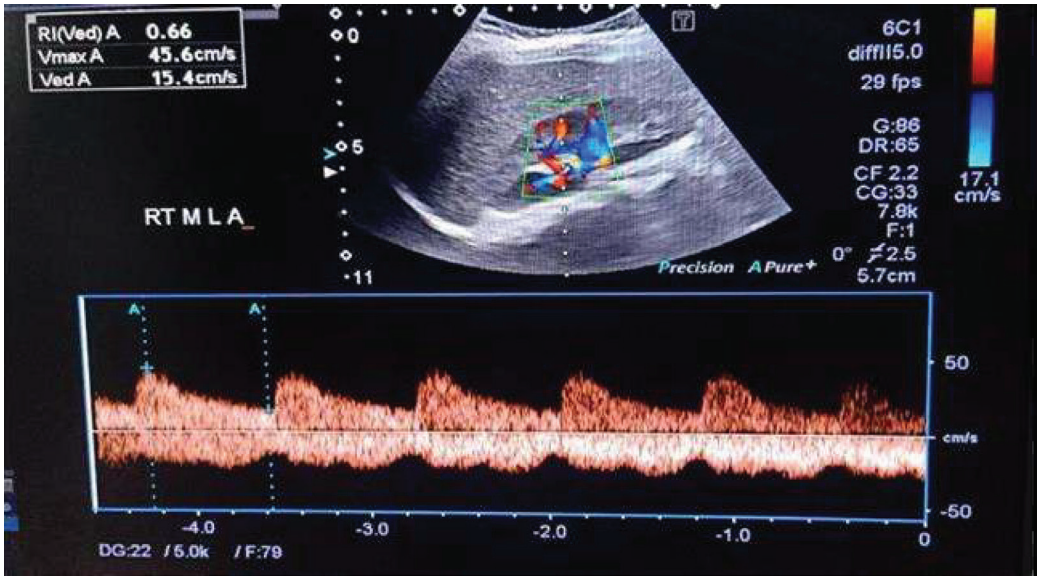

FIGURE 2 - Color duplex ultrasound measurements of the right and middle pole interlobar artery resistive index.

No statistically significant differences were found between the studied groups regarding diastolic and systolic BP measurements (Tab. 1).

TABLE 1 - Clinical, laboratory and radiological findings in the studied groups

	Patients n = 60	Controls n = 60	p value
Age (years)	9.6 ± 3.6	9.7 ± 3.7	0.83
Male/female n	39/21	43/17	0.43
BMI (kg/m^2)	21.3 ± 5.6	20.1 ± 3.8	0.19
SBP (mm Hg)	102.1 ± 10.3	103.5 ± 8.4	0.41
DBP (mm Hg)	65.2 ± 9.0	64.9 ± 8.2	0.83
Laboratory findings			
WBCs (10^9/L)	5.6 (4.9-6.6)	5.1 (4.7-6.2)	0.21
Hemoglobin (mg/dL)	13.0 ± 1.3	12.9 ± 1.4	0.9
Platelets (10^9/L)	381.4 ± 105.2	332.4 ± 94.2	0.008
Albumin (g/dL)	1.7 ± 0.4	3.5 ± 0.3	<0.001
Urea (mg/dL)	19.5 ± 5.3	18.0 ± 4.6	0.1
Creatinine (mg/dL)	0.37 ± 0.22	0.33 ± 0.22	0.27
ACR (mg/g)	5945.5 ± 2866.6	75.4 ± 122.4	<0.001
Cholesterol (mg/dL)	456.3 ± 139.5	163.8 ± 126.3	<0.001
Triglycerides (mg/dL)	214.6 ± 112.0	123.6 ± 38.7	<0.001
Annexin-V (ng/mL)	5.9 ± 2.6	2.1 ± 0.8	<0.001
IL-13 (ng/L)	19.2 ± 7.6	3.4 ± 1.4	<0.001
Ultrasound findings			
CIMT (mm)	0.49 ± 0.06	0.35 ± 0.03	<0.001
Right RI	0.61 ± 0.02	0.60 ± 0.02	0.5
Left RI	0.60 ± 0.02	0.60 ± 0.02	0.73

ACR = albumin/creatinine ratio; BMI = body mass index; CIMT = carotid intima-media thickness; DBP = diastolic blood pressure; IL-13 = interleukin-13; RI = resistive index; SBP = systolic blood pressure; WBCs = white blood cells.

In addition, they expressed significantly higher An-V (5.9 ± 2.6 vs. 2.1 ± 0.8 ng/mL, p<0.001) and IL-13 (19.2 ± 7.6 vs. 3.4 ± 1.4 ng/L) levels when compared with healthy counterparts. Moreover, it was shown that patients had significantly higher CIMT (0.49 ± 0.06 vs. 0.35 ± 0.03, p<0.001) as compared to controls. No significant differences were noted between the studied groups regarding right or left RIs (Tab. 1).

Correlation analysis identified significant direct correlation between serum An-V levels and ACR (r = 0.55), cholesterol (r = 0.48), triglycerides (r = 0.36), IL-13 (r = 0.92) and CIMT (r = 0.53). Similar correlations could be found between serum IL-13 levels and CIMT measurements and the corresponding parameters (ACR, cholesterol, triglycerides) (Tab. 2).

TABLE 2 - Correlations between CIMT, annexin-V, IL-13 and clinical, laboratory and radiological data

	CIMT		Annexin-V		IL-13	
	r	p	r	p	r	p
Age	0.003	0.98	−0.034	0.71	−0.027	0.77
BMI	−0.02	0.88	−0.01	0.88	−0.04	0.7
SBP	−0.06	0.67	−0.13	0.15	−0.11	0.25
DBP	−0.14	0.3	−0.09	0.32	−0.04	0.68
Disease duration	−0.05	0.73	−0.14	0.29	−0.16	0.23
WBCs	0.006	0.96	−0.005	0.97	0.01	0.19
Hemoglobin	0.08	0.56	−0.1	0.3	−0.06	0.51
Platelets	0.06	0.67	0.13	0.15	0.19	0.043
Albumin	−0.77	<0.001	0.55	<0.001	0.65	<0.001
Urea	−0.2	0.12	0.13	0.16	0.16	0.1
Creatinine	−0.09	0.49	0.13	0.15	0.12	0.18
ACR	0.77	<0.001	0.55	<0.001	0.65	<0.001
Cholesterol	0.7	<0.001	0.48	<0.001	0.58	<0.001
Triglycerides	0.31	0.017	0.36	<0.001	0.39	<0.001
Annexin-V	0.53	<0.001	–	–	0.92	<0.001
IL-13	0.64	<0.001	0.92	<0.001	–	–
CIMT	–	–	0.53	<0.001	0.64	<0.001
Right RI	−0.08	0.54	0.08	0.37	0.06	0.53
Left RI	−0.06	0.67	0.04	0.69	−0.05	0.56

ACR = albumin/creatinine ratio; BMI = body mass index; CIMT = carotid intima-media thickness; DBP = diastolic blood pressure; IL-13 = interleukin-13; RI = resistive index; SBP = systolic blood pressure; WBCs = white blood cells.

The present study included 38 (63.3%) steroid-sensitive patients. Comparison between steroid-sensitive and steroid-resistant patients regarding An-V and IL-13 levels, CIMT measurements and other clinical parameters revealed no statistically significant differences (Tab. 3).

Discussion

The present study found an association between increased CIMT levels and higher levels of serum An-V and IL-13 levels, which is a novel finding to the best of our knowledge. The study compared clinical, laboratory and Doppler ultrasound parameters in children with INS and healthy controls. The study found that patients exhibited significantly higher CIMT measurements as compared to healthy controls. Similar results were reported by previous studies (17,28-32), while Kniazewska et al (33) and Rahul et al (34) found no significant differences in CIMT measurements between children with INS and healthy counterparts. This may be explained by the different clinical profile of the studied groups. Elevated CIMT in INS children is usually explained by concurrent hypertension and dyslipidemia. Notably, our patients had significantly higher serum cholesterol and triglyceride levels as compared

TABLE 3 - Annexin-V and IL-13 levels and CIMT in steroid-sensitive and steroid-resistant patients

	Steroid sensitive n = 38	Steroid resistant n = 22	p value
Age (years)	9.8 ± 3.7	9.3 ± 3.4	0.56
Male/female n	23/15	16/6	0.34
BMI (kg/m^2)	20.5 ± 4.6	22.7 ± 7.1	0.16
SBP (mm Hg)	102.1 ± 8.5	102.0 ± 12.8	0.99
DBP (mm Hg)	63.2 ± 6.4	68.6 ± 11.6	0.05
Laboratory findings			
WBCs (10^9/L)	5.5 (4.9-6.1)	5.7 (4.9-9.6)	0.42
Hemoglobin (mg/dL)	12.9 ± 1.4	13.3 ± 1.2	0.29
Platelets (10^9/L)	380.3 ± 95.4	383.2 ± 122.7	0.92
Albumin (g/dL)	1.7 ± 0.4	1.8 ± 0.3	0.81
Urea (mg/dL)	20.3 ± 5.9	18.2 ± 4.0	0.14
Creatinine (mg/dL)	0.40 ± 0.21	0.31 ± 0.21	0.11
Cholesterol (mg/dL)	464.3 ± 153.9	442.5 ± 112.6	0.56
Triglycerides (mg/dL)	210.0 ± 110.4	222.6 ± 117.0	0.68
Annexin-V (ng/mL)	19.8 ± 8.0	18.3 ± 7.1	0.55
IL-13 (ng/L)	6.3 ± 2.6	5.2 ± 2.4	0.55
Ultrasound findings			
CIMT (mm)	0.493 ± 0.061	0.488 ± 0.056	0.76
Right RI	0.611 ± 0.024	0.609 ± 0.026	0.79
Left RI	0.608 ± 0.019	0.607 ± 0.024	0.85

BMI = body mass index; CIMT = carotid intima-media thickness; DBP = diastolic blood pressure; IL-13 = interleukin-13; RI = resistive index; SBP = systolic blood pressure; WBCs = white blood cells.

to controls while both groups expressed comparable systolic and diastolic BP values.

The present study proposed to assess if serum An-V and IL-13 levels are related to dyslipidemia and CIMT measurements in those patients. The study showed significantly higher concentrations of An-V in children with INS in comparison with healthy controls. Jakubowska and Kiliś-Pstrusińska (16) also reported higher concentrations of plasma An-V in children with INS. Moreover, we detected a positive correlation between serum An-V with ACR in line with the conclusions of Simsek and colleagues (35). The cause of elevated plasma An-V concentrations in INS is still unknown. It is well recognized that An-V pathophysiological function is linked to cell apoptosis, and increased circulating lymphocyte apoptosis have been observed in children with nephrotic syndrome (35). Interestingly, Ye and colleagues (36) had demonstrated higher level of anti-annexin antibodies in children with INS, which significantly correlated with urine protein level. In addition, An-V levels were well correlated with dyslipidemia and CIMT in our study. To the best of our knowledge, this is a new finding in children with INS. In support of this result, one study on adult diabetic population observed positive correlation between serum An-V levels and CIMT (37).

Moreover, the present study detected a significantly higher concentration of IL-13 in INS patients in comparison with healthy controls. The overexpression of IL-13 is probably related to downregulation of podocin, nephrin and dystroglycan (essential molecules in preserving the slit diaphragm integrity of the glomeruli) (38).

Our findings are also supported by the studies of Kimata et al (39) who reported increased levels of urinary IL-13 in untreated children with INS. The present study also documented a significant positive correlation between serum IL-13 levels and ACR, cholesterol and triglyceride levels in INS patients. The relation between IL-13 levels in dyslipidemia observed by the present study may be explained by the interesting experimental work of Low et al (40). In their study on cytokine-induced rat MCD model, they showed that IL-13 induced changes in hepatic handling of cholesterol that resulted in hypercholesterolemia even before the onset of proteinuria. Our results may have therapeutic implications. Possible blockade of IL-13 pathways was recently studied in many inflammatory conditions (41-43). Use of similar approach in INS may be tried in the forthcoming future.

Notably, no significant differences were found between patients and controls regarding renal hemodynamic parameters. This reflects the fact that in spite of the increased CIMT in the studied patients, the renal hemodynamics remained unaffected. Also, the study showed no significant difference in CIMT between steroid response and SRNS and this came in agreement with Ahmed et al (17) who reported no significant difference in the CIMT between different steroid response and resistant groups. Also Rahul et al (34) found no significant difference in CIMT between steroid-sensitive nephrotic syndrome (SSNS) and SRNS patients.

Finally, we noticed that our patients expressed significantly higher platelet count. This comes in agreement with Gulleroglu et al (44) who reported increased platelet count and platelet volume in children with INS. The precise mechanism of this finding is still unknown. However, it has been noted that platelet hyper-aggregation and high platelet numbers are associated with hypoalbuminemia and hypercholesterolemia. The contribution of these cofactors to the development and clinical presentation of INS remains to be elucidated. Findings of the present study are limited by its cross-sectional design and the relatively small sample size. In conclusion, the present study suggests an association between early atherosclerosis expressed as elevated CIMT measurements in children with INS and elevated serum levels of An-V and IL-13. Further studies are recommended to confirm these findings and to explore their practical implications.

Acknowledgment

The authors are grateful to the patients' families for their participation in this work.

Disclosures

Conflict of interest: The authors have no conflicts of interest in this work.

Financial support: This research received no external funding.

Ethical approval: Written informed consent was completed by each child's parents. The study protocol was approved by Al-Azhar

University local Ethics Committee, Faculty of Medicine (for girls), the council number is 202107919, and all procedures were in accordance with the Helsinki Declaration.

Consent of publication: Not applicable.

Data availability statement: Data of this study will be available from the corresponding author upon reasonable request.

Authors' Contributions: All authors contributed significantly to the work reported, whether that is in the conception, study design, implementation, data collection, analysis and interpretation, or in each of these areas. They also participated in writing, revising or critically evaluating the article, gave their final approval for the version that would be published, decided on the journal to which the article would be submitted and agreed to be held accountable for all aspects of the work.

References

1. Chanchlani R, Parekh RS. Ethnic differences in childhood nephrotic syndrome. Front Pediatr. 2016;4:39. CrossRef PubMed
2. Wine R, Vasilevska-Ristovska J, Banh T, et al; H3 Africa Kidney Disease Research Network. Trends in the epidemiology of childhood nephrotic syndrome in Africa: a systematic review. Glob Epidemiol. 2021;3:100061. CrossRef PubMed
3. Özlü SG, Demircin G, Tökmeci N, et al. Long-term prognosis of idiopathic nephrotic syndrome in children. Ren Fail. 2015;37(4):672-677. CrossRef PubMed
4. Carter SA, Mistry S, Fitzpatrick J, et al. Prediction of short- and long-term outcomes in childhood nephrotic syndrome. Kidney Int Rep. 2019;5(4):426-434. CrossRef PubMed
5. Kitsou K, Askiti V, Mitsioni A, Spoulou V. The immunopathogenesis of idiopathic nephrotic syndrome: a narrative review of the literature. Eur J Pediatr. 2022;181(4):1395-1404. CrossRef PubMed
6. Guo HL, Li L, Xu ZY, et al. Steroid-resistant nephrotic syndrome in children: a mini-review on genetic mechanisms, predictive biomarkers and pharmacotherapy strategies. Curr Pharm Des. 2021;27(2):319-329. CrossRef PubMed
7. da Silva Filha R, Burini K, Pires LG, Brant Pinheiro SV, Simões E Silva AC. Idiopathic nephrotic syndrome in pediatrics: an up-to-date. Curr Pediatr Rev. 2022;18(4):251-264. CrossRef PubMed
8. Matera MG, Ora J, Calzetta L, Rogliani P, Cazzola M. Investigational anti IL-13 asthma treatments: a 2023 update. Expert Opin Investig Drugs. 2023;32(5):373-386. CrossRef PubMed
9. Iwaszko M, Biały S, Bogunia-Kubik K. Significance of interleukin (IL)-4 and IL-13 in inflammatory arthritis. Cells. 2021;10(11):3000. CrossRef PubMed
10. Shi J, Song X, Traub B, Luxenhofer M, Kornmann M. Involvement of IL-4, IL-13 and their receptors in pancreatic cancer. Int J Mol Sci. 2021;22(6):2998. CrossRef PubMed
11. Shobeiri SS, Sankian M. Polyvinyl alcohol can stabilize FITC conjugated recombinant annexin V for apoptotic cells detection. Protein Pept Lett. 2022;29(9):806-814. CrossRef PubMed
12. Simonsen AC, Boye TL, Nylandsted J. Annexins bend wound edges during plasma membrane repair. Curr Med Chem. 2020;27(22):3600-3610. CrossRef PubMed
13. Horimoto AMC, de Jesus LG, de Souza AS, Rodrigues SH, Kayser C. Anti-annexin V autoantibodies and vascular abnormalities in systemic sclerosis: a longitudinal study. Adv Rheumatol. 2020;60(1):38. CrossRef PubMed
14. Bratseth V, Margeirsdottir HD, Chiva-Blanch G, et al. Annexin V^+ microvesicles in children and adolescents with type 1 diabetes: a prospective cohort study. J Diabetes Res. 2020;2020:7216863. CrossRef PubMed
15. Hu Y, Liu G, Zhang H, et al. A comparison of [^{99m}Tc]duramycin and [^{99m}Tc]annexin V in SPECT/CT imaging atherosclerotic plaques. Mol Imaging Biol. 2018;20(2):249-259. CrossRef PubMed
16. Jakubowska A, Kiliś-Pstrusińska K. Annexin V in children with idiopathic nephrotic syndrome treated with cyclosporine A. Adv Clin Exp Med. 2020;29(5):603-609. CrossRef PubMed
17. Ahmed HM, Ameen EE, Awad MS, Botrous OE. Assessment of carotid intima media thickness and left ventricular mass index in children with idiopathic nephrotic syndrome. Vasc Health Risk Manag. 2021;17:349-356. CrossRef PubMed
18. Hyla-Klekot L, Bryniarski P, Pulcer B, Ziora K, Paradysz A. Dimethylarginines as risk markers of atherosclerosis and chronic kidney disease in children with nephrotic syndrome. Adv Clin Exp Med. 2015;24(2):307-314. CrossRef PubMed
19. Vaziri ND. HDL abnormalities in nephrotic syndrome and chronic kidney disease. Nat Rev Nephrol. 2016;12(1):37-47. CrossRef PubMed
20. Geraci G, Buccheri D, Zanoli L, et al. Renal haemodynamics and coronary atherosclerotic burden are associated in patients with hypertension and mild coronary artery disease. Exp Ther Med. 2019;17(4):3255-3263. CrossRef PubMed
21. Youssef DM, Fawzy FM. Value of renal resistive index as an early marker of diabetic nephropathy in children with type-1 diabetes mellitus. Saudi J Kidney Dis Transpl. 2012;23(5):985-992. CrossRef PubMed
22. Moriconi D, Mengozzi A, Duranti E, et al. The renal resistive index is associated with microvascular remodeling in patients with severe obesity. J Hypertens. 2023;41(7):1092-1099. CrossRef PubMed
23. Ghafori M, Rashedi A, Montazeri M, Amirkhanlou S. The relationship between Renal Arterial Resistive Index (RRI) and renal outcomes in patients with resistant hypertension. Iran J Kidney Dis. 2020;14(6):448-453. PubMed
24. Provenzano M, Rivoli L, Garofalo C, et al. Renal resistive index in chronic kidney disease patients: possible determinants and risk profile. PLoS One. 2020;15(4):e0230020. CrossRef PubMed
25. Primary nephrotic syndrome in children: clinical significance of histopathologic variants of minimal change and of diffuse mesangial hypercellularity. A report of the International Study of Kidney Disease in Children. Kidney Int. 1981;20(6):765-771. CrossRef PubMed
26. Trautmann A, Vivarelli M, Samuel S, et al; International Pediatric Nephrology Association. IPNA clinical practice recommendations for the diagnosis and management of children with steroid-resistant nephrotic syndrome. Pediatr Nephrol. 2020;35(8):1529-1561. CrossRef PubMed
27. Flynn JT, Kaelber DC, Baker-Smith CM, et al; SUBCOMMITTEE ON SCREENING AND MANAGEMENT OF HIGH BLOOD PRESSURE IN CHILDREN. Clinical practice guideline for screening and management of high blood pressure in children and adolescents. Pediatrics. 2017;140(3):e20171904. CrossRef PubMed
28. Hooman N, Isa-Tafreshi R, Otukesh H, Mostafavi SH, Hallaji F. Carotid artery function in children with idiopathic nephrotic syndrome. Nefrologia. 2013;33(5):650-656. CrossRef PubMed
29. Youssef DM, Gomaa MA, El-Akhras A, et al. Brachial artery flow-mediated dilatation and carotid intima-media thickness in children with idiopathic nephrotic syndrome. Iran J Kidney Dis. 2018;12(6):331-340. PubMed
30. Skrzypczyk P, Kuźma-Mroczkowska E, Kułagowska J, Brzewski M, Okarska-Napierała M, Pańczyk-Tomaszewska M. Carotid intima-media thickness in children with idiopathic nephrotic syndrome: a single center cross-sectional study. Clin Nephrol. 2019;91(6):353-362. CrossRef PubMed

31. Paripović A, Stajić N, Putnik J, Gazikalović A, Bogdanović R, Vladislav V. Evaluation of carotid intima media thickness in children with idiopathic nephrotic syndrome. Nephrol Ther. 2020;16(7):420-423. CrossRef PubMed
32. Kamel AS, AlGhawass MME, Sayed MA, Roby SA. Evaluation of carotid intima media thickness in children with idiopathic nephrotic syndrome. Ital J Pediatr. 2022;48(1):195. CrossRef PubMed
33. Kniazewska MH, Obuchowicz AK, Wielkoszyński T, et al. Atherosclerosis risk factors in young patients formerly treated for idiopathic nephrotic syndrome. Pediatr Nephrol. 2009;24(3):549-554. CrossRef PubMed
34. Rahul I, Krishnamurthy S, Satheesh S, Biswal N, Bobby Z, Lakshminarayanan S. Brachial artery flow-mediated dilatation and carotid intima medial thickness in pediatric nephrotic syndrome: a cross-sectional case-control study. Clin Exp Nephrol. 2015;19(1):125-132. CrossRef PubMed
35. Simsek B, Buyukcelik M, Soran M, et al. Urinary annexin V in children with nephrotic syndrome: a new prognostic marker? Pediatr Nephrol. 2008;23(1):79-82. CrossRef PubMed
36. Ye Q, Zhang Y, Zhuang J, et al. The important roles and molecular mechanisms of annexin A_2 autoantibody in children with nephrotic syndrome. Ann Transl Med. 2021;9(18):1452. CrossRef PubMed
37. Bilgir O, Vural HA, Bilgir F, Akan OY, Demir I. Serum annexin V and anti-annexin V levels and their relationship with metabolic parameters in patients with type 2 diabetes. Rev Assoc Med Bras (1992). 2019 Sep 12;65(8):1042-1047. CrossRef
38. Lai KW, Wei CL, Tan LK, et al. Overexpression of interleukin-13 induces minimal-change-like nephropathy in rats. J Am Soc Nephrol. 2007;18(5):1476-1485. CrossRef PubMed
39. Kimata H, Fujimoto M, Furusho K. Involvement of interleukin (IL)-13, but not IL-4, in spontaneous IgE and IgG4 production in nephrotic syndrome. Eur J Immunol. 1995;25(6):1497-1501. CrossRef PubMed
40. Low LD, Lu L, Chan CY, et al. IL-13-driven alterations in hepatic cholesterol handling contributes to hypercholesterolemia in a rat model of minimal change disease. Clin Sci (Lond). 2020;134(2):225-237. CrossRef PubMed
41. Le Floc'h A, Allinne J, Nagashima K, et al. Dual blockade of IL-4 and IL-13 with dupilumab, an IL-4Rα antibody, is required to broadly inhibit type 2 inflammation. Allergy. 2020;75(5):1188-1204. CrossRef PubMed
42. Pelaia C, Pelaia G, Crimi C, et al. Biological therapy of severe asthma with dupilumab, a dual receptor antagonist of interleukins 4 and 13. Vaccines (Basel). 2022;10(6):974. CrossRef PubMed
43. Kariyawasam HH. Chronic rhinosinusitis with nasal polyps: mechanistic insights from targeting IL-4 and IL-13 via IL-4Rα inhibition with dupilumab. Expert Rev Clin Immunol. 2020;16(12):1115-1125. CrossRef PubMed
44. Gulleroglu K, Yazar B, Sakalli H, Ozdemir H, Baskin E. Clinical importance of mean platelet volume in children with nephrotic syndrome. Ren Fail. 2014;36(5):663-665. CrossRef PubMed

JCB
J Circ Biomark 2024; 13: 14-22
ISSN 1849-4544 | DOI: 10.33393/jcb.2024.3149
ORIGINAL RESEARCH ARTICLE

Comparative evaluation of serum and gingival crevicular fluid levels of interleukin 21 in periodontally diseased and healthy patients

Shabnam Gulfishan[1], Suhail Ahmed Syed[2], Pathakota Krishnajaneya Reddy[1], Preeti Krishnan[1], Aravinda B. Reddy[1], Ibrahim Fazal[3]

[1]Department of Periodontics, Sri Sai College of Dental Surgery, Vikarabad, Telangana - India
[2]Redesign Clinics, Banjara Hills, Hyderabad, Telangana - India
[3] Department of Periodontics and Implantology, Brny Medical Complex, Al-Rashidiyah, Al-Ahsa - Saudi Arabia

ABSTRACT

Background: Periodontitis is an inflammatory reaction to subgingival pathogenic microorganisms that causes gradual deterioration of the gingiva, periodontal ligament, and alveolar bone. Interleukin (IL)-21 is the most recently found member of type I cytokine family that is upregulated during inflammation. The current study aims to investigate the biological plausibility of IL-21 as a biomarker for chronic periodontitis.

Materials and methods: This cross-sectional clinico-biochemical investigation included 15 systemically healthy, 15 periodontally healthy, 15 chronic gingivitis, and 15 chronic periodontitis subjects aged 25 to 60 years. Following subject enrollment, gingival crevicular fluid (GCF) and blood samples were then taken from each subject. The concentration of IL-21 in all samples was determined using enzyme-linked immunosorbent assay (ELISA) kit. The data was examined using the Kruskal-Wallis test and the Spearman correlation test.

Results: Serum IL-21 levels in chronic periodontitis patients were substantially greater than in periodontally healthy individuals. GCF IL-21 levels were substantially greater in gingivitis and chronic periodontitis patients compared to periodontally healthy individuals. In terms of clinical indicators, serum IL-21 levels correlated significantly with bleeding index (BI) in the chronic periodontitis group. In chronic periodontitis group, disease severity as evaluated by probing pocket depth (PPD) and clinical attachment loss (CAL) did not correlate with serum or GCF IL-21 levels.

Conclusion: According to the current study's findings, periodontally involved patients had higher IL-21 levels than periodontally healthy patients, suggesting it can be used as biomarker. Further studies with larger sample size can shed more light on the clinical advantage of IL-21 as a possible marker for disease activity and progression.

Keywords: Blood samples, Cytokines, Gingival crevicular fluid, Interleukin 21, Periodontal diseases, Periodontitis

Introduction

Host inflammatory response is triggered by bacterial biofilm, which is one of the factors contributing to multifactorial disease known as periodontitis (1). A prolonged exposure to bacteria and endotoxins is necessary for the development of gingival inflammation and progressive dysbiotic condition eventually leading to destruction, although it only accounts for 20% of the variation in the clinical manifestation of periodontitis (2). The primary cause of the soft and hard tissue destruction linked to periodontitis is the host immune system's inflammatory response to the bacterial challenge. As a result, the inflammatory response plays a major role in determining the disease's destructive nature (3). This includes the active expression of catabolic cytokines and inflammatory mediators like interleukin (IL)-1β and IL-6 through the activation of lymphocytes, fibroblasts, monocytes/macrophages, and other cellular components. Through tissue-derived matrix metalloproteinases, these cytokines and inflammatory mediators can act alone or in combination to promote collagen degradation and alveolar bone resorption (4).

Traditional methods for diagnosing periodontal diseases include clinical and radiographic examinations. These traditional measures provide information only about the existing disease and are incapable of predicting disease progression. As a result, advances in oral and periodontal disease diagnostic research are shifting toward methods for identifying and quantifying periodontal risk using objective measures such as

Received: May 27, 2024
Accepted: August 20, 2024
Published online: September 20, 2024

Corresponding author:
Ibrahim Fazal
email: ibrahim.f.dhinda@gmail.com

biomarkers. One of these biomarkers that can be detected in several inflammatory conditions is IL-21 (5,6).

Gingival crevicular fluid (GCF) is produced by the blood vessel gingival plexus, which is located next to the epithelial lining of the dentogingival space. Several molecular components originating from the host response are carried by GCF, which is regarded as a major defense against periodontal infection. GCF-present host response mediators can help with both the status of disease activity and the identification of different periodontal diseases (7). Numerous cytokines, including IL-1, IL-6, IL-8, and IL-12, have been thoroughly examined in relation to chronic periodontitis, and research has been done on their role in the breakdown of periodontal tissues (8-11). The research of IL-21, a recently discovered cytokine, has received more attention in recent years.

IL-21, an inflammatory cytokine mostly expressed by activated T-helper (Th)1 and Th17 cells, two distinct proinflammatory lineages, is not expressed by Th2 cells in humans (12,13). It operates by binding to the type I cytokine receptor IL-21R. Because it has been linked to the pathophysiology of inflammatory breakdown in a number of systemic disorders, including rheumatoid arthritis, colitis, and inflammatory bowel disease, IL-21 has recently attracted attention (14-16). Given the critical function that IL-21 plays in inflammation (17), excessive IL-21 production amplifies local inflammation and exacerbates tissue damage and destruction (18).

The levels of IL-21 may rise as a result of periodontal diseases' propensity for chronic inflammation. Few studies have been conducted on IL-21 in patients with chronic periodontitis (14,19). However, no research has been done to compare GCF and serum IL-21 levels in healthy individuals, gingivitis patients, or periodontitis patients (19). Thus, the current study aims to measure the levels of IL-21 in the blood and GCF of patients with chronic periodontitis, compare them with those of gingivitis and healthy individuals, and assess the usefulness of this information as a diagnostic tool for periodontal disease.

Materials and methods

This cross-sectional study included 45 patients, ages 25 to 60, who were patients at Sri Sai College of Dental Surgery's Outpatient Department of Periodontics in Vikarabad, Telangana. The Institutional Ethical Committee gave its approval before the trial started. This study included three groups: Group A, or the healthy group, consisted of 15 participants who were 25-60 years old and had a systemically healthy periodontium with probing pocket depth (PPD) of less than 3 mm. Group B, which consisted of 15 individuals aged 25-60 years who were systemically healthy, had gingivitis. They exhibited clinical symptoms of inflammation and had a score of less than 2, using Modified Gingival Index (MGI). Group C, or the periodontitis group, consisted of 15 individuals, aged 25 to 60, who were in general health but had moderate to severe chronic periodontitis. At least four of their teeth had PPDs or clinical attachment loss (CAL) of at least 5 mm, bleeding when probed, and radiographic signs of bone loss. All the parameters, such as plaque index (PI), MGI, Saxton's bleeding index (BI), PPD, and CAL, were recorded in all the groups.

Inclusion criteria

Patients between the ages of 25 and 50, patients in general good health, subjects with at least 18 fully erupted teeth, subjects with bleeding during probing, PPD of at least 5 mm, and clinical attachment level of at least 6 mm were included.

Exclusion criteria

Atherosclerotic vascular disease (including peripheral artery disease, stroke, and cardiovascular diseases), immunological disorders, osteoporosis, arthritis, a history of periodontal intervention within the previous 6 months, anti-inflammatory and nonsteroidal anti-inflammatory medication use within 3 months of the periodontal assessment, and pregnancy or lactation were the exclusion criteria.

The Ethics Committee for Human Trials of Sri Sai College of Dental Surgery approved the research, which was carried out in Sri Sai College of Dental Surgery in compliance with the World Medical Association's 2008 Declaration of Helsinki (reference no: 615/SSCDS/IRB-E/2017). Each patient or their family member gave their informed consent after the periodontal exam, GCF, and blood sample removal were fully explained.

GCF and serum sample collection for IL-21

After instructing the subjects to sit comfortably upright in the dentist chair, the selected test site was air-dried and isolated with cotton rolls. To avoid contamination and obstruction of the microcapillary pipette, supragingival plaque was removed with an ultrasonic scaler while avoiding contact with the marginal gingiva.

The following day, GCF was collected using a calibrated volumetric microcapillary pipette (Sigma Aldrich Chemical Company, USA, Catalog No. p0549) with a black color code. The pipette was used to insert the tip at the entrance of the gingival crevice (unstimulated) and leave it there for 5 to 20 minutes. A 3 µL GCF standard volume was obtained. Adequate GCF was difficult to get from periodontally healthy persons (Fig. 1) and gingivitis subjects; therefore, pooled samples were collected from numerous sites to ensure that each subject received the minimal amount required (3 µL).

FIGURE 1 - Method of gingival crevicular fluid collection.

When chronic periodontitis is present, gathering GCF takes less time and is less laborious since the site with the highest PPD can provide the necessary amount. The collected samples were wrapped in aluminum foil and kept at 80°C until the assay time. Samples tainted with blood or saliva and those with air bubbles were rejected.

For serum samples, after disinfecting the skin over the antecubital fossa, a 20-gauge needle was used to venipuncture 3 mL of blood into a 5-mL syringe. A sample of collected blood was left to coagulate for approximately half an hour at room temperature (Fig. 2). After separating the serum component, the sample was centrifuged for 10 minutes at 3000 rpm. It was then moved to a polycarbonate container and kept at −80°C until the test was scheduled.

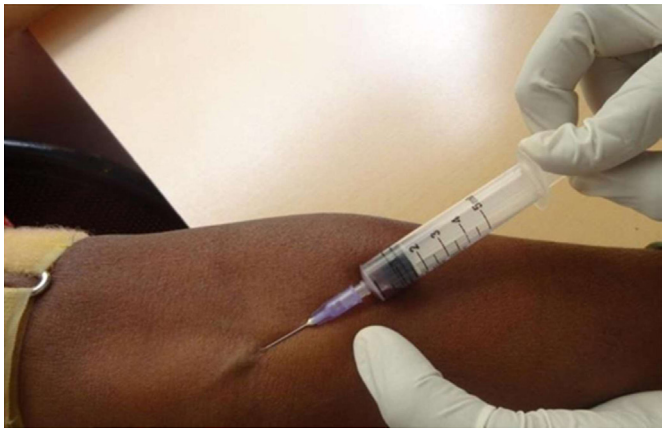

FIGURE 2 - Collection of blood samples.

Estimation of interleukin 21 levels

Using a commercially available human IL-21, or IL-21 enzyme-linked immunosorbent assay (ELISA) kit (BioAssay Technology Laboratory affiliated to Shanghai Korain Biotech Co., Ltd., Shanghai, China) (Fig. 3), the levels of GCF and serum IL-21 were determined. Phosphate-buffered saline was used to dilute GCF samples to a level of 100 µL.

Assay principle

An ELISA kit is intended to detect various biomarkers in bodily fluid samples. Human IL-21 antibody was precoated onto the plate. The sample's IL-21 was introduced, and it binds to the antibodies coated on the wells. After that, biotinylated human IL-21 antibody was added, and it binds to the sample's IL-21.

Next, streptavidin-horseradish peroxidase (HRP), which binds to the IL-21 antibody that has been biotinylated, was added. During a washing phase, unbound streptavidin-HRP is removed following incubation. After that, the substrate solution was added, and color changed proportionately to the concentration of human IL-21. The addition of an acidic stop solution ends the process, and the absorbance is measured at 450 nm.

Sensitivity

The sensitivity or minimum detectable dose of human IL-21 is reported to be 2.46 ng/L.

Assay procedure

1. Every reagent, standard solution, and sample was made in accordance with the directions. Prior to use, all reagents were brought to room temperature, and the experiment was conducted.

FIGURE 3 - Enzyme-linked immunosorbent assay kit.

2. After figuring out how many strips were needed for the assay, the strips were put into the frames and used. The leftover strips were kept between 2 and 8°C.
3. The standard well was later filled with 50 µL of standard solution.
4. In addition, 40 µL of the sample and 10 µL of the anti-IL-21 antibody were added to the sample wells. Following a thorough mixing of 50 µL streptavidin-HRP into both the standard and sample wells, the plate was sealed with a sealer and allowed to sit at 37°C for 60 minutes (Fig. 4).

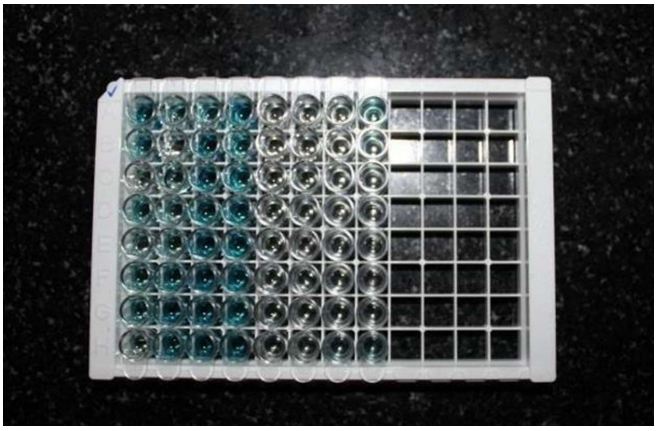

FIGURE 4 - After addition of samples in enzyme-linked immunosorbent assay plates.

5. All of the wells were aspirated, filled to the brim with wash buffer, and automatically cleaned five times. The plate was blotted onto paper towels or other absorbent material.
6. Subsequently, 50 µL of substrate solution A and 50 µL of substrate solution B were applied to each well. The plate was sealed with a fresh sealer and left in the dark at 37°C for 10 minutes.
7. The last step involved adding 50 µL of Stop Solution to each well, which instantly caused the color to shift to yellow (Fig. 5).

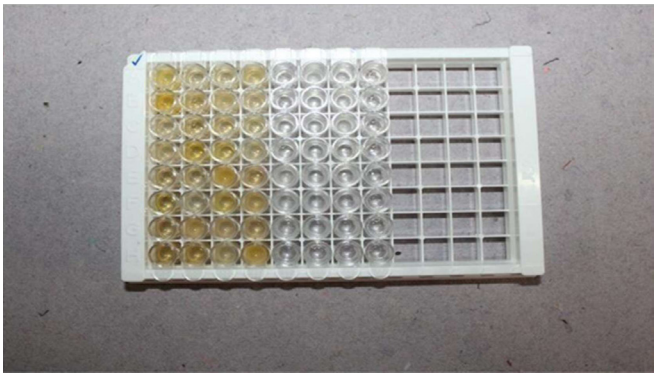

FIGURE 5 - Enzyme-linked immunosorbent assay microplates after addition of stop solution.

8. Within 10 minutes of administering the stop solution, each well's optical density (OD value) was ascertained using a microplate reader set to 450 nm (Tab. 1).

TABLE 1 - Reagents required

Components	Quantity
Standard solution (1600 ng/L)	0.5 mL ×1
Precoated ELISA plate	12 × 8 well strips ×1
Standard diluent	3 mL ×1
Streptavidin-HRP	6 mL ×1
Stop solution	6 mL ×1
Substrate solution A	6 mL ×1
Substrate solution B	6 mL ×1
Wash buffer concentrate (30×)	20 mL ×1
Biotinylated human IL-21 antibody	1 mL ×1
User instruction	1
Plate sealer	2
Zipper bag	1

ELISA = enzyme-linked immunosorbent assay; HRP = horseradish peroxidase; IL = interleukin; NS = no statistical significance; S = statistical significance (p≤0.05).

Statistical analysis

Statistical Package for the Social Sciences (SPSS) for Windows (Version 22.0, Released 2013; Armonk, NY: IBM Corp.) was used for providing statistical analysis.

The data was presented as mean ± standard deviation (SD). Using SPSS version 20.0 software, the following statistical tests were used to analyze the parameters.

1. The Kruskal-Wallis test was used to do intergroup analysis for the following variables: serum, GCF IL-21, MGI, PI, PPD, CAL, age, and gender.
2. In group A, the relationship between age and gender and serum and GCF IL-21 levels was assessed. In group B, there was a correlation between the levels of serum and GCF IL-21 and the clinical indices MGI, PI, and BI, as well as age and gender. In group C, the levels of serum and GCF IL-21 were correlated with age, gender, and clinical indices and parameters, such as MGI, PI, BI, PPD, and CAL. The Spearman correlation coefficient test was used to perform all of these group-specific correlations.

Results

Of the 15 individuals in group A, 9 (60%) were male and 6 (40%) were female; of the 15 patients in group B, 8 (55%) were male and 7 (45%) were female; of the 15 patients in group C, 7 (45%) were male and 8 (55%) were female (Tab. 2). According to Table 2, the participants in groups A, B, and C had mean ages of 34.07 ± 2.99, 33.93 ± 2.79, and 34.67 ± 2.35, respectively.

Plaque index

Groups A, B, and C had mean PI scores of 0.73 ± 0.353, 1.09 ± 0.171, and 1.97 ± 0.395, respectively. Group C had the highest mean PI score, followed by group B, and group A had the lowest value, according to the intergroup comparison of mean PI scores. The results showed that there was no statistically significant difference between groups A and B, but

there was between groups B and C and between groups A and C (Tab. 2).

Modified gingival index

MGI was used to determine the gingival status, and the mean values for groups A, B, and C were 0.39 ±0.195, 1.08 ± 0.258, and 1.76 ± 0.509 (Fig. 6). The mean gingival index intergroup comparison showed that group C had high values, whereas group B had moderate values that were greater than those of group A. There is statistical significance in the outcomes for each of the three groups (Tab. 2).

Bleeding index

Saxton's BI was used to measure bleeding, and the mean values for groups A, B, and C were 0.32 ± 0.315, 0.77 ± 0.277, and 1.33 ± 0.132, respectively. According to the intergroup comparison of mean BI values, group C had the highest bleeding scores, group B had moderate scores, and group A had the lowest or minimum value when compared to the other groups (Fig. 6). The findings between groups A and C, as well as between groups B and C, are statistically significant; however, the results between groups A and B are not (Tab. 2).

TABLE 2 - Intergroup comparison of demographic data and clinical parameters using Kruskal-Wallis test and post hoc analysis

	Group			p-Value
	A	B	C	
	Mean ± SD	Mean ± SD	Mean ± SD	
Age (years)	34.07±2.99	33.93±2.79	34.67±2.35	0.736 (NS)
Sex – Male	60.0%	55.0%	45.0%	
Female	40.0%	45.0%	55.0%	
PI	0.73 ± 0.353	1.09 ± 0.171	1.97 ± 0.395	0.000
				A vs. B (NS)
				B vs. C (S)
				A vs. C (S)
MGI	0.39 ± 0.195	1.08 ± 0.258	1.76 ± 0.509	0.000
				A vs. B (S)
				B vs. C (S)
				A vs. C (S)
BI	0.32 ± 0.315	0.77 ± 0.277	1.33 ± 0.132	0.000
				A vs. B (NS)
				B vs. C (S)
				A vs. C (S)
Mean (mm) PPD	1.27 ± 0.346	1.82 ± 0.568	4.22 ± 0.538	0.000
				A vs. B (NS)
				B vs. C (S)
				A vs. C (S)
Mean (mm) CAL	0	0	4.55 ± 0.864	0.000
				A vs. B (NS)
				B vs. C (S)
				A vs. C (S)

BI = bleeding index; CAL = clinical attachment loss; MGI = Modified Gingival Index; NS = no statistical significance; PI = plaque index; PPD = probing pocket depth; S = statistical significance (p≤0.05); SD = standard deviation.

Probing pocket depth

The mean PPD was 1.27 ± 0.346 mm in group A, 1.82 ± 0.568 mm in group B, and 4.22 ± 0.538 (Fig. 6) in group C; the intergroup comparison of mean PPD scores of groups A and B revealed statistically significant high score for group C (Tab. 2)

Clinical attachment loss

Mean CAL was 0.00 mm in groups A and B and 4.55 ± 0.864 mm (Fig. 6) in group C. There was a statistically significant difference of CAL values in group C vs. other groups (Tab. 2).

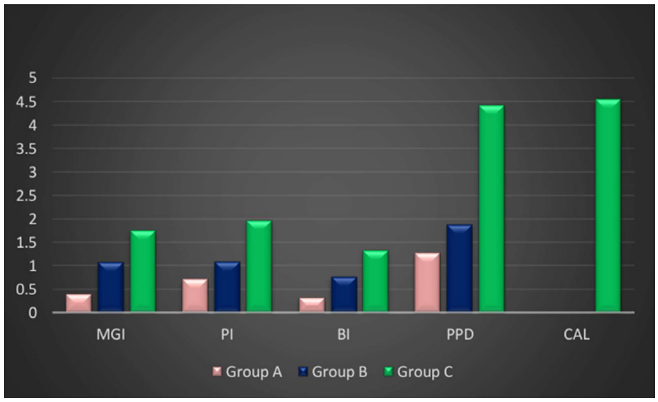

FIGURE 6 - Intergroup comparison of clinical parameters. BI = bleeding index; CAL = clinical attachment loss; MGI = Modified Gingival Index; PI = plaque index; PPD = probing pocket depth.

Concentration of IL-21 in serum

The amount of IL-21 in the serum was reported in nanograms per milliliter. All of the participants in groups A, B, and C had measurable amounts of IL-21 in their serum. Group A patients had the highest observed level of IL-21 in their serum at 57 ng/mL, whereas group B had 100 ng/mL and group C 545 ng/mL. Group A subjects' serum had a minimum IL-21 level of 30 ng/mL, group B's was 66 ng/mL, and group C's was 83 ng/mL. The mean serum concentrations in groups A, B, and C were 44.866 ± 8.9, 87.33 ± 10.14, and 139.3 ± 113.5 ng/mL, in that order. Group C had greater values than group A in this statistically significant comparison of serum IL-21 levels. Between groups A and B and between groups B and C, however, there was no discernible change (Tabs. 3 and 4).

TABLE 3 - Mean IL-21 concentrations in serum and GCF in groups A, B, and C

Group	IL-21 levels	Mean ± SD	Minimum (ng/mL)	Maximum (ng/mL)
A	Serum	44.866 ± 8.9	30	57
	GCF	21.933 ± 9.1	10	40
B	Serum	87.33 ± 10.14	66	100
	GCF	66.400 ± 9.47	55	80
C	Serum	139.3 ± 113.5	83	545
	GCF	66.400 ± 7.28	59	82

GCF = gingival crevicular fluid; IL = interleukin; NS = no statistical significance; S = statistical significance (p≤0.05); SD = standard deviation.

TABLE 4 - Intergroup comparison of IL-21 levels in serum and GCF

	Group			p-Value
	A	B	C	
	Mean ± SD	Mean ± SD	Mean ± SD	
Serum IL-21 concentration (ng/mL)	44.866 ± 8.9	87.33 ± 10.1	139.3 ± 11.3	≤0.001 A vs. B = (NS) A vs. C = (S) B vs. C = (NS)
GCF IL-21 concentration (ng/mL)	21.933 ± 9.1	66.400 ± 9.47	66.400 ± 7.82	≤0.001 A vs. B = (S) A vs. C = (S) B vs. C = (NS)

GCF = gingival crevicular fluid; IL = interleukin; NS = no statistical significance; S = statistical significance (p≤0.05); SD = standard deviation.

In GCF, the highest levels of IL-21 were 40 ng/mL in the GCF of patients in group A, 80 ng/mL in group B, and 82 ng/mL in group C. In group A, the minimum IL-21 levels were 10 ng/mL; in groups B and C, the levels were 55 and 59 ng/ml, respectively, in the GCF. In groups A, B, and C, the corresponding mean GCF concentrations were 21.933 ± 9.1, 66.400 ± 9.47, and 66.400 ± 7.28 ng/mL. Compared to group A, groups B and C had statistically significant higher IL-21 levels (Tabs. 2 and 4).

Regarding the correlation between IL-21 and demographics, there was statistically significant correlation between age for each of the three groups and serum IL-21 levels and GCF. In other groups, there was no statistically significant relationship between age and serum and GCF IL-21 levels (Tab. 5).

When the correlation between IL-21 and clinical parameters was estimated, no statistically significant association was seen in group B between serum IL-21 levels and GCF with clinical indicators, such as PI, MGI, and BI (Tab. 6). With the exception of BI, which is substantially correlated with serum IL-21 levels, group C's GCF and serum IL-21 concentration did not significantly correlate with any of the clinical indicators examined. There were no discernible relationships found between the levels of PPD, CAL, and IL-21 (Tab. 7).

TABLE 5 - Correlations between serum and GCF IL-21 concentration with age in the groups A, B, and C using Spearman correlation coefficient

			Serum IL-21	GCF IL-21
Group A	Age	Spearman correlation coefficient	−0.287	−0.058
		p-value	0.2990	0.837
Group B	Age	Spearman correlation coefficient	−0.151	−0.333
		p-value	0.590	−0.226
Group C	Age	Spearman correlation coefficient	−0.391	−0.292
		p-value	0.149	0.290

GCF = gingival crevicular fluid; IL = interleukin; NS = no statistical significance; S = statistical significance (p≤0.05).

TABLE 6 - Correlation between serum and GCF IL-21 concentration with clinical indices of group B using Spearman correlation coefficient

		PI	MGI	BI
Serum IL-21	Spearman correlation coefficient	−0.259	−0.298	0.095
	p-value	0.35	0.28	0.73
GCF IL-21	Spearman correlation coefficient	0.10	0.25	−0.291
	p-value	0.97	0.36	0.29

BI = bleeding index; GCF = gingival crevicular fluid; IL = interleukin; MGI = Modified Gingival Index; NS = no statistical significance; PI = plaque index; S = statistical significance (p≤0.05).

Discussion

Periodontitis is the sixth most common disease in humans, affecting 740 million people worldwide. Periodontitis is a bacterially induced chronic tissue destructive inflammation of the teeth. This periodontal microbiota causes the release of proinflammatory mediators both locally and systemically. As the paradigm of chronic infection in dental pathology, periodontal disease shares several pathogenic pathways with cardiovascular diseases as a result of the low-grade state of systemic inflammation posed by periodontitis (20).

Early diagnosis is essential since disease progression is unpredictable and irreversible. The diagnostic and prognostic efficacy of traditional clinical diagnostic parameters, such as bleeding on probing, PPD, and CAL, is limited (21). Therefore, developments in the diagnosis of periodontal disease are moving in the direction of techniques that allow periodontal risk to be recognized and measured using objective metrics like biomarkers. Diagnostic evidence of the infection/host immune response axis can be obtained through site-specific examination of GCF and subject-based data based on serum assays (6).

TABLE 7 - Correlation between serum and GCF IL-21 concentration with clinical parameters of group C using Spearman correlation coefficient

		Mean PPD	Mean CAL	MGI	PI	BI
Serum IL-21	Spearman correlation coefficient	0.246	0.136	0.199	−0.169	−0.621
	p-value	0.378	0.629	0.478	0.546	0.013
GCF IL-21	Spearman correlation coefficient	0.473	0.361	−0.474	−0.189	0.097
	p-value	0.075	0.186	0.074	0.500	0.730

BI = bleeding index; CAL = clinical attachment loss; GCF = gingival crevicular fluid; IL = interleukin; MGI = Modified Gingival Index; NS = no Statistical significance; PI = plaque index; PPD = probing pocket depth; S = statistical significance (p≤0.05).

Although there is an array of evidence and research about biomarkers for periodontal disease in the literature, appropriate molecular indicators of destruction of both soft and hard tissues that can take the place of clinical gold standards are still missing. However, scientists have been aggressively looking for clear indicators of periodontitis (22).

IL-21 is a pleiotropic cytokine that influences immunological responses. IL-21 promotes the growth of Th17 cells, which contribute significantly to periodontitis. In addition to periodontitis, it has been linked to inflammatory disorders such as rheumatoid arthritis and systemic lupus erythematosus (23). The available information on the connection of IL-21 with chronic periodontitis is limited. This study aims to assess IL-21 levels in serum and GCF of chronic periodontitis patients, correlate them with clinical indicators, and compare them to levels in gingivitis patients and healthy people. IL-21 increases the host's immunological response and local inflammation. This study suggests that IL-21 plays a significant role in the etiology of periodontal disease (24).

In this investigation, group C had significantly higher mean serum IL-21 concentrations (139.3 ± 113.5 ng/mL) than group A (44.866 ± 8.9 ng/mL), but not group B (87.33 ± 10.1 ng/mL). Lokhande et al (25) found that the periodontitis group had considerably higher serum levels of IL-21 (497.78 ± 297.06) compared to the healthy group (65.34 ± 42.66), which is in accordance with current investigation, where serum levels showed no statistically significant difference between groups B and C.

The current study is the first of its type to measure GCF levels of IL-21 in distinct degrees of periodontal inflammation, including gingivitis and periodontitis, when compared to a healthy cohort. In this investigation, groups C and B had considerably higher mean GCF concentrations of IL-21 (66.400 ± 7.82 and 66.400 ± 9.47 ng/mL, respectively) compared to group A (21.933±9.1 ng/mL). There was no significant difference between groups B and C, demonstrating that IL-21 is a generic inflammatory marker.

The current study suggests that IL-21 may play a role in periodontitis by causing inflammation and tissue damage. The current investigation found no significant correlation between illness severity (defined by PPD and CAL) and IL-21 levels in GCF or serum in group C. Dutzan et al (23) found a substantial positive association between GCF levels of IL-21 and PPD and CAL, which contradicts our findings. Lokhande et al (25) found a strong association between PPD and serum IL-21 levels, but no correlation between IL-21 levels in saliva or serum with CAL.

Zhao et al (26) found that nonsurgical periodontal therapy decreased Th17-related cytokines (IL-17, IL-21) in GCF of chronic periodontitis patients. Reduced IL-21 levels suggest a link between periodontal inflammation and disease activity.

Napimoga et al (27) conducted a study on the local levels of IL-21 and IL-21 receptor in gingival tissues of chronic periodontitis and periodontally healthy subjects, as well as their relationship with salivary immunoglobulin A (IgA) levels. The study found that chronic periodontitis patients had considerably greater mean IgA levels and messenger ribonucleic acid (mRNA) levels for IL-21 compared to those who were periodontally healthy, which has consistent results with our study. Elevated IgA levels in the study suggest that IL-21 plays a considerable role in periodontal damage, sometimes even more than periodontal bacteria themselves.

Vahabi et al (28) conducted a study that compared salivary concentrations of IL-17 and IL-18 in patients with chronic periodontitis and healthy individuals. They concluded that an elevated salivary IL-18 level in chronic periodontitis patients has the potential to be a biomarker for periodontal tissue destruction, which was in accordance with our study where we concluded that elevated levels of IL-21 were found in chronic periodontitis individuals.

The current study's lack of association could be attributed to the small sample size, disease progression, and site specificity. Although clinical parameters indicate cumulative damage, it is impossible to assess the current state of disease activity within tissues. It has been proposed that disease activity is not continuous, but rather consists of active and remission states. If a sample is collected from a remission site that was previously active, the levels may not correlate with clinical criteria. More research is needed with bigger patient samples with different levels of active and inactive areas.

GCF collection in periodontitis locations may not produce comparable amounts due to variations in production and flow rates based on the periodontium's inflammatory condition. Our study found a strong positive connection between serum levels of IL-21 and BI in group C. Gingival bleeding is an early and clear indicator of gingival irritation. Since IL-21 is an inflammatory biomarker, there may be a positive link between these two traits.

The study found no significant association between age and GCF or serum IL-21 levels across three groups. Age is a

variable that requires a bigger sample size for evaluation, and no attributes can be made at this time. Chronic periodontitis is a polymicrobial disease with multiple causes. The host's susceptibility is determined by interactions between bacteria, the immune system, and the environment, with the host factor playing a significant influence. Estimating host response indicators may aid in monitoring disease progression in advanced gingivitis or early periodontitis patients, as early tissue damage can be challenging to diagnose (29). Estimating host response indicators may aid in assessing disease progression. More cross-sectional and interventional studies with higher sample sizes are needed to determine the efficacy of IL-21 as a biomarker in diagnosis and treatment.

Conclusion

To the best of our knowledge, the current study is the first of its kind to quantify GCF and serum levels of IL-21 in various stages of periodontal inflammation, including gingivitis and periodontitis, when compared to a healthy cohort. Despite the limitations of this study, IL-21 could be a viable biomarker for detecting periodontitis. Further cross-sectional and interventional research with bigger sample sizes are needed to compare the association of IL-21 levels in various types of periodontal disease and consider it as a potential diagnostic biomarker.

DISCLOSURES

Conflict of interest: The authors declare no conflict of interest.

Financial support: This research received no specific grant from any funding agency in the public, commercial, or not-for-profit sectors.

Authors contribution: All authors contributed equally to this manuscript.

Compliance with ethics guidelines: The study protocol is approved by the University Ethics Committee for Human Trials of Sri Sai College of Dental Surgery, Vikarabad, Telangana (Ref no. 615/SSCDS/IRB-E/2017). Written informed consent has been obtained from the participants.

Availability of data and materials: All data generated or analyzed during this study are included in this published article (and its supplementary information files).

References

1. Salvi GE, Lang NP. Host response modulation in the management of periodontal diseases. J Clin Periodontol. 2005;32(s6) (suppl 6):108-129. CrossRef PubMed
2. Grossi SG, Zambon JJ, Ho AW, et al. Assessment of risk for periodontal disease. I. Risk indicators for attachment loss. J Periodontol. 1994;65(3):260-267. CrossRef PubMed
3. Gemmell E, Yamazaki K, Seymour GJ. Destructive periodontitis lesions are determined by the nature of the lymphocytic response. Crit Rev Oral Biol Med. 2002;13(1):17-34. CrossRef PubMed
4. Offenbacher S. Periodontal diseases: pathogenesis. Ann Periodontol. 1996;1(1):821-878. CrossRef PubMed
5. Taba M Jr, Kinney J, Kim AS, Giannobile WV. Diagnostic biomarkers for oral and periodontal diseases. Dent Clin North Am. 2005;49(3):551-571, vi. CrossRef PubMed
6. Fazal I, Shetty B, Yadalam U, Khan SF, Nambiar M. Effectiveness of periodontal intervention on the levels of N-terminal pro-brain natriuretic peptide in chronic periodontitis patients. J Circ Biomark. 2022;11:48-56. CrossRef PubMed
7. AlRowis R, AlMoharib HS, AlMubarak A, Bhaskardoss J, Preethanath RS, Anil S. Oral fluid-based biomarkers in periodontal disease – part 2. Gingival crevicular fluid. J Int Oral Health. 2014;6(5):126-135. PubMed
8. Engebretson SP, Grbic JT, Singer R, Lamster IB. GCF IL-1beta profiles in periodontal disease. J Clin Periodontol. 2002;29(1):48-53. CrossRef PubMed
9. Irwin CR, Myrillas TT. The role of IL-6 in the pathogenesis of periodontal disease. Oral Dis. 1998;4(1):43-47. CrossRef PubMed
10. Harada A, Sekido N, Akahoshi T, Wada T, Mukaida N, Matsushima K. Essential involvement of interleukin-8 (IL-8) in acute inflammation. J Leukoc Biol. 1994;56(5):559-564. CrossRef PubMed
11. Tsai IS, Tsai CC, Ho YP, Ho KY, Wu Y-M, Hung CC. Interleukin-12 and interleukin-16 in periodontal disease. Cytokine. 2005; 31(1):34-40. CrossRef PubMed
12. de Rham C, Ferrari-Lacraz S, Jendly S, Schneiter G, Dayer JM, Villard J. The proinflammatory cytokines IL-2, IL-15 and IL-21 modulate the repertoire of mature human natural killer cell receptors. Arthritis Res Ther. 2007;9(6):R125. CrossRef. PubMed
13. Sarra M, Pallone F, Monteleone G. Interleukin-21 in chronic inflammatory diseases. Biofactors. 2013;39(4):368-373. CrossRef PubMed
14. Rasmussen TK, Andersen T, Hvid M, et al. Increased interleukin 21 (IL-21) and IL-23 are associated with increased disease activity and with radiographic status in patients with early rheumatoid arthritis. J Rheumatol. 2010;37(10):2014-2020. CrossRef PubMed
15. Gerlach K, Daniel C, Lehr HA, et al. Transcription factor NFATc2 controls the emergence of colon cancer associated with IL-6-dependent colitis. Cancer Res. 2012;72(17):4340-4350. CrossRef PubMed
16. Abraham C, Cho J. Interleukin-23/Th17 pathways and inflammatory bowel disease. Inflamm Bowel Dis. 2009;15(7):1090-1100. CrossRef PubMed
17. Nurieva R, Yang XO, Martinez G, et al. Essential autocrine regulation by IL-21 in the generation of inflammatory T cells. Nature. 2007;448(7152):480-483. CrossRef PubMed
18. Onoda T, Rahman M, Nara H, et al. Human CD4+ central and effector memory T cells produce IL-21: effect on cytokine-driven proliferation of CD4+ T cell subsets. Int Immunol. 2007; 19(10):1191-1199. CrossRef PubMed
19. Pelletier M, Girard D. Biological functions of interleukin-21 and its role in inflammation. ScientificWorldJournal. 2007;7:1715-1735. CrossRef PubMed
20. Shetty B, Fazal I, Khan SF, et al. Association between cardiovascular diseases and periodontal disease: more than what meets the eye. Drug Target Insights. 2023;17:31-38. CrossRef PubMed
21. Persson GR. Site-based versus subject-based periodontal diagnosis. Periodontol 2000. 2005;39(1):145-163. CrossRef PubMed
22. Loos BG, Tjoa S. Host-derived diagnostic markers for periodontitis: do they exist in gingival crevice fluid? Periodontol 2000. 2005;39(1):53-72. CrossRef PubMed
23. Dutzan N, Rivas C, García-Sesnich J, et al. Levels of interleukin-21 in patients with untreated chronic periodontitis. J Periodontol. 2011 Oct;82(10):1483-1489. CrossRef. PubMed.
24. Dutzan N, Vernal R, Vaque JP, et al. Interleukin-21 expression and its association with proinflammatory cytokines in untreated chronic periodontitis patients. J Periodontol. 2012; 83(7):948-954. CrossRef PubMed

25. Lokhande RV, Ambekar JG, Bhat KG, Dongre NN. Interleukin-21 and its association with chronic periodontitis. J Indian Soc Periodontol. 2019;23(1):21-24. CrossRef PubMed
26. Zhao L, Zhou Y, Xu Y, Sun Y, Li L, Chen W. Effect of non-surgical periodontal therapy on the levels of Th17/Th1/Th2 cytokines and their transcription factors in Chinese chronic periodontitis patients. J Clin Periodontol. 2011;38(6):509-516. CrossRef PubMed
27. Napimoga MH, Nunes LH, Maciel AA, et al. Possible involvement of IL-21 and IL-10 on salivary IgA levels in chronic periodontitis subjects. Scand J Immunol. 2011;74(6):596-602. CrossRef PubMed
28. Vahabi S, Yadegari Z, Pournaghi S. The comparison of the salivary concentration of interleukin-17 and interleukin-18 in patients with chronic periodontitis and healthy individuals. Dent Res J (Isfahan). 2020;17(4):280-286. CrossRef PubMed
29. Khiste SV, Ranganath V, Nichani AS, Rajani V. Critical analysis of biomarkers in the current periodontal practice. J Indian Soc Periodontol. 2011;15(2):104-110. CrossRef PubMed

JCB
J Circ Biomark 2024; 13: 23-24
ISSN 1849-4544 | DOI: 10.33393/jcb.2024.3197
CORRESPONDENCE

Comments to: Relation between interleukin-13 and annexin-V levels and carotid intima-media thickness in nephrotic syndrome

Christian Saleh, M.D.

Basel - Switzerland

Elsehmawy et al. wrote, "in children with idiopathic nephrotic syndrome (INS), atherosclerotic changes may accelerate progression to chronic kidney disease and are mainly related to dyslipidemia" (1). The authors aimed with their study to "assess the relation between carotid intima-media thickness (CIMT) measurements, renal Doppler resistive index (RI) and serum levels of interleukin-13 (IL-13) and annexin-V (An-V) in children with INS…" (1). As surrogate marker for preclinical atherosclerosis the authors used the carotid intima-media thickness (CIMT), measured by ultrasonography (1). The study was based on 60 children with INS and 60 healthy controls matched for age and gender (1). The patients had significantly higher CIMT as compared to controls (0.49 ± 0.06 vs. 0.35 ± 0.03, p<0.001) (1). The authors concluded that "the present study suggests an association between early atherosclerosis expressed as elevated CIMT measurements in children with INS and elevated serum levels of An-V and IL-13… In children with INS, atherosclerotic changes may accelerate progression to chronic kidney disease and are mainly related to dyslipidemia" (1). Some comments to the CIMT findings/conclusions of this study are needed. Elsehmawy et al. wrote, "Measurement of CIMT was done using the ultrasound machine …with high-frequency linear probe (7.5 MHz) …The arterial wall of the common carotid artery was assessed bilaterally in a longitudinal view…. Measurements were taken from the far wall of each common carotid artery 1 cm proximal to bifurcation. The measurements were made three times on each side and the average of the measurements was taken. The mean of measurements of the left and right common carotid arteries was calculated" (1). The authors (1) measured CIMT only at one predetermined carotid artery (CA) segment, the far wall of the common carotid artery (CCA) for higher spatial resolution (2). The major disadvantage of a one-site CIMT measurement method is to miss potential atherosclerotic altered vessel segments, given that atherosclerosis is a systemic disease yet, importantly, presents asymmetrically (3). A composite CIMT measure including all CA sections, e.g. both walls (far/near) of the CCA, bifurcation and internal CA, provides a more precise estimate of the CIMT (4); the authors (1) missed to mention and to discuss in the analysis of their results this important methodological aspect and limitation in their CIMT evaluation. Furthermore, Elsehmawy et al. (1) did not specify if the CIMT measurement was synchronized with the cardiac cycle and made, as recommended, at the end-diastole (2). CIMT values are subject to obvious vessel diameter changes that occur during the cardiac phases, with thinner values in systole (lumen expansion) and greater values in diastole (lumen reduction) (5). The differences between the patients and controls can be due to measurements that occurred during different cardiac phases and therefore cannot be compared. Sub-millimetric differences in CIMT values will classify subjects into normal or abnormal CIMT groups (2). A meticulous and detailed CIMT measurement protocol is fundamental when CIMT is used as surrogate marker (2,4). In conclusion, CIMT values less than 0.6 mm are considered as normal (2). The mean CIMT of the group of patients (0.49 ± 0.06 mm) (1) falls within the normal CIMT range and is void of diagnostic and prognostic value. The CIMT values of this study (1), given the methodological flaws, should be considered with caution.

Disclosures

Conflict of interest: The authors declare no conflict of interest.

Financial support: This research received no specific grant from any funding agency in the public, commercial, or not-for-profit sectors.

Author contribution: CS wrote and revised the manuscript.

References

1. Elsehmawy AA, Gouda RM, Diab FEAE, et al. Relation between interleukin-13 and annexin-V levels and carotid intima-media thickness in nephrotic syndrome. J Circ Biomark. 2024;13(1):7-13. CrossRef PubMed
2. Touboul PJ, Hennerici MG, Meairs S, et al. Mannheim carotid intima-media thickness and plaque consensus (2004-2006-2011). An update on behalf of the advisory board of the 3rd, 4th and 5th watching the risk symposia, at the 13th, 15th and 20th European Stroke Conferences, Mannheim,

Received: July 8, 2024
Accepted: August 26, 2024
Published online: September 25, 2024

Corresponding author:
Christian Saleh, M.D.
email: chs12us75010@yahoo.com

Germany, 2004, Brussels, Belgium, 2006, and Hamburg, Germany, 2011. Cerebrovasc Dis. 2012;34(4):290-296. CrossRef PubMed

3. Nixdorff U. [Intima-media thickness is a suitable surrogate marker for systemic atherosclerosis – contra]. Dtsch Med Wochenschr. 2009;134(40):2007. CrossRef PubMed
4. Bots ML, Evans GW, Riley WA, Grobbee DE. Carotid intima-media thickness measurements in intervention studies: design options, progression rates, and sample size considerations: a point of view. Stroke. 2003;34(12):2985-2994. CrossRef PubMed
5. Polak JF, Johnson C, Harrington A, et al. Changes in carotid intima-media thickness during the cardiac cycle: the multi-ethnic study of atherosclerosis. J Am Heart Assoc. 2012;1(4):e001420. CrossRef PubMed

JCB
J Circ Biomark 2024; 13: 25-26
ISSN 1849-4544 | DOI: 10.33393/jcb.2024.3284
CORRESPONDENCE

Author's reply to: Comments to: Relation between interleukin-13 and annexin-V levels and carotid intima-media thickness in nephrotic syndrome

Asmaa A. Elsehmawy

Pediatric Department, Al-Azhar University, Cairo - Egypt

- **Use of multiple measurement sites:** The use of a single site for carotid intima-media thickness (CIMT) measurement at the far wall of the common carotid artery (CCA) was a methodological decision aimed at maintaining consistency. Several studies have shown that the CIMT values measured at different segments (CCA, carotid bifurcation, and internal carotid artery) predict future cardiovascular events to nearly the same extent (1), so we have chosen the common site of measurements in all studies. CIMT should measure at least 5 mm below the end of CCA and in the far wall to eliminate interindividual variability induced by physiological remodeling and to reduce the dependence on instrument gain (2). However, we agree that a composite measure including multiple sites would provide a more comprehensive assessment.
- **Measurement of CIMT with cardiac cycle synchronization**: While it is acknowledged that synchronizing CIMT measurements with the cardiac cycle enhances precision, it is important to consider the specific context of pediatric patients. Children generally have higher heart rates and more variable cardiac cycles compared to adults, which can pose additional challenges in achieving precise synchronization. Therefore, several studies on children measured CIMT and did not mention synchronization with the cardiac cycle (3-5); however, we were careful with all cases and control to start measurements after 10 minutes of rest, repeating measurements three times on each side and the average of the measurements was taken. Despite these challenges, future research should aim to incorporate cardiac cycle synchronization to improve the accuracy of CIMT measurements in pediatric populations.
- **Variability in cardiac phases:** The differences observed in CIMT measurements during different phases of the cardiac cycle (systole and diastole) are particularly relevant in children due to their higher heart rates and rapid changes in vascular dynamics. The thinner walls during systole and thicker walls during diastole can lead to significant measurement variability. Addressing this variability requires advanced imaging techniques and equipment capable of real-time cardiac cycle synchronization as semiautomated edge detection software and CIMT should be measured at the same point on the echocardiogram to overcome this variation (6), which may not always be available in all clinical settings.
- **Diagnostic and prognostic value**: We appreciate the critique regarding the diagnostic and prognostic value of CIMT measurements. The CIMT values in our patient group (0.49 ± 0.06 mm) align with normal ranges, suggesting limited prognostic utility in this context. The study's aim was primarily to explore associations rather than definitive prognostic predictions.

In conclusion, while our study has methodological limitations, it highlights important associations between CIMT and nephrotic syndrome in children. We recognize the need for advanced techniques to mitigate the impact of cardiac cycle variability and enhance the precision of CIMT measurements. We recommend that future research focus on these methodological improvements to provide more accurate assessments of cardiovascular risk in pediatric populations.

Disclosures

Conflict of interest: The authors have no conflicts of interest in this work.

Financial support: This research received no external funding.

References

1. Nezu T, Hosomi N, Aoki S, Matsumoto M. Carotid intima-media thickness for atherosclerosis. J Atheroscler Thromb. 2016;23(1):18-31. CrossRef PubMed
2. Touboul PJ, Hennerici MG, Meairs S, et al. Mannheim carotid intima-media thickness and plaque consensus (2004-2006-2011). An update on behalf of the advisory board of the 3rd, 4th and 5th watching the risk symposia, at the 13th, 15th and 20th European Stroke Conferences, Mannheim, Germany, 2004, Brussels, Belgium, 2006, and Hamburg, Germany, 2011. Cerebrovasc Dis. 2012;34(4):290-296. CrossRef. Epub 2012 Nov 1. PubMed

Received: August 27, 2024
Accepted: August 27, 2024
Published online: September 25, 2024

Corresponding author:
Asmaa A. Elsehmawy
email: asmaawakeel@yahoo.com

3. Mehta A, Mishra S, Ahmad K, Tiwari HC, Singh V, Singh A. Carotid intima media thickness in children with nephrotic syndrome: an observational case control study. Sudan J Paediatr. 2019;19(2):110-116. CrossRef PubMed
4. Paripović A, Stajić N, Putnik J, Gazikalović A, Bogdanović R, Vladislav V. Evaluation of carotid intima media thickness in children with idiopathic nephrotic syndrome. Nephrol Ther. 2020;16(7):420-423. CrossRef PubMed
5. El-Bana SM, Sharawe MA, Mahmoud AH. Carotid intimal medial thickness in children and young adolescents with nephrotic syndrome. Alex J Pediatrics. 2005;19(2):437-441. Online
6. Menees S, Zhang D, Le J, Chen J, Raghuveer G. Variations in carotid artery intima-media thickness during the cardiac cycle in children. J Am Soc Echocardiogr. 2010;23(1):58-63. CrossRef PubMed

JCB
J Circ Biomark 2024; 13: 27-35
ISSN 1849-4544 | DOI: 10.33393/jcb.2024.3046
ORIGINAL RESEARCH ARTICLE

A novel liquid biopsy assay for detection of *ERBB2* (HER2) amplification in circulating tumor cells (CTCs)

Giuseppe Di Caro[1], Ernest T. Lam[1], David Bourdon[1], Martin Blankfard[1], Nilesh Dharajiya[1], Megan Slade[1], Emily Williams[1], Dong Zhang[1], Rick Wenstrup[1], Lee Schwartzberg[2]

[1]Epic Sciences, San Diego, California - USA
[2]Renown Health-Pennington Cancer Institute, Reno, Nevada - USA

ABSTRACT

Purpose: Circulating tumor cell (CTC)-based *ERBB2* (HER2) assay is a laboratory test developed by Epic Sciences using single-cell genomics to detect *ERBB2* (HER2) amplification in CTCs found in the peripheral blood of metastatic breast cancer (MBC) patients.

Patients and methods: Peripheral blood was collected in Streck tubes and centrifugation was used to remove plasma and red blood cells. The remaining nucleated cells were deposited on glass slides, immunofluorescent-stained with proprietary antibodies, scanned by a high-definition digital scanner, and analyzed by a proprietary algorithm. In addition, single-cell genomics was performed on selected CTC. Analytical validation was performed using white blood cells from healthy donors and breast cancer cell lines with known levels of *ERBB2* amplification. Clinical concordance was assessed on MBC patients whose blood was tested by the CTC *ERBB2* (HER2) assay and those results are compared to results of matched metastatic tissue biopsy (immunohistochemistry [IHC] 3+ or IHC2+/in situ hybridization [ISH+]).

Results: Epic's *ERBB2* (HER2) assay detected 2-fold *ERBB2* amplification with 85% sensitivity and 94% specificity. In the clinical concordance study, among the 50% of the cases that had *ERBB2* status results from CTCs found to be chromosomally-unstable, the CTC *ERBB2* (HER2) assay showed sensitivity of 69% and specificity of 78% when compared to HER2 status by metastatic tissue biopsy.

Conclusions: The CTC *ERBB2* (HER2) assay can consistently detect *ERBB2* status in MBC cell lines and in the population of patients with MBC with detectable chromosomally unstable CTCs for whom tissue biopsy is not available or is infeasible.

Keywords: Analytical validation, Breast cancer, Circulating tumor cells, Epic CTC platform, HER2, Liquid biopsy

Introduction

ERBB2 genomic amplification is a cancer driver occurring in approximately 20% of breast cancer patients (1). Several pharmacological strategies are designed to be efficacious against cancers with HER2 tumor-specific overexpression (1). Clinically established routine tissue biopsies detect HER2 overexpressed or *ERBB2* "amplified" HER2 by detecting the number of copies of *ERBB2* by in situ hybridization (ISH) or by protein overexpression by immunohistochemistry (IHC) (2-4).

Received: February 14, 2024
Accepted: August 26, 2024
Published online: October 4, 2024

This article includes supplementary material

Corresponding author:
Giuseppe Di Caro
email: giuseppe.dicaro@epicsciences.com; giuseppe.dicaro19@gmail.com

During the initial diagnosis of metastatic cancer, the standard of care is to verify concordance of current HER2 status with the primary tumor by performing a tissue biopsy on the first or most available metastatic site. Previous studies of metastatic breast cancer (MBC) patients have demonstrated a degree of tumor tissue heterogeneity (5-12) and discordance in the HER2 status between metastatic sites and the primary tumor (13-15). Lack of knowledge about potential change in HER2 status may increase the chance that the therapy for patients thought to continue to have HER2-positive MBC will be ineffective at the expense of toxicity. At the same time, patients with a change to HER2-positive status may miss out on an effective treatment. The occurrence of receptor conversion makes longitudinal monitoring important, yet it is challenging to implement due to the invasive nature of tissue biopsies. While assessment of HER2 status through tissue biopsy IHC or ISH is the standard of care, a significant population of MBC patients do not receive an assessment of HER2 status and even fewer receive serial longitudinal tissue biopsies (16-18). As a result, tumor evolution and biomarker

receptor conversion, which can contribute to treatment resistance, are often missed. Studies are ongoing to assess whether HER2 receptor conversion impacts treatment efficacy and survival.

When tissue biopsy is contraindicated, refused, or otherwise not available, liquid biopsy can be an alternative. Typical liquid biopsy assays are limited to analysis of only the cell-free deoxyribonucleic acid (cfDNA) component of blood. In contrast, Epic Sciences' liquid biopsy assay identifies candidate circulating tumor cells (CTCs), confirms they are genomically unstable, and assesses *ERBB2* amplification within those selected cells. CTCs are very rare (on the order of one in two million cells), making both their detection and analysis challenging. Historically, the detection of CTCs relied on enrichment techniques based on preconceived knowledge about their biological phenotype, which may not account for evolving and emerging CTCs. Enrichment limits the ability to perform standardized clinical pathology for CTC biomarker assessment (morphology, protein, and molecular identification) on individual isolated cells (19-23). To overcome these limitations, Epic Sciences developed a cell-based assay to analyze the entire population of blood cells from a tube of blood providing a broad and unbiased identification of CTCs. Epic's assay then performs a thorough and high-definition phenotypic assessment, which includes evaluation by a clinical pathologist of cell morphology and immunofluorescence (IF) protein expression. A subset of CTCs is also selected to obtain genomic data matching cell morphology and IF data.

Using the cell-based assay (24), Epic Sciences previously developed an assay for detecting AR-V7-positive CTCs in patients with metastatic castration-resistant prostate cancer and informing the selection of treatment associated with superior survival on taxane therapy over androgen receptor signaling inhibitor-directed therapy (25-33). Epic's AR-V7 test was approved by MolDX (Molecular Diagnostic Services Program) for Medicare reimbursement. Epic's CTC *ERBB2* assay expands Epic's core technology to detect *ERBB2* amplification in CTCs from patients with MBC in a multistep workflow. This report describes both the analytical validation and clinical concordance studies that Epic Sciences completed to assess the performance of the CTC *ERBB2* Assay.

Methods

CTC ERBB2 assay workflow

Epic's CTC *ERBB2* assay workflow is shown in Figure 1 (further described in the Supplementary methods section). The assay uses a non-enrichment approach where all nucleated blood cells from a patient are placed on microscope slides (24). The slides are stained by IF and scanned by a high-definition imaging system. The image data are analyzed by an algorithm to detect CTC candidates from among the approximately three million white blood cells (WBCs) on each slide (Fig. 1). To minimize the manual cell classification effort, Epic developed an image analysis algorithm, BRIA (Breast Cancer Imaging Algorithm), to improve standardization and scalability of the assay. BRIA excludes the majority of the non-CTCs and identifies CTC candidates. The identified CTC candidates and their coordinates are tracked through the entire workflow from IF cell analysis to genomics. Using an in-house-developed Clinical Viewer for classification, interpretation, and reporting, CTC candidates are manually classified and confirmed by trained, California-licensed clinical laboratory scientists (Figs. 1 and 2).

Following CTC classification, the laboratory director (a medical doctor and board-certified clinical pathologist) reviews the CTC candidates and, by prioritizing CTCs with high HER2 IF staining intensities, selects CTCs for further genomic characterization via single-cell isolation and low-pass whole-genome sequencing (24,34) for detection

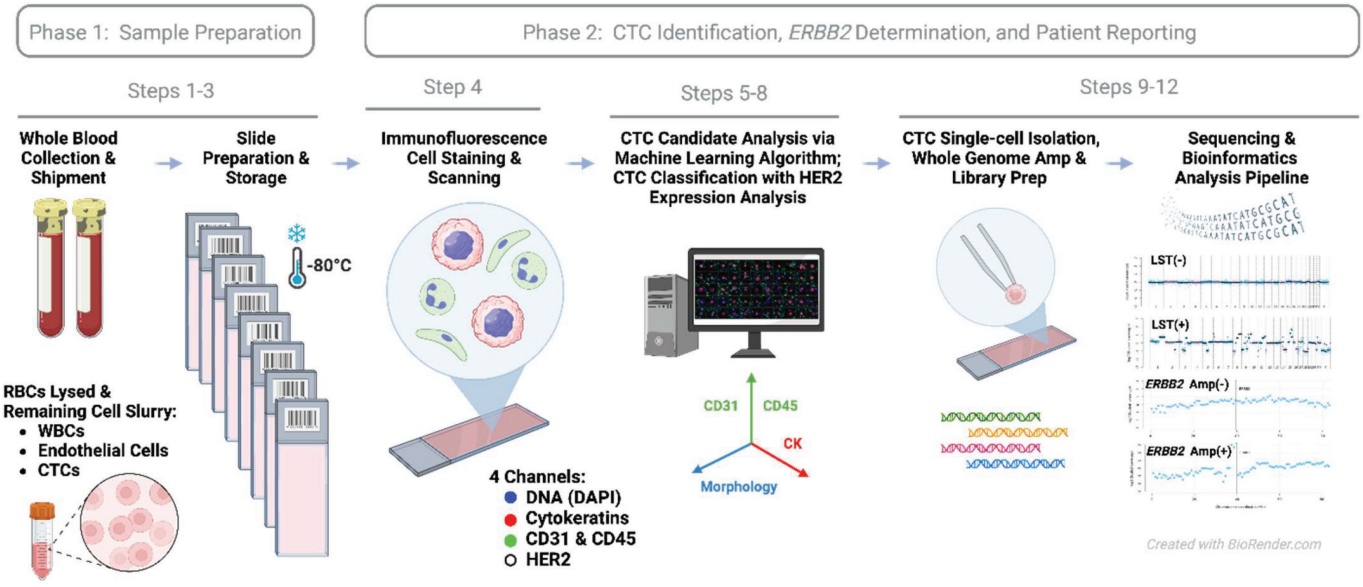

FIGURE 1 - Workflow of Epic Sciences' CTC *ERBB2* assay. The assay is performed entirely at Epic Sciences' CAP/CLIA laboratory. After deposition of blood cells onto glass slides, CTC candidates are identified through an immunofluorescence-based (IF) assay, then the laboratory director (a board-certified clinical pathologist) selects cells for genomic characterization via single-cell isolation and low-pass whole-genome sequencing by prioritizing those with higher MFI readings in the HER2 channel. Step numbers correspond to the workflow as described in Supplementary methods. CTC = circulating tumor cell; MFI = median cellular fluorescence intensity.

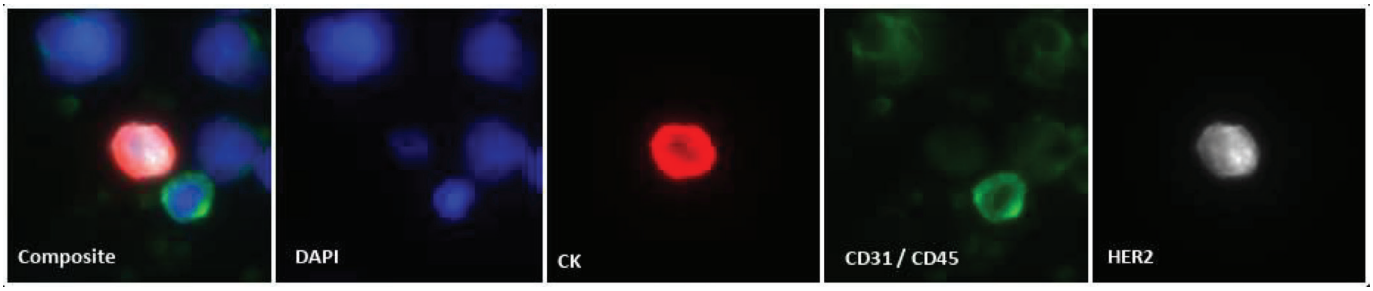

FIGURE 2 - Example HER2 protein expression visualized by immunofluorescence. Immunofluorescence staining of a CTC and surrounding cells as tested on Epic's CTC detection assay. The composite image is the overlay of four distinct fluorescent channels demonstrating the identification of nuclear DNA (DAPI, blue), pan-cytokeratins (CK, red), endothelial (CD31) and white blood cell (CD45) markers (green), and HER2 protein (white). The CTC shown expresses marked levels of CK and HER2, yet lacks the presence of CD31/CD45 protein markers. Image shown is 40× magnification. CTC = circulating tumor cell; DAPI = 4',6-diamidino-2-phenylindole; DNA = deoxyribonucleic acid.

of *ERBB2* amplification and chromosomal instability. DNA extraction from the CTCs is done via cell lysis, Proteinase K, and Tris buffer. Sequencing library preparation comes after whole-genome amplification (WGA). Both WGA and library preparation are done with the Sigma-Aldrich SEQPLEX-I WGA kit. Patient-level *ERBB2* status is determined based on assessment of *ERBB2* amplification levels across the chromosomally unstable CTCs using a clinical decision tree scoring system (Fig. 3). The board-certified pathologist(s) at Epic use Epic's Clinical Viewer to review QC data, interpret the results, and generate the clinical report.

CTC immunofluorescence

The CTC HER2 test utilizes a 4-channel IF assay workflow as outlined in Figure 1. Centrifugation facilitates plasma separation from red blood cells (RBCs). Following removal of plasma, RBCs are lysed, and the remaining nucleated cells are deposited on glass slides and adhered to microscope slides at a density of approximately 3×10^6 cells per slide and stored at −80°C prior to testing. To begin, the IF assay slides are thawed, proteins fixed with paraformaldehyde, cell membranes permeabilized via methanol treatment, washed and placed in

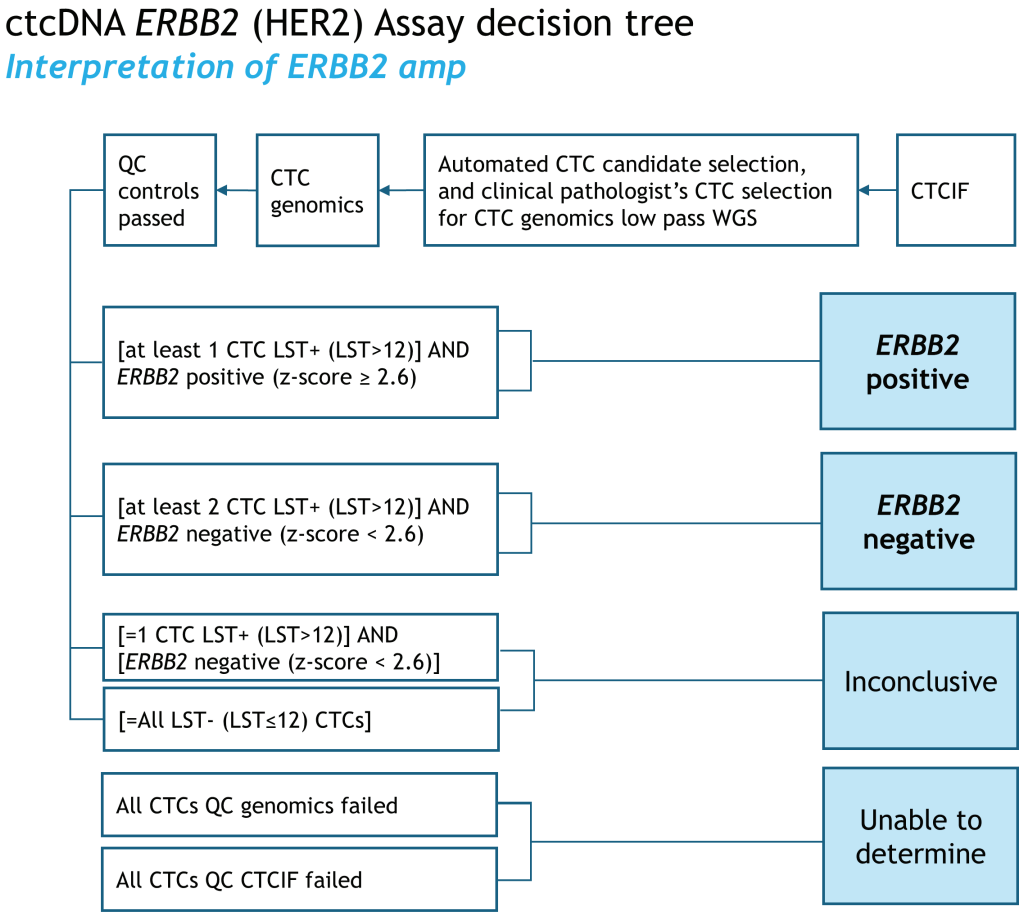

FIGURE 3 - Clinical scoring decision tree for Epic's CTC *ERBB2* (HER2) assay. CTCs that fail genomics QC metrics are excluded from the analysis. If the resulting *ERBB2* Z-score is ≥2.6 on at least one CTC and at least one LST+ CTC (LST > 12) is present, the case is positive. The case is negative if the resulting *ERBB2* Z-scores are <2.6 and at least two LST+ CTC (LST > 12) are present. The result is inconclusive if all CTCs are LST− (LST ≤12) or if the *ERBB2* Z-scores are <2.6 and only one LST+CTC (LST > 12) is present. However, If the patient sample is deemed "Inconclusive," additional CTCs may be prioritized and selected for sequencing, if available. The case is "unable to determine" if no CTCs are available for further analysis. CTC = circulating tumor cell; LST = large-scale state transition.

automated slide staining instrument. Each slide is subjected to nuclear staining with 4',6-diamidino-2-phenylindole (DAPI), as well as staining with fluorescently labeled antibodies specific to CD45 (WBC marker), CD31 (endothelial cell marker), cytokeratins (CKs; CTC marker), and HER2 through a sequential immunoassay workflow. CD31 (marking endothelial cells) and CD45 (marking WBCs) are exclusionary labels that allow us to filter out the endothelial cells and WBCs. DAPI channel is used for nuclear staining. The anti-pan CK antibody detects multi-CK types within the 555 nm channel as a marker for tumor cells. The Tyramide Signal Amplification (TSA) reagent system is used to generate the signal detected at 488 nm for the HER2 biomarker. Following fluorescent slide scanning image analysis is performed through BRIA.

Breast cancer imaging algorithm

BRIA consists of four main components: cell detection, segmentation, feature extraction, and CTC candidate identification. BRIA's cell detection and segmentation components were leveraged from its predecessor (24) used for AR-V7, with the addition of 42 newly developed image intensity features. BRIA's input is a high-resolution image from the ZEISS™ Axio automated scanning platform. BRIA first detects cells with DAPI signal. A multiscale feature enhancement algorithm is used to detect edges and blobs that are defined using the DAPI signal to enable detection of cell centers. The detected cells are further computationally characterized to extract relevant features from the biomarker intensity data in each of the channels (DAPI, CKs, CD45, and CD31). Specifically, there are 9 cell morphology, 42 biomarker signal intensity, and 24 image texture features. The feature values are used as input to the machine-learning generated algorithm that identifies CTC candidates for manual review.

Copy number variation pipeline for ERBB2 and large-scale state transition detection

A copy-number-analysis pipeline was developed for analysis of the CTC sequencing data. The pipeline was previously described and is similar to typical whole-genome sequencing workflows (35). Briefly, it aligns the Illumina sequencing reads to the human reference genome (hg38) and tallies the read coverage of 1-Mb bins across the genome. Using the alignment data, it computes key bioinformatic QC metrics for identifying samples with 1) insufficient sequencing data, 2) significant fractions of low-quality alignments, or 3) excessive coverage noise. Samples not passing bioinformatic QC are excluded from analysis (counts shown in Supplementary Tab. 2). Consistent with typical coverage scaling approaches, the bin coverage is scaled relative to an autosomal baseline. This normalizes for the average gene count in autosomes, and the resulting *ERBB2*/autosomal-average ratio compensates for the presence of multiple copies of chromosomes. In contrast, ISH-based *ERBB2* assays typically use CEP17 as the reference point.

Analytical validation

Breast cancer imaging algorithm

To validate BRIA's ability to identify CTC candidates, its cell-level performance was evaluated on an analytical validation dataset that consisted of manually confirmed CTC candidates, non-CTCs, and visual artifacts from patients' samples. The cell-level performance of the HER2 IF protein analysis (Supplementary Fig. 1) was assessed using a high-marker-expressing cell line (MDA-MB-453) and a low-marker-expressing cell line (MDA-MB-231). Also, several breast cancer cell lines spiked into healthy donors' blood were tested for their HER2 median cellular fluorescence intensity (MFI) values on Epic's assay (Supplementary Fig. 2).

Copy number variation pipeline for *ERBB2* and large-scale state transition detection

The accuracy for *ERBB2* amplification detection was assessed using MDA-MB-453 cells as positives and WBCs as negatives; sensitivity and specificity were computed. The precision for *ERBB2* amplification detection was assessed across two manufacturing lots of the sequencing-reagent kits, two operators, and two sequencing runs. To assess how the results were impacted by the additional variables, positive percent agreement (PPA) and negative percent agreement (NPA) were computed by comparing the mode across all replicates to each replicate result (Tab. 1).

Clinical concordance

Patients were included in the concordance study with distant metastases and with HER2 status as determined in a matched metastatic tissue biopsy using the standard, IHC, and/or ISH performed at each cancer center site and were tested by Epic's CTC ER assay. The concordance of *ERBB2* amplification was detected by single-cell CTC genomics. Contemporaneous is defined as patients with blood collection performed within about 30 days before tissue biopsy. By computing typical concordance metrics (PPA, NPA, positive predictive value [PPV], and negative predictive value [NPV]), we inferred the probability that the assay will provide a correct diagnosis of HER2 status as determined in a matched metastatic tissue biopsy. The two-sided 95% confidence interval for PPA and NPA was calculated using the Wilson score method and the Bayesian Rule formula (36,37).

TABLE 1 - Analytical validation summary data

Biomarker	LOD (n = 138)	AV cutoff	Accuracy (n = 162)		Precision (n = 162)	
			Sensitivity	Specificity	PPA	NPA
ERBB2 amplification	2-fold amplification	>1.77 (*ERBB2* Z-score)	0.85	0.94	0.85	0.94

The sensitivity and specificity of ***ERBB2*** amplification detection were computed using WBCs and MDA-MB-453 cells as expected negatives and positives, respectively. Based on the expected statuses, true positives and true negatives, and false positives and false negatives were counted for all samples that passed QC.
AV = analytical validation; LOD = limit of detection; NPA = negative percentage agreement; PPA = positive percentage agreement; WBC = white blood cell.

Results

Analytical validation

BRIA and immunofluorescence

BRIA was built to reliably identify CTC candidates from patient slides with minimal manual review. It is based on earlier versions of Epic's proprietary digital pathology used in its CTC assays (AR-V7 and others) (24-33,35,38). BRIA classifies cell candidates captured from slide images into two classes, "CTC" and "non-CTC," using a predictive model. In the analytical validation analysis, the evaluation of the BRIA predictive model relies on "true positive," which refers to a manually confirmed CTC that BRIA classified as "CTC," and "true negative" refers to a non-CTC that BRIA classified as "non-CTC." These labels are used in the calculation of BRIA's cell-level performance metrics. At the cell level, BRIA had 99% sensitivity, 96% specificity, and 97% overall percentage agreement (OPA) for the validation dataset (Supplementary Tab. 1). The analytical performance at the cell level of the IF HER2 protein analysis was evaluated between the high-marker-expressing cell line (MDA-MB-453) and the low-marker-expressing cell line (MDA-MB-231) (Supplementary Fig. 1), and revealed a sensitivity, specificity, and accuracy of 94%, 97%, and 95%, respectively (Supplementary Fig. 1). To demonstrate the assay's ability to cover the dynamic range of intensity levels of HER2, Epic spiked cells from several breast cancer cell lines into tubes of healthy donor blood and tested the spiked blood on Epic's CTC *ERBB2* assay. The resulting single-cell data showed that the overall HER2 intensity levels were consistent with expectations for well-characterized cell lines based on reported IHC values (39,40) (Supplementary Fig. 2).

Single-cell genomic assay

To validate the single-cell genomic pipeline's ability to identify *ERBB2* copy number amplification and chromosomal instability, we analyzed WBCs from healthy donors and well-characterized breast cancer cell lines (SK-BR-3, MDA-MB-453, and MCF-7) with known chromosomal instability and known *ERBB2* amplification status as negative and positive controls, respectively. The experiments, cell types, and the number of cells used for analytical validation are summarized in Supplementary Tab. 2. To evaluate the limit of detection (LOD) for the detection of chromosomal instability, a copy number variation simulator was used to introduce different amounts of large copy number changes (which would result in large-scale state transitions [LSTs]) to the WBC base genomes (Supplementary Fig. 3). Modified genomes with at least 10 breakpoints were consistently called as chromosomally unstable (sensitivity of 91%), which was considered the LOD for chromosomal instability detection (Fig. 3). *ERBB2* amplification

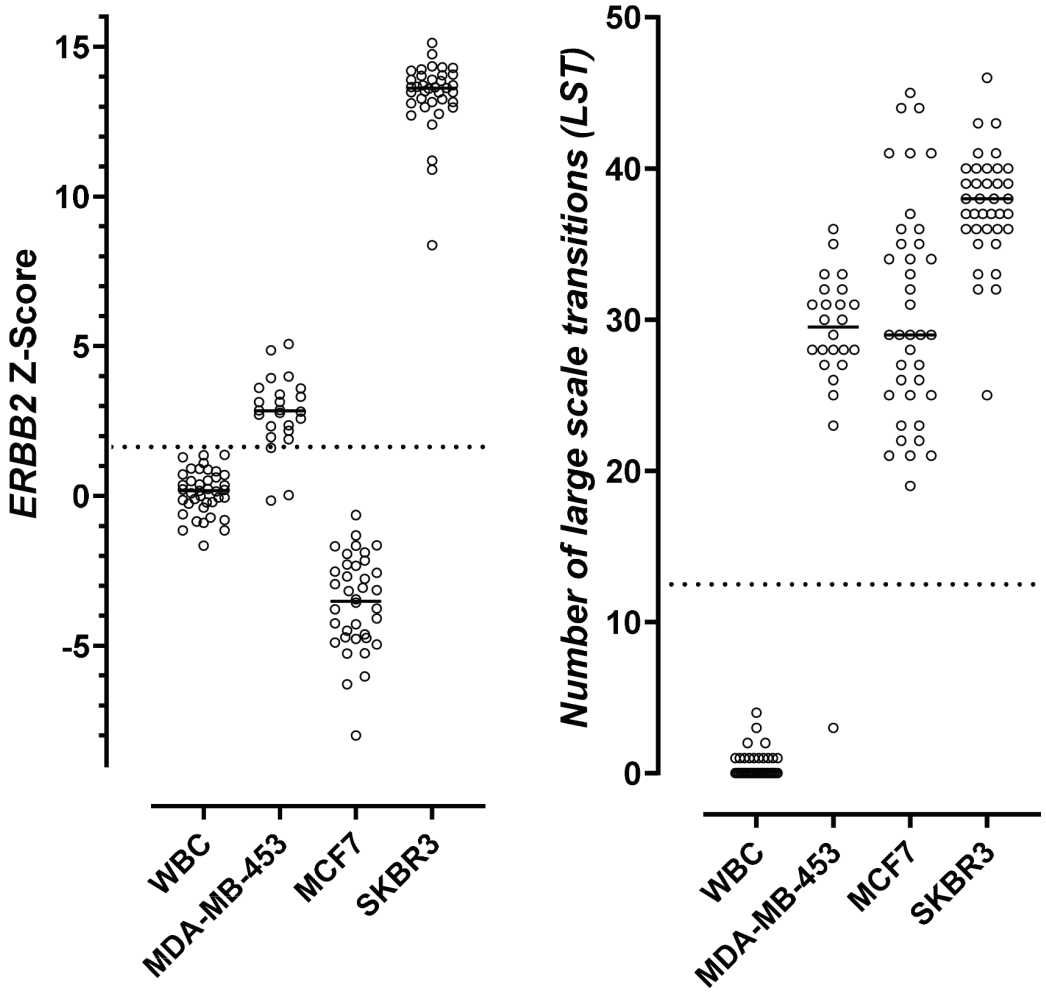

FIGURE 4 - Distributions of *ERBB2* Z-scores and numbers of LSTs in WBCs and cells from characterized breast cancer cell lines. WBCs are negative controls with expected chromosomal stability (right) and *ERBB2* non-amplified (left). Breast cancer cell lines MDA-MB-453 and SKBR3 are positive controls with expected chromosomal instability (right) and *ERBB2* amplification (left). Breast cancer cell line MCF7 has expected chromosomal instability (right) and no *ERBB2* amplification (left). The dotted line on the left represents the *ERBB2* Z-score cutoff (1.77) that was used in analytical validation for defining *ERBB2* amplification positivity. The dotted line on the right highlights the LST cutoff (12). LST, large-scale state transitions; WBC = white blood cell.

was not detected in WBCs and MCF-7 cells but was detected in MDA-MB-453 and SK-BR-3 cells (Tab. 1 and Fig. 3). Given that MDA-MB-453 cells had an expected 2-fold *ERBB2* amplification, that 2-fold level was considered the LOD for detection of *ERBB2* amplification. The sensitivity and specificity for detecting the 2-fold *ERBB2* amplification were 85% and 94%, respectively (Tab. 1). Precision was assessed across two sequencing runs, two lots, and two operators and the overall PPA and NPA were 85% and 94%, respectively (Tab. 1).

Clinical concordance

Patients with tissue biopsy results who were diagnosed with MBC with distant metastases were tested by Epic's CTC *ERBB2* (HER2) assay (n = 128; Supplementary Fig. 4). Fifty percent (64/128) of patients tested in the clinical concordance cohort were found to be reported as either *ERBB2* positive or *ERBB2* negative by CTC *ERBB2* (HER2) assay, based on the scoring system described in Figure 4 and were included in the Clinical Concordance set (n = 64) analysis, 50% were considered inconclusive due to lack of chromosomal instability or by quality control parameters and were excluded from analysis (Supplementary Fig. 4). The Clinical Concordance set reported here (n = 64) and the clinical and histopathological features at diagnosis of the Clinical Concordance set are shown in Table 2. In Supplementary Figure 5, we show the distributions of the maximum *ERBB2* Z-score among LST+CTC per patient with *ERBB2* amp status (mean: Z-score 7.5) and *ERBB2* non-amp (mean: Z-score 0.65) status. To test the correlation between the *ERBB2* CTC assay results and stage of metastatic disease Supplementary Figure 6 shows the distributions of the maximum *ERBB2* Z-score among LST+CTC per patient across those who received first-line (1L) (mean: Z score 2.7) or second-line and higher (>1L+) therapy (mean: Z-score 3.7) for metastatic disease after the blood was drawn for CTC analysis and found no significant differences. Similarly, as shown in Supplementary Figure 7, we found no significant difference between the distribution of the number of LST+CTC in patients who received first-line (1L) (mean: 5.0 LST+ CTC) or second-line and higher (>1L+) therapy (mean: 4.8 LST+ CTC) for metastatic disease after the blood was drawn for CTC analysis. Epic's CTC *ERBB2* (HER2) assay scoring system was applied to the Clinical Concordance set; the concordance analysis showed a sensitivity of 69% and specificity of 78% to the comparator results of the tissue biopsies (Tab. 3). Based on the rationale that HER2 status determination on bone biopsy samples has reported decreased sensitivity of ISH analysis of *ERBB2* gene amplification (17,41), a subgroup analysis of only patients with non-bone tissue biopsies was performed (Supplementary Fig. 4) and, as expected, it showed that concordance was improved, with sensitivity of 86% and specificity of 75% (Tab. 3). Based on the rationale that HER2 status can change during the course of treatment and progression, a second subgroup analysis was performed to include only patients with contemporaneous tissue biopsies (Supplementary Fig. 4). When including only patients with HER2 status assessed by tissue biopsies that were both contemporaneous (to the comparator blood draw) and were performed on non-bone tissue (Supplementary Fig. 4), the concordance to tissue biopsy improved to a sensitivity of 100% and a specificity of 75% (Tab. 3). These results provide evidence of the contribution of time as a source of discordance between the results of Epic's CTC *ERBB2* (HER2) assay and the tissue biopsy comparators.

TABLE 2 - Clinical and histopathological features of the clinical patients set

Clinical and histopathological features	% of patients with MBC (number/total)
Line of treatment	
1. First line	83% (53/64)
2. Second line or above	14% (9/64)
3. Unknown	3% (2/64)
Tissue biopsies	
1. Contemporaneous	89% (57/64)
2. Non-contemporaneous	11% (7/64)
3. IHC performed	97% (62/64)
4. ISH performed	37% (24/64)
5. Tissue site	
a) Bone	39% (25/64)
b) Non-bone	61% (39/64)
c) Liver	28% (18/64)
d) Breast	16% (10/64)
e) Lymph node	11% (7/64)
f) Lung	2% (1/64)
g) Omentum	2% (1/64)
h) Pleural fluid	2% (1/64)
i) Stomach	2% (1/64)
6. Non-bone	61% (39/64)
7. HER2+	20% (13/64)
a) HER2+ by IHC	11% (7/62)
b) HER2+ by ISH	25% (6/24)
8. ER+	78% (50/64)

ER = estrogen receptor; IHC = immunohistochemistry; ISH = in situ hybridization; MBC = metastatic breast cancer.

Discussion

This report shows the analytical and clinical performance of Epic's CTC *ERBB2* (HER2) cell-based liquid biopsy assay's ability to detect *ERBB2* amplifications in MBC patients. The assay is a test intended for a population with very limited options available to get individualized sequential information about the treatment that is most likely to be efficacious.

A substantial improvement in the CTC *ERBB2* (HER2) assay's characterization of CTCs over conventional liquid biopsy assays is that, as a criteria of CTC classification and enumeration, it takes advantage of a characteristic genomic feature of tumor cells, which is the presence of chromosomal instability, a biological mechanism of tumor evolution and adaptation to environmental pressures that enables

TABLE 3 - Clinical concordance summary data

Sample	N	PPA	NPA	PPV	NPV	Comments
Clinical Concordance set	64	0.69	0.78	0.45	0.91	Overall population
Subgroup analysis limited to patients with *non-bone biopsies*	39	0.86	0.75	0.46	0.96	Removal of patients with *bone biopsies improves sensitivity*
Subgroup analysis limited to patients with *only contemporaneous non-bone biopsies*	35	1.00	0.75	0.50	1.00	Removal of patients with *non-contemporaneous* tissue biopsy and *bone biopsies* further improves sensitivity in the Clinical Concordance set

Concordance of Clinical Concordance set patients (and subgroups of patients with non-bone and contemporaneous tissue samples) with results from tissue biopsy. When including only patients with HER2 status assessed by tissue biopsies that were both contemporaneous and from non-bone tissue, the concordance to tissue biopsies improved to a sensitivity of 100% and a specificity of 75%.
NPA = negative percent agreement; NPV = negative predictive value; PPA = positive percent agreement; PPV = positive predictive value.

tumor progression and metastatic capabilities (42-44). Peer-reviewed data showed that genomic sequencing applied to CTCs from Epic Sciences' assay allowed identification of high chromosomal instability within CTCs (35,42,45) that was independently associated with worse survival in men with high-risk metastatic castration-resistant prostate cancer treated with abiraterone/enzalutamide that may benefit alternative treatments (42). In this report, concordance of *ERBB2* status was analyzed only in the subgroup of patients with CTCs with high LSTs by the CTC *ERBB2* (HER2) assay, which indicates the detection of chromosomal instability. Only 50% of patients were found to have CTCs with high numbers of chromosomal instability. Clinical studies will be performed to test whether patients with detection of chromosomally unstable CTCs reported here will associate with patient's outcome.

Typically, reliable tumor identification in histopathological tissue biopsy analysis of HER2 status does not require genomic assessment but instead requires a pathologist to visually examine patterns of cell shapes and regions of tissue structure to identify cancer cells by morphological assessment and to perform proper semiquantitative scoring of HER2 expression on those cancer cells. However, liquid biopsy assays are limited to the analysis of those few rare CTCs (or ctDNA) in the sample that are in suspension, without their tissue contexture, and sometimes may be morphologically indistinguishable from circulating nontumor cells by the trained pathologist (or from DNA shed from endogenous germ-line cells, called cell-free DNA [cfDNA]). To avoid this problem, detection of chromosomal instability in CTCs, a common feature of metastatic cancer cells (42,43), increases the probability that the CTCs on which *ERBB2* is evaluated represent truly neoplastic components of the tumor, thus making the *ERBB2* CTC assay diagnostic assessments tumor specific. Therefore, as compared to analysis based on cfDNA, Epic's assay can detect *ERBB2* amplifications with high sensitivity because it is evaluating a pool of DNA that comes entirely from a tumor cell with chromosomal instability, as detected by high numbers of LSTs. Development efforts are ongoing to test whether artificial intelligence algorithms trained on thousands of chromosomally unstable CTCs will be capable of differentiating subsets of cancer cells by using only morphological patterns.

Potential confounding factors impacting our concordance analysis are the following: First, there are no available orthogonal assays to demonstrate concordance in the same blood sample. As an alternative, we measured concordance comparing the blood assay results to metastatic tumor tissue biopsies rather than comparing the same blood sample analyzed with different CTC-based assays. Second, bone tissues often represent the location of first distant metastasis in patients (46) but bone biopsies utilizing older decalcification techniques could be falsely negative for HER2 overexpression or *ERBB2* amplification (17,41). In fact, bone biopsies from bone-only metastatic patients are often excluded from clinical trials of HER2 expression as exemplified by the recently published DAISY trial (47). Additional factors contribute to assay variability, such as lack of central laboratory verification for pathological tissue biopsy results. These may reflect variations in pathologists' assessment of HER2 status in tissue biopsies that do not control and are not accounted for within reported analytical variation. Validation studies using a contemporaneous dataset of tissue biopsy samples analyzed in central pathology labs will be needed to confirm these correlative findings in a larger dataset. Clinical utility studies have been designed to test whether the CTC *ERBB2* assay will inform improved treatment decision-making to HER2-targeted therapies over the current standard of care for MBC patients.

Acknowledgments

Research support for this study was funded by Epic Sciences. The data are available within the article and the Supplementary Information provided with this article. For additional data that may be under restricted access in compliance with patient consent and ethical principles for data sharing request, please contact the corresponding author.

Disclosures

Conflict of interest: E.T.L., E.W., D.Z., D.B., M.B., N.D., M.S., and R.W. are or have been employed by Epic Sciences. L.S. has received honoraria for consulting from Epic Sciences.

Funding: The research and the work presented were funded by Epic Sciences.

Author contributions: G.D.C. designed the clinical study, performed the statistical analysis, and drafted the manuscript. E.T.L., E.W., and D.Z. designed and developed the genomic platform and performed statistical analysis. D.B. and M.B. designed and developed

the immunofluorescent platform. N.D. is a board-certified clinical pathologist who reviewed the CTC candidates and interpreted the clinical results. M.S. coordinated clinical study samples' accrual, clinical data collection, and data entry. L.S. and R.W. provided scientific guidance, revised the manuscript draft with all authors contributing and providing feedback and advice.

References

1. Carey LA, Perou CM, Livasy CA, et al. Race, breast cancer subtypes, and survival in the Carolina breast cancer study. JAMA. 2006;295(21):2492-2502. CrossRef
2. Martínez-Sáez O, Prat A. Current and future management of HER2-positive metastatic breast cancer. JCO Oncol Pract. 2021;17(10):594-604. CrossRef
3. Wolff AC, Hammond MEH, Hicks DG, et al; American Society of Clinical Oncology; College of American Pathologists. Recommendations for human epidermal growth factor receptor 2 testing in breast cancer: American Society of Clinical Oncology/College of American Pathologists clinical practice guideline update. J Clin Oncol. 2013;31(31):3997-4013. CrossRef PubMed
4. Gradishar WJ, Moran MS, Abraham J, et al. Breast Cancer, Version 3.2022, NCCN Clinical Practice Guidelines in Oncology. J Natl Compr Canc Netw. 2022;20(6):691-722. CrossRef PubMed
5. Gilson P, Merlin JL, Harlé A. Deciphering tumour heterogeneity: from tissue to liquid biopsy. Cancers (Basel). 2022;14(6):1384. CrossRef PubMed
6. Hiley C, de Bruin EC, McGranahan N, Swanton C. Deciphering intratumor heterogeneity and temporal acquisition of driver events to refine precision medicine. Genome Biol. 2014 Aug 27;15(8):453. CrossRef PubMed
7. Zardavas D, Irrthum A, Swanton C, Piccart M. Clinical management of breast cancer heterogeneity. Nat Rev Clin Oncol. 2015;12(7):381-394. CrossRef PubMed
8. Pasha N, Turner NC. Understanding and overcoming tumor heterogeneity in metastatic breast cancer treatment. Nat Cancer. 2021;2(7):680-692. CrossRef PubMed
9. Hapach LA, Carey SP, Schwager SC, et al. Phenotypic heterogeneity and metastasis of breast cancer cells. Cancer Res. 2021;81(13):3649-3663. CrossRef PubMed
10. Lee JK, Choi YL, Kwon M, Park PJ. Mechanisms and consequences of cancer genome instability: lessons from genome sequencing studies. Annu Rev Pathol. 2016;11(1):283-312. CrossRef PubMed
11. Tellez-Gabriel M, Ory B, Lamoureux F, Heymann MF, Heymann D. Tumour heterogeneity: the key advantages of single-cell analysis. Int J Mol Sci. 2016;17(12):2142. CrossRef PubMed
12. McGranahan N, Swanton C. Clonal heterogeneity and tumor evolution: past, present, and the future. Cell. 2017;168(4):613-628. CrossRef PubMed
13. Kaufman PA, Bloom KJ, Burris H, et al. Assessing the discordance rate between local and central HER2 testing in women with locally determined HER2-negative breast cancer. Cancer. 2014 Sep 1;120(17):2657-2664. CrossRef. Epub 2014 Jun 13. PubMed
14. Paik S, Bryant J, Tan-Chiu E, et al. Real-world performance of HER2 testing – National Surgical Adjuvant Breast and Bowel Project experience. J Natl Cancer Inst. 2002 Jun 5;94(11):852-854. CrossRef. PubMed
15. Schrijver WAME, Suijkerbuijk KPM, van Gils CH, van der Wall E, Moelans CB, van Diest PJ. Receptor conversion in distant breast cancer metastases: a systematic review and meta-analysis. J Natl Cancer Inst. 2018 Jun 1;110(6):568-580. CrossRef. PubMed
16. Aktas B, Kasimir-Bauer S, Müller V, et al; DETECT Study Group. Comparison of the HER2, estrogen and progesterone receptor expression profile of primary tumor, metastases and circulating tumor cells in metastatic breast cancer patients. BMC Cancer. 2016;16(1):522. CrossRef PubMed
17. Schrijver WAME, van der Groep P, Hoefnagel LD, et al. Influence of decalcification procedures on immunohistochemistry and molecular pathology in breast cancer. Mod Pathol. 2016;29(12):1460-1470. CrossRef PubMed
18. Van Poznak C, Somerfield MR, Bast RC, et al. Use of biomarkers to guide decisions on systemic therapy for women with metastatic breast cancer: American Society of Clinical Oncology clinical practice guideline. J Clin Oncol. 2015;33(24):2695-2704. CrossRef PubMed
19. Micalizzi DS, Maheswaran S, Haber DA. A conduit to metastasis: circulating tumor cell biology. Genes Dev. 2017 Sep 15;31(18):1827-1840. CrossRef. PubMed
20. Alix-Panabières C, Pantel K. Liquid biopsy: from discovery to clinical application. Cancer Discov. 2021;11(4):858-873. CrossRef PubMed
21. Alix-Panabières C, Pantel K. Liquid biopsy: from discovery to clinical application. Cancer Discov. 2021 Apr;11(4):858-873. CrossRef. PubMed
22. Joosse SA, Gorges TM, Pantel K. Biology, detection, and clinical implications of circulating tumor cells. EMBO Mol Med. 2015;7(1):1-11. CrossRef PubMed
23. Keomanee-Dizon K, Shishido SN, Kuhn P. Circulating tumor cells: high-throughput imaging of CTCs and bioinformatic analysis. In: Recent results in cancer research. Vol 215. Springer: New York LLC; 2020:89-104. CrossRef
24. Werner SL, Graf RP, Landers M, et al. Analytical validation and capabilities of the epic CTC platform: enrichment-free circulating tumour cell detection and characterization. J Circ Biomark. 2015;4:3. CrossRef PubMed
25. Scher HI, Lu D, Schreiber NA, et al. Association of AR-V7 on circulating tumor cells as a treatment-specific biomarker with outcomes and survival in castration-resistant prostate cancer. JAMA Oncol. 2016;2(11):1441-1449. CrossRef PubMed
26. Armstrong AJ, Luo J, Nanus DM, et al. Prospective multicenter study of circulating tumor cell AR-V7 and taxane versus hormonal treatment outcomes in metastatic castration-resistant prostate cancer. JCO Precis Oncol. 2020;4(4):1285-1301. CrossRef PubMed
27. Graf RP, Hullings M, Barnett ES, Carbone E, Dittamore R, Scher HI. Clinical utility of the nuclear-localized AR-V7 biomarker in circulating tumor cells in improving physician treatment choice in castration-resistant prostate cancer. Eur Urol. 2020;77(2):170-177. CrossRef PubMed
28. Lu D, Krupa R, Harvey M, et al. Development of an immunofluorescent AR-V7 circulating tumor cell assay – a blood-based test for men with metastatic prostate cancer. J Circ Biomark. 2020;9(1):13-19. CrossRef PubMed
29. Scher HI, Graf RP, Schreiber NA, et al. Nuclear-specific AR-V7 protein localization is necessary to guide treatment selection in metastatic castration-resistant prostate cancer. Eur Urol. 2017;71(6):874-882. CrossRef PubMed
30. Scher HI, Graf RP, Schreiber NA, et al. Phenotypic heterogeneity of circulating tumor cells informs clinical decisions between AR signaling inhibitors and taxanes in metastatic prostate cancer. Cancer Res. 2017;77(20):5687-5698. CrossRef PubMed
31. Beltran H, Jendrisak A, Landers M, et al. The initial detection and partial characterization of circulating tumor cells in neuroendocrine prostate cancer. Clin Cancer Res. 2016;22(6):1510-1519. CrossRef PubMed
32. Bjartell AS. Re: The initial detection and partial characterization of circulating tumor cells in neuroendocrine prostate cancer. Eur Urol. 2016;70(4):700. CrossRef PubMed

33. Fujii T, Reuben JM, Huo L, et al. Androgen receptor expression on circulating tumor cells in metastatic breast cancer. PLoS One. 2017;12(9):e0185231. CrossRef PubMed
34. Dago AE, Stepansky A, Carlsson A, et al. Rapid phenotypic and genomic change in response to therapeutic pressure in prostate cancer inferred by high content analysis of single circulating tumor cells. PLoS One. 2014;9(8):e101777. CrossRef PubMed
35. Greene SB, Dago AE, Leitz LJ, et al. Chromosomal instability estimation based on next generation sequencing and single cell genome wide copy number variation analysis. PLoS One. 2016;11(11):e0165089. CrossRef PubMed
36. Efron B. Mathematics. Bayes' theorem in the 21st century. Science. 2013 Jun 7;340(6137):1177-1178. CrossRef PubMed
37. Bours MJ. Bayes' rule in diagnosis. J Clin Epidemiol. 2021;131: 158-160. CrossRef PubMed
38. Zhang L, Beasley S, Prigozhina NL, et al. Detection and characterization of circulating tumour cells in multiple myeloma. J Circ Biomark. 2016;5:10. CrossRef PubMed
39. Subik K, Lee JF, Baxter L, et al. The expression patterns of ER, PR, HER2, CK5/6, EGFR, Ki-67 and AR by immunohistochemical analysis in breast cancer cell lines. Breast Cancer (Auckl). 2010 May 20;4:35-41. Erratum in: Breast Cancer (Auckl). 2018 Oct 16;12:1178223418806626. PubMed
40. McCabe A, Dolled-Filhart M, Camp RL, Rimm DL. Automated quantitative analysis (AQUA) of in situ protein expression, antibody concentration, and prognosis. J Natl Cancer Inst. 2005; 97(24):1808-1815. CrossRef PubMed
41. Gertych A, Mohan S, Maclary S, et al. Effects of tissue decalcification on the quantification of breast cancer biomarkers by digital image analysis. Diagn Pathol. 2014;9(1):213. CrossRef PubMed
42. Brown LC, Halabi S, Schonhoft JD, et al. Circulating tumor cell chromosomal instability and neuroendocrine phenotype by immunomorphology and poor outcomes in men with mCRPC treated with abiraterone or enzalutamide. Clin Cancer Res. 2021;27(14):4077-4088. CrossRef PubMed
43. Manié E, Popova T, Battistella A, et al. Genomic hallmarks of homologous recombination deficiency in invasive breast carcinomas. Int J Cancer. 2016;138(4):891-900. CrossRef PubMed
44. Sansregret L, Swanton C. The role of aneuploidy in cancer evolution. Cold Spring Harb Perspect Med. 2017;7(1):a028373. CrossRef PubMed
45. Malihi PD, Graf RP, Rodriguez A, et al. Single-cell circulating tumor cell analysis reveals genomic instability as a distinctive feature of aggressive prostate cancer. Clin Cancer Res. 2020;26(15):4143-4153. CrossRef PubMed
46. Parkes A, Clifton K, Al-Awadhi A, et al. Characterization of bone only metastasis patients with respect to tumor subtypes. NPJ Breast Cancer. 2018;4(1):2. CrossRef PubMed
47. Mosele F, Deluche E, Lusque A, et al. Trastuzumab deruxtecan in metastatic breast cancer with variable HER2 expression: the phase 2 DAISY trial. Nat Med. 2023;29(8):2110-2120. CrossRef PubMed

JCB
J Circ Biomark 2024; 13: 36-44
ISSN 1849-4544 | DOI: 10.33393/jcb.2024.3146
ORIGINAL RESEARCH ARTICLE

Altered amino and fatty acids metabolism in Sudanese prostate cancer patients: insights from metabolic analysis

Dalia Ahmed[1–3], Ebtesam A. Abdel-Shafy[3,4], Elsadig Ahmed Adam Mohammed[5,6], Husam Elden Alnour Bakhet Alnour[1], Amar Mohamed Ismail[7,8], Stefano Cacciatore[3], Luiz Fernando Zerbini[9]

[1]Department of Histopathology and Cytology, Faculty of Medical Laboratory Science, Al-Neelain University, Khartoum - Sudan
[2]Department of Histopathology and Cytology, Faculty of Medical Laboratory Science, Omdurman Ahlia University, Omdurman - Sudan
[3]Bioinformatics Unit, International Centre for Genetic Engineering and Biotechnology, Cape Town - South Africa
[4]National Research Centre, Cairo - Egypt
[5]Department of Histopathology and Cytology, Faculty of Medical Laboratory Science, National Ribat University, Khartoum - Sudan
[6]Department of Histology and Cytology, National Ribat University Hospital, Khartoum - Sudan
[7]Department of Biochemistry and Molecular Biology, Faculty of Science and Technology, Al-Neelain University, Khartoum - Sudan
[8]Department of Biomedical Science, Faculty of Pharmacy, Omer Al-Mokhtar University, Al Bayda - Libya
[9]Cancer Genomics, International Centre for Genetic Engineering and Biotechnology, Cape Town - South Africa

ABSTRACT

Introduction: Prostate cancer (PCa) management presents a multifaceted clinical challenge, intricately linking oncological considerations with cardiovascular health. Despite the recognized importance of lipid metabolism and hypertension in this interwoven relationship, their involvement in PCa development remains partially understood. This study aimed to explore variations in plasma metabolome among Sudanese PCa patients and their associated comorbidities.

Methods: Plasma samples were collected from 50 patients across four hospitals in Sudan and profiled by nuclear magnetic resonance (NMR) spectroscopy. One-dimensional proton NMR spectra were acquired for each sample using standard nuclear Overhauser effect spectroscopy pulse sequence presat on a 500 MHz Bruker Avance III HD NMR spectrometer. Metabolite concentrations were quantified using R scripts developed in-house. Univariate and multivariate analyses were generated in the R software.

Results: Patients were categorized into four distinct metabotypes based on their metabolic profiles, and statistical analyses were conducted to evaluate the significance of observed differences. Our findings revealed high levels of fatty acids, phospholipids, cholesterol, valine, leucine, and isoleucine associated with non-hypertensive patients. In contrast, hypertensive patients were associated with high GlycA and GlycB levels and altered amino acid metabolism.

Conclusion: These findings underscore the intricate interplay between metabolic dysregulation and hypertension in PCa patients. Further research is warranted to elucidate the precise molecular pathways underlying lipid metabolism in PCa and to explore the therapeutic potential of targeting these pathways. In conclusion, our study contributes to a deeper understanding of the metabolic landscape of PCa in Sudanese patients, emphasizing the importance of personalized approaches in cancer management.

Keywords: Africa, Metabolomics, NMR, Prostate cancer, Sudan

Introduction

Prostate cancer (PCa) poses a significant global health challenge, characterized by its increasing incidence and substantial impact on patient morbidity and mortality (1). With advancements in anticancer therapies leading to improved survival rates, the emergence of cardiovascular toxicities and hypertension (HTN) presents clinicians with intricate management dilemmas (2). Understanding the complex biochemical alterations associated with PCa is vital for advancing diagnostic and therapeutic strategies (3). Metabolomics offers a comprehensive snapshot of the metabolome, the complete set of small molecule metabolites within a biological system, providing insights into dynamic changes occurring in cellular metabolism (4,5). It has emerged as a pivotal tool in elucidating the intricate metabolic changes underlying PCa development and progression (6–9). Particularly, the

Received: May 22, 2024
Accepted: November 20, 2024
Published online: December 16, 2024

This article includes supplementary material

Corresponding author:
Stefano Cacciatore
email: stefano.cacciatore@icgeb.org

investigation of altered metabolic pathways involving lipids, fatty acids, and free amino acids holds immense importance in understanding the molecular mechanisms driving PCa pathogenesis (10,11).

Among the plethora of molecular factors implicated in PCa pathogenesis, lipids have emerged as pivotal players, governing diverse cellular processes crucial for tumor progression (12). Emerging evidence suggests a complex interplay between lipid metabolism, HTN, and androgen deprivation therapies (ADTs) in PCa patients, adding further layers of complexity to patient care (13,14). Dysregulated lipid metabolism not only fuels the energy demands of proliferating cancer cells but also contributes to the structural integrity of cellular membranes and facilitates signaling pathways crucial for PCa progression (15). Fatty acids, the building blocks of complex lipids, are intricately involved in various cellular processes, including energy production, membrane synthesis, and signaling modulation (16). Perturbations in fatty acid metabolism have been implicated in PCa pathophysiology, influencing tumor aggressiveness, therapeutic resistance, and disease prognosis (17). Metabolomic studies have unveiled alterations in fatty acid composition and metabolism associated with PCa, highlighting their potential as biomarkers for disease diagnosis and therapeutic targets for intervention (10,18). Moreover, free amino acids play pivotal roles in cellular metabolism, serving as precursors for protein synthesis, energy production, and signaling molecules (19). Alteration in amino acid metabolism has been implicated in PCa progression, influencing cell proliferation, invasion, and metastasis (20,21). Metabolomic profiling has uncovered variations in amino acid levels and metabolism in PCa, offering insights into the relation between metabolic rewiring and oncogenic signaling pathways (8,11).

Most metabolomic PCa studies are conducted predominantly in European and Asian populations. The generalization of findings to other ethnic groups may be limited due to inherent genetic, environmental, and lifestyle differences (22). Therefore, investigating altered metabolic pathways in diverse populations, including those from African regions like Sudan, is crucial for elucidating population-specific variations in PCa biology. Sudan presents a unique demographic landscape characterized by its distinct genetic ancestry, dietary habits, and environmental exposures (23). The region is characterized by a rich diversity highlighted by the extensive presence of major continental African language families, including Niger-Congo (NC), Nilo-Saharan (NS), and Afro-Asiatic (AA) (24). Our study aims to reveal underlying metabolic phenotypes across Sudanese PCa patients to better understand the triggering mechanisms and corresponding tumor heterogeneity.

Material and methods

Study patients and sample collection

The study encompasses a cohort of Sudanese patients diagnosed with PCa. They were primarily treated at the Urology Department of four facilities: Omdrman Teaching Hospital (OTH), Kuwaiti Specialized Hospital (KSH), Soba University Hospital (SUH), and Military Crop (MC). Ethical approval was provided by the National Health Research Ethics Committee of the Sudanese Federal Ministry of Health. The prevalence of comorbidities such as HTN and type 2 diabetes mellitus (T2DM) was documented. Further insights into PCa characteristics including prostate-specific antigen (PSA) levels, biopsy types, perineural invasion (PNI), and disease grading were recorded from Grade 1 to Grade 5. Written consent was obtained from all the participants for tissue and blood examinations. All clinical data were collected regarding their age and clinical history. Five milliliters of blood was collected in Vacuette® ethylenediaminetetraacetic acid (EDTA) tube by medical staff. Blood plasma was separated by centrifugation (1000 g for 10 min at 4°C) and stored at –80°C. Serum PSA level was estimated.

Nuclear magnetic resonance sample preparation and analysis

Plasma samples were thawed at room temperature. An aliquot of 350 µL of a phosphate sodium buffer (70 mM Na_2HPO_4; 20% (v/v) ^2H_2O; 6.1 mM NaN_3; 4.6 mM sodium 3-trimethylsilyl [2,2,3,3-$^2H_4$]-propionate; pH 7.4) was added to 350 µL of each sample. The mixture was homogenized by vortexing for 30 s, before 600 µL of this mixture was transferred into a 5-mm nuclear magnetic resonance (NMR) tube for analysis. One-dimensional (1D) proton (^{1}H)-NMR spectra were acquired on a 500 MHz Bruker Avance III HD NMR spectrometer equipped with a triple-resonance inverse ^{1}H probe head and x, y, z gradient coils. A standard nuclear Overhauser effect spectroscopy (NOESY) pulse sequence presat (noesygppr1d) was used on plasma samples (25). Pooled samples were used as a quality control sample and were included in each batch for qualitative assessment of repeatability by overlaying the raw spectra. The peaks of the identified metabolites were fitted by combining a local baseline and Voigt functions based on the multiplicity of the NMR signal (26). To validate the efficacy of the different deconvolution models, the root-mean-square deviation was determined. The absolute concentration of each metabolite was calculated according to the previously reported equation (27). The number of protons contributing to the unknown signals was imputed to 1. The concentration of carbohydrates was also estimated by considering the equilibrium between their cyclic forms. GlycA and GlycB signals were quantified by integrating the areas between 2.00 and 2.05 ppm and between 2.09 and 2.05 ppm, respectively, above a local baseline, aiming to remove the signal of lipoproteins.

Statistical and data analysis

*S*tatistical analysis and graphical illustrations of the data were generated in the R (version 4.3.2) and R studio (version 1.1.456) software using scripts developed in-house. Wilcoxon rank sum test and Kruskal-Wallis rank sum test were used to compare differences in numerical covariates (e.g., age and metabolite concentration). Fisher's exact test was used to assess differences between categorical variables (e.g., ethnicity). Spearman's test was used to calculate the correlation coefficient (rho) between variables. Unsupervised analysis was performed on the metabolic profiles using the KODAMA algorithm (28,29). Hierarchical clustering (Ward linkage) (30) was used on the KODAMA's output to identify clusters with similar

metabolic patterns. Silhouette median value was used to evaluate the optimal number of clusters with the number of possible clusters varying from 2 to 10 (31). The p values less than 0.05 were considered to be significant. To account for multiple tests, a false discovery rate (FDR) of <10% was applied. Linear scaling was used for normalization. Logistic regression models were used to calculate odds ratio (OR) estimates with 95% confidence intervals (CIs) of association between HTN and measured NMR metabolites using ggforestplot R package (32).

Results

Patients' demographic and clinicopathological characteristics

The participants recruited for this study are representative of the three predominant ethnic groups prevailing in Sudan. The ethnic distribution among the 50 patients included in the study reveals a predominant representation of AA, constituting 48% (n = 24) of the cohort, followed by 34% (n = 17) identified as NC, and 18% (n = 9) as NS. Regarding hospital distribution, KSH accounted for 58% (n = 29) of the total recruited patients, followed by MC at 16% (n = 8), OTH at 14% (n = 7), and SUH at 12% (n = 6). The patients from these three ethnic groups exhibited comparable age distributions and prevalence of disease comorbidities such as HTN and T2DM. No significant differences were observed in PSA levels across ethnic groups. Most of the recruited patients were diagnosed utilizing tissues from transurethral resection of the prostate (TURP), accounting for 68% (n = 34), followed by needle biopsy at 26% (n = 13), prostatectomy at 4% (n = 2), and transurethral laser vaporization of the prostate (TVP) at 2% (n = 1). PNI was observed in 11 tissue samples. Regarding disease grading, 34% of patients were classified as grade 5 PCa (n = 17), 34% as grade 4 (n = 17), 10% as grade 3 (n = 5), 12% as grade 2 (n = 6), and 10% as grade 1 (n = 5). There were no significant differences in clinicopathological parameters observed among patients belonging to the three ethnic groups. A detailed summary of the clinical and demographic characteristics of PCa within the analyzed cohort is presented in Table I.

TABLE 1 - Demographic and clinical features of the study's patients according to their ethnicity

Feature	AA (n = 24)	NC (n = 17)	NS (n = 9)	p-Value
Hospital				0.083
KSH, n (%)	16 (66.7)	10 (58.8)	3 (33.3)	
MC, n (%)	2 (8.3)	5 (29.4)	1 (11.1)	
OTH, n (%)	2 (8.3)	2 (11.8)	3 (33.3)	
SUH, n (%)	4 (16.7)	0 (0.0)	2 (22.2)	
Age (years), median [IQR]	74.5 [65-77]	75 [62-78]	65 [63-71]	0.124
Hypertension				0.922
No, n (%)	9 (37.5)	5 (29.4)	3 (33.3)	
Yes, n (%)	15 (62.5)	12 (70.6)	6 (66.7)	
T2DM				0.321
No, n (%)	12 (50.0)	12 (70.6)	4 (44.4)	
Yes, n (%)	12 (50.0)	5 (29.4)	5 (55.6)	
PSA (ng/mL), median [IQR]	42.35 [24.4-63]	54 [37.4-62.1]	50.5 [44.9-94.2]	0.238
Biopsy type				0.858
Needle biopsy, n (%)	8 (33.3)	3 (17.6)	2 (22.2)	
Prostatectomy, n (%)	1 (4.2)	1 (5.9)	0 (0.0)	
TVP, n (%)	1 (4.2)	0 (0.0)	0 (0.0)	
TURP, n (%)	14 (58.3)	13 (76.5)	7 (77.8)	
PNI				0.345
No, n (%)	20 (83.3)	11 (64.7)	8 (88.9)	
Yes, n (%)	4 (16.7)	6 (35.3)	1 (11.1)	
Grade				0.572
1, n (%)	3 (12.5)	1 (5.9)	1 (11.1)	
2, n (%)	5 (20.8)	0 (0.0)	1 (11.1)	
3, n (%)	1 (4.2)	3 (17.6)	1 (11.1)	
4, n (%)	7 (29.2)	7 (41.2)	3 (33.3)	
5, n (%)	8 (33.3)	6 (35.3)	3 (33.3)	

AA = Afro-Asiatic; IQR = interquartile range; KSH = Kuwaiti Specialized Hospital; MC = Military Crop; NC = Niger-Congo; NS = Nilo-Saharan; OTH = Omdurman Teaching Hospital; PNI = perineural invasion; PSA = prostate-specific antigen; SUH = Soba University Hospital; T2DM = type 2 diabetes mellitus; TURP = transurethral resection of prostate; TVP = transurethral laser vaporization of prostate.

Metabolic profiling

NMR spectroscopy was used to profile the plasma metabolome. The metabolic profiles from the three ethnic backgrounds were analyzed (Tab. S1), revealing no significant differences in the metabolic landscape across different ethnicities. However, we reported strong correlations in certain metabolic groups, as shown in Figure 1A. Lipid metabolites encompassing cholesterol, glycerol phospholipid, lipid = CH-CH_2-CH = , lipid alpha-CH_2, lipid beta-CH_2, lipid CH_2, lipid CH_3, and unsaturated lipid -CH = CH- exhibited distinctive patterns. They showed a significant correlation with the amino acids valine, leucine, and isoleucine. The glutamine was negatively related to glutamate levels. Pyruvate exhibited a negative correlation with glutamate and histidine while displaying a positive correlation with citrate, glycine, and lactate. As expected, the inflammatory NMR markers GlycA and GlycB were negatively correlated with the concentration level of histidine, as reported previously (33). Additionally, GlycA and GlycB were also negatively correlated with the lipid levels.

Metabolic phenotype analysis

The plasma metabolic profile of PCa patients is heterogeneous and shaped by different factors, including inflammation and lipid metabolism. To elucidate metabolic patterns in PCa patients, we employed the unsupervised KODAMA method to analyze quantified NMR metabolite concentrations. By grouping patients with similar metabolic profiles together, four distinct metabolic phenotypes (metabotypes) were identified, as visualized in the heatmap of Figure 2B. The demographic and clinical variations among four identified patient metabotypes are illustrated in Table II. While some differences exist, many parameters do not reach statistical significance among the metabotypes. Significantly divergent HTN prevalence (p-value = 0.028) was observed among the predicted patient groups. Metabotypes A, B, and D exhibited a higher proportion of hypertensive patients (76.2%, 70%, and 80%, respectively) compared to metabotype B, which predominantly comprised non-hypertensive patients (77.8%). The variations in metabolic signature across four metabotypes with corresponding cancer grade and HTN status are represented in Figure 2C.

Through a detailed metabolic comparison illustrated in Table S2, it becomes evident that these metabotypes exhibit distinct metabolic patterns, each characterized by unique compositions of metabolites. Among the 38 NMR metabolites measured, 23 metabolites exhibited significant differences between the predicted metabotypes, each forming a distinct metabolic pattern that characterized the identified metabotypes uniquely (Fig. 2A). The metabotype A is characterized by elevated levels of formate, glutamine, and acetate. In contrast, metabotype B displayed an elevated set of fatty acids and lipid metabolites associated with high levels of some amino acids. Conversely, the metabotype C exhibited higher levels of ascorbate, glutamate, and histidine, while metabotype D showed a distinct pattern of elevated levels of inflammatory biomarkers GlycA and GlycB. These findings indicate unique metabolic signatures associated with each group. Since high circulating cholesterol increases the risk of PCa aggressiveness (15), its level across the four metabotype groups is visualized relative to the HTN status of corresponding patients (Fig. 2B). Additionally, GlycB, serving as an inflammatory biomarker and previously reported to be correlated with a high lipidomic profile (33), also displayed regarding the HTN status of patients from different metabotypes (Fig. 2C).

Association of hypertension with patient characteristics

Our findings indicate that despite a higher proportion of non-hypertensive patients falling under metabotype B, their

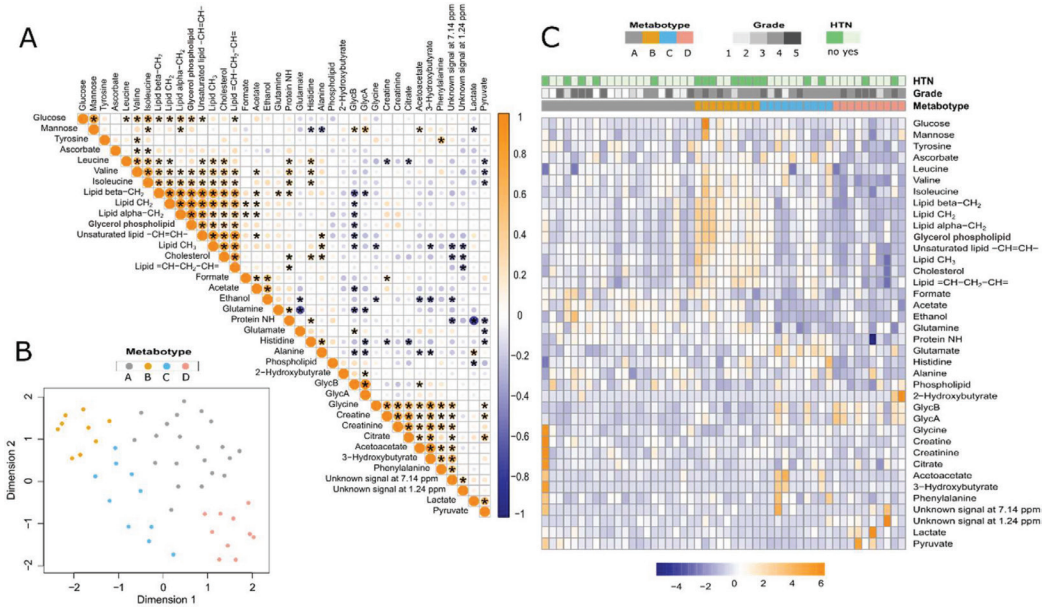

FIGURE 1 - Descriptive analysis for NMR metabolic profile of PCa patients. A) Correlation matrix of Spearman's rank correlation coefficients between the estimated metabolites. B) KODAMA plot visualizing four metabotypes. C) Heatmap showing the comparison of immune cell profiles across four metabotypes. HTN = hypertension; NMR = nuclear magnetic resonance; PCa = prostate cancer.

lipid metabolite levels remain elevated compared to other groups. To uncover potential metabolic patterns associated with hypertension, a thorough examination of demographic, clinical (Tab. S3), and metabolic (Tab. S4) data comparing patients with and without HTN has been performed. Our analysis unveiled significantly elevated levels of PSA in hypertensive patients compared to the non-hypertensive group (p-value = 0.037), remarking the association between hypertension and prostate health. A discrepancy in the T2DM prevalence was observed between hypertensive and non-hypertensive groups (p-value = 0.021). Most hypertensive patients (81.8%) were found to be non-diabetic while 94.1% of non-hypertensive patients presented with T2DM. Moreover, hypertensive patients exhibited significantly higher concentrations of various lipid metabolites compared to their non-hypertensive counterparts. These included unsaturated lipid -CH = CH- (p-value = 0.021), lipid alpha-CH_2 (p-value = 0.007), lipid CH_2 (p-value = 0.002), lipid beta-CH_2 (p-value = 0.02), and glycerol phospholipid (p-value = 0.005), as evidenced by our statistical analysis (Fig. 3, Tab. S4). These findings underscore the intricate metabolic alterations associated with hypertension and the need for further explorations in understanding the pathophysiology of hypertension and its complications in PCa patients.

TABLE 2 - Variation in demographic and clinical parameters among different metabotypes

Feature	Metabotype A (n = 21)	Metabotype B (n = 9)	Metabotype C (n = 10)	Metabotype D (n = 10)	p-Value
Hospital					0.073
KSH, n (%)	8 (38.1)	7 (77.8)	5 (50.0)	9 (90.0)	
MC, n (%)	4 (19.0)	0 (0.0)	3 (30.0)	1 (10.0)	
OTH, n (%)	5 (23.8)	2 (22.2)	0 (0.0)	0 (0.0)	
SUH, n (%)	4 (19.0)	0 (0.0)	2 (20.0)	0 (0.0)	
Ethnicity					0.342
AA, n (%)	13 (61.9)	4 (44.4)	2 (20.0)	5 (50.0)	
NC, n (%)	4 (19.0)	4 (44.4)	5 (50.0)	4 (40.0)	
NS, n (%)	4 (19.0)	1 (11.1)	3 (30.0)	1 (10.0)	
Age (year), median [IQR]	75 [65–80]	70 [63–72]	71.5 [68-75]	61 [57.5-74]	0.237
HTN					0.027
No, n (%)	5 (23.8)	7 (77.8)	3 (30.0)	2 (20.0)	
Yes, n (%)	16 (76.2)	2 (22.2)	7 (70.0)	8 (80.0)	
T2DM					0.408
No, n (%)	14 (66.7)	3 (33.3)	6 (60.0)	5 (50.0)	
Yes, n (%)	7 (33.3)	6 (66.7)	4 (40.0)	5 (50.0)	
PSA (ng/mL), median [IQR]	42.7[31-61.7]	35.8[24.9-43.7]	49.0[44-57.5]	72.8[46.6-91.6]	0.231
Biopsy type					0.611
Needle biopsy, n (%)	4 (19.0)	2 (22.2)	4 (40.0)	3 (30.0)	
…Prostatectomy, n (%)	1 (4.8)	0 (0.0)	1 (10.0)	0 (0.0)	
TVP, n (%)	0 (0.0)	0 (0.0)	0 (0.0)	1 (10.0)	
TURP, n (%)	16 (76.2)	7 (77.8)	5 (50.0)	6 (60.0)	
PNI					0.521
No, n (%)	17 (81.0)	8 (88.9)	8 (80.0)	6 (60.0)	
Yes, n (%)	4 (19.0)	1 (11.1)	2 (20.0)	4 (40.0)	
Grade					0.056
1, n (%)	5 (23.8)	0 (0.0)	0 (0.0)	0 (0.0)	
2, n (%)	5 (23.8)	0 (0.0)	1 (10.0)	0 (0.0)	
3, n (%)	2 (9.5)	1 (11.1)	1 (10.0)	1 (10.0)	
4, n (%)	2 (9.5)	6 (66.7)	5 (50.0)	4 (40.0)	
5, n (%)	7 (33.3)	2 (22.2)	3 (30.0)	5 (50.0)	

AA = Afro-Asiatic; HTN = hypertension; IQR = interquartile range; KSH = Kuwaiti Specialized Hospital; MC = Military Crop; NC = Niger-Congo; NS = Nilo-Saharan; OTH = Omdurman Teaching Hospital; PNI = perineural invasion; PSA = prostate-specific antigen; SUH = Soba University Hospital; T2DM = type2 diabetes mellitus; TURP = transurethral resection of prostate; TVP = transurethral laser vaporization of prostate.

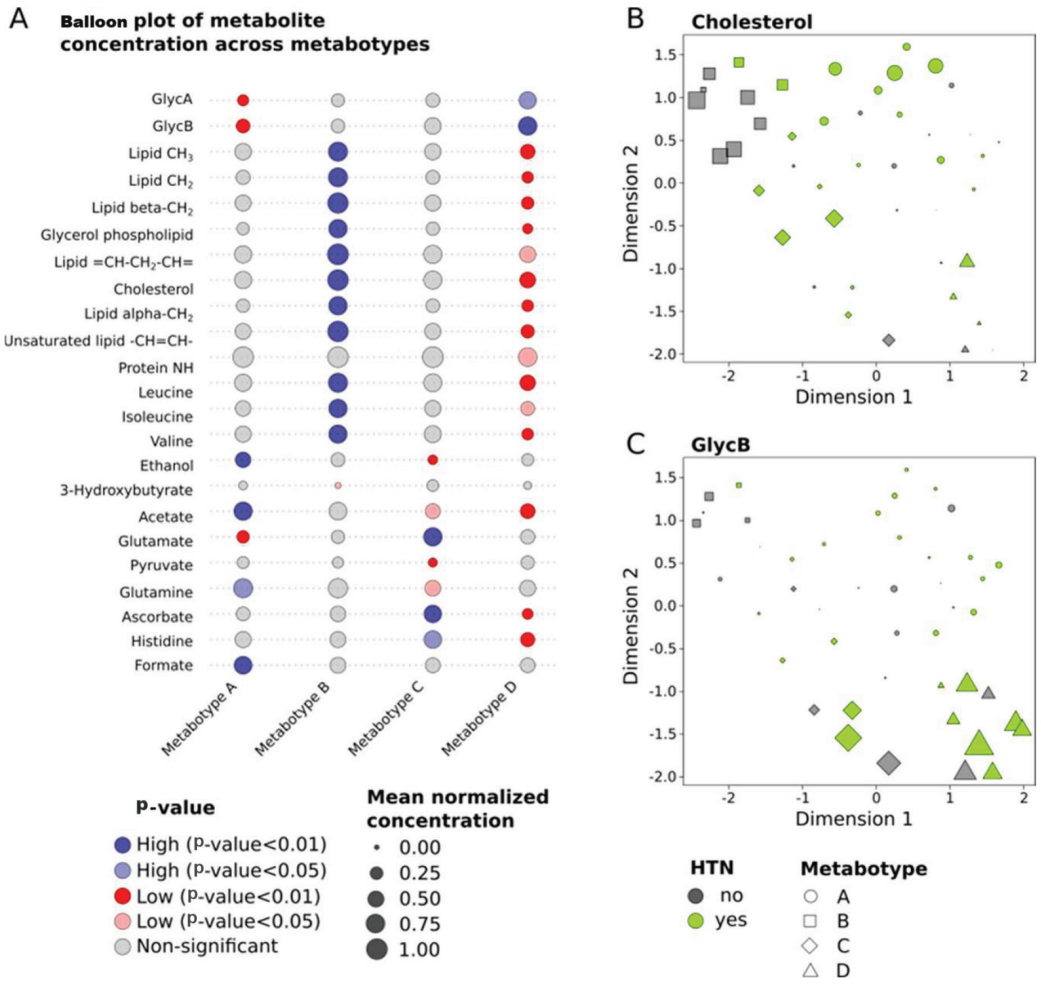

FIGURE 2 - Variations in significant metabolites across four predicted metabotypes. A) Balloon plot representing the different metabolite concentrations across the four metabotypes. The KODAMA plots illustrate the distribution of cholesterol (B) and GlycB concentrations (C), with concentrations represented by varying point sizes across four distinct metabotypes. HTN = hypertension.

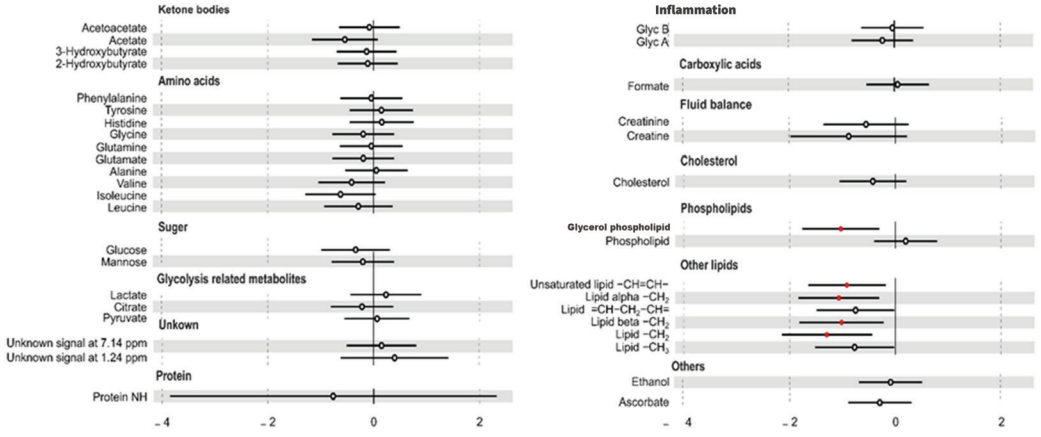

FIGURE 3 - Association between hypertension (HTN) and metabolite concentrations. Odds ratio for HTN per 1-standard deviation increment in metabolite concentration with 95% confidence interval (CI). The red circle represents significant values.

Discussion

Despite the lack of specific metabolomic studies of PCa in Sudanese patients, this research tries to investigate the metabolic profile within the Sudanese context. Mostly, Sudanese PCa patients frequently present with late-stage diagnoses characterized by elevated PSA levels and Gleason scores (34).

The diverse ethnic composition of our study, with a predominant representation of ethnicities such as AA, NC, and NS, mirrors the demographic diversity typical of this African region (25). Metabolic stratification of PCa patients using machine learning techniques offers a promising approach to elucidate the disease's heterogeneity and enhance personalized

treatment strategies. By analyzing metabolomic profiles from plasma samples, machine learning algorithms can categorize patients into distinct metabolic subtypes based on their unique metabolic signatures. Several studies have showcased the feasibility and potential of this approach. For instance, Cacciatore et al (2021) utilized KODAMA, a clustering algorithm to stratify PCa patients into different metabotypes using metabolomic profiling data (33). Their findings highlighted distinct inflammatory metabolic patterns associated with PCa aggressiveness in South African patients.

In our study, we applied KODAMA to categorize Sudanese PCa patients based on their NMR-measured metabolic data, identifying four distinct metabolic groups. These groups differed in PCa grade distribution and exhibited significant variability in hypertension prevalence. An increased level of lipid metabolites, including fatty acids, cholesterol, and glycerol phospholipids, was observed in patients within the second metabotype (metabotype B). This metabolic signature revealed a potential link between lipid metabolism and the clinical characteristics of PCa patients grouped within this group. Unlike other metabotypes, this group is dominated by non-hypertensive patients, which implies another factor that can interfere with the recorded raised lipid metabolites. Previous research implicated dysregulated lipid metabolism in cancer progression, including PCa (35–37). Accumulation of phospholipids and cholesterol in the circulation interacts with androgens and the immune system and triggers PCa development (38). The extended utilization of ADT is recognized for inducing alterations in the lipid profile both during and following treatment (39,40). It may be potentially contributing to the enhanced lipid biosynthesis in metabotype B group. Furthermore, our analysis also revealed a positive correlation between estimated lipid metabolites and certain amino acids, particularly valine, leucine, and isoleucine, which are classified as branched-chain amino acids (BCAAs). These BCAAs play pivotal roles in crucial cellular processes such as protein synthesis, energy production, and cellular signaling (41). The dysregulation of BCAA metabolism has been implicated in the pathogenesis of various cancers, including PCa (42). The genes encoding these amino acids have been reported to be expressed at higher levels in PCa tumor tissue compared to non-transformed tissue (43). Previous studies have illuminated the relation between lipid and amino acid metabolism in various cancer types (44,45). Specifically, cancer cells, including those of PCa, often exhibit heightened demands for lipid synthesis and fatty acid oxidation to fuel their growth and meet their energy requirements, while simultaneously orchestrating the transport and metabolic pathways of amino acids to sustain proliferation and ensure survival (46). Aside from BCAAs, our results also highlighted variations in the concentrations of other metabolites such as glutamine, glutamate, histidine, and pyruvate across the detected metabotype groups. The abnormal metabolism of amino acids in PCa cells often manifests as a disruption in glutamic acid metabolism, which is synthesized from glutamine to fulfill the demands of growth and proliferation (47). Plasma samples from PCa patients have been shown to exhibit elevated levels of valine, glutamine, creatine, tyrosine, phenylalanine, histidine, and 3-methylhistidine (48). Increased levels of BCAAs, glutamate, and a reduction in the levels of glycine, dimethylglycine, fumarate, and 4-imidazole-acetate have been identified as discriminative factors between PCa patients and those with benign prostatic hyperplasia (49). Lipid oxidation might be initiated by glycosylation of phospholipids leading to formation of advanced glycation end products. This pathway might increase the severity of inflammatory diseases, and the initiation and progression of malignant tumors (50). GlycA and GlycB are identifiable as two distinct signals in NMR spectroscopy that indicate the glycation status of the most abundant acute-phase inflammatory proteins, reflecting the patient inflammatory status (51). From our results, there was increased concentrations of GlycA and GlycB in the fourth metabotype (metabotype D) associated with low levels of lipid metabolites. Consistent with our results, a previous study reported a similar PCa metabotype, characterized by a high level of GlycB and reduced concentration of lipids (33). The possible origin of this metabotype is still under investigation.

Conclusion

This study sheds light on the metabolic landscape of PCa in Sudanese patients, emphasizing the potential of metabolomics in enhancing personalized treatment strategies. The identified metabolic subtypes using machine learning techniques provide valuable insights into disease heterogeneity, guiding targeted interventions. The associations between lipid metabolites and PCa characteristics underscore the importance of metabolic dysregulation in disease progression. Further research into the interplay between lipid and amino acid metabolism, informed by our findings and previous studies, promises to deepen our understanding of PCa pathogenesis and identify novel therapeutic targets.

Limitations and future directions

While the study provided valuable insights into the metabolic variations among PCa patients with comorbidities like hypertension, this study has some limitations that should be considered. The relatively small sample size (50 patients) limits the generalizability of the findings, and the focus on a specific population in Sudan may not fully capture metabolic variations across different regions or ethnic groups. Finally, while NMR spectroscopy was useful for metabolomic profiling, it may have missed other relevant metabolites that more sensitive techniques like mass spectrometry could detect. Despite these limitations, the study offers practical insights identifying distinct metabolic phenotypes in PCa patients, particularly concerning hypertension. The findings may also contribute to the development of biomarkers for early detection and risk stratification, particularly in patients with metabolic comorbidities like hypertension. Further research could explore these metabolic pathways to inform targeted therapies.

Acknowledgments

We would like to express our deep and sincere gratitude and appreciation to all urology and histopathology surgeons, clinicians, and technical staff for their efforts in performing this study.

Disclosures

Conflicts of Interest: The authors declare no conflicts of interest.

Financial support: The research was funded by the International Centre for Genetic Engineering and Biotechnology (L.F.Z. and S.C.), and the UN Technology Bank for Least Developed Countries, TWAS and ICGEB under South-North and South-South Fellowships (D.A.).

Informed consent statement: Informed consent was taken from all the participants.

Author contributions: Conceptualization, D.A., S.C., and L.F.Z.; methodology, S.C.; formal analysis, D.A., E.A.A.S., S.C.; resources, D.A., E.A.A.M., H.E.A.B.A., A.M.I., S.C., and L.F.Z.; clinical data curation, D.A., E.A.A.M., H.E.A.B.A., A.M.I.; writing – original draft preparation, D.A. and E.A.A.S.; writing – review and editing, S.C. and L.F.Z.; visualization, E.A.A.S.; supervision, S.C. and L.F.Z.; project administration, S.C. and L.F.Z.; funding acquisition, D.A., S.C., and L.F.Z. All authors have read and agreed to the published version of the manuscript.

Institutional review board statement: Specimen collection and research contents were examined and approved by the National Health Research Ethics Committee of the Sudanese Federal Ministry of Health (6-9-2021). The study was performed in accordance with the Declaration of Helsinki.

Data availability statement: All data produced in the present study are available upon reasonable request to the authors. NMR spectra were deposited at the MetaboLight database.

References

1. Bray F, Ferlay J, Soerjomataram I, Siegel RL, Torre LA, Jemal A. Global cancer statistics 2018: GLOBOCAN estimates of incidence and mortality worldwide for 36 cancers in 185 countries. CA Cancer J Clin. 2018;68(6):394-424. CrossRef PubMed
2. Choi Y, Park B, Jeong BC, et al. Usefulness of early extracorporeal shock wave lithotripsy in colic patients with ureteral stones. Korean J Urol. 2015;56(12):853-859. CrossRef PubMed
3. Wasim S, Lee SY, Kim J. Complexities of prostate cancer. Int J Mol Sci. 2022;23(22):14257. CrossRef PubMed
4. Danzi F, Pacchiana R, Mafficini A, et al. To metabolomics and beyond: a technological portfolio to investigate cancer metabolism. Signal Transduct Target Ther. 2023;8(1):137. CrossRef PubMed
5. Li Z, Zhang H. Reprogramming of glucose, fatty acid and amino acid metabolism for cancer progression. Cell Mol Life Sci. 2016;73(2):377-392. CrossRef PubMed
6. Kdadra M, Höckner S, Leung H, Kremer W, Schiffer E. Metabolomics biomarkers of prostate cancer: a systematic review. Diagnostics (Basel). 2019;9(1):21. CrossRef PubMed
7. Vandergrift LA, Decelle EA, Kurth J, et al. Metabolomic prediction of human prostate cancer aggressiveness: magnetic resonance spectroscopy of histologically benign tissue. Sci Rep. 2018;8(1):4997. CrossRef PubMed
8. Struck-Lewicka W, Kordalewska M, Bujak R, et al. Urine metabolic fingerprinting using LC-MS and GC-MS reveals metabolite changes in prostate cancer: a pilot study. J Pharm Biomed Anal. 2015;111:351-361. CrossRef PubMed
9. Ren S, Shao Y, Zhao X, et al. Integration of metabolomics and transcriptomics reveals major metabolic pathways and potential biomarker involved in prostate cancer. Mol Cell Proteomics. 2016;15(1):154-163. CrossRef PubMed
10. Yang M, Ayuningtyas A, Kenfield SA, et al. Blood fatty acid patterns are associated with prostate cancer risk in a prospective nested case-control study. Cancer Causes Control. 2016;27(9):1153-1161. CrossRef PubMed
11. Sroka WD, Boughton BA, Reddy P, et al. Determination of amino acids in urine of patients with prostate cancer and benign prostate growth. Eur J Cancer Prev. 2017;26(2):131-134. CrossRef PubMed
12. Li J, Ren S, Piao HL, et al. Integration of lipidomics and transcriptomics unravels aberrant lipid metabolism and defines cholesteryl oleate as potential biomarker of prostate cancer. Sci Rep. 2016;6(1):20984. CrossRef PubMed
13. Hahn AW, Thoman W, Koutroumpakis E, et al. Cardiometabolic healthcare for men with prostate cancer: an MD Anderson Cancer Center experience. Cardiooncology. 2023;9(1):33. CrossRef PubMed
14. Zhang H, Zhou Y, Xing Z, Sah RK, Hu J, Hu H. Androgen metabolism and response in prostate cancer anti-androgen therapy resistance. Int J Mol Sci. 2022;23(21):13521. CrossRef PubMed
15. Zeković M, Bumbaširević U, Živković M, Pejčić T. Alteration of lipid metabolism in prostate cancer: multifaceted oncologic implications. Int J Mol Sci. 2023;24(2):1391. CrossRef PubMed
16. Koundouros N, Poulogiannis G. Reprogramming of fatty acid metabolism in cancer. Br J Cancer. 2020;122(1):4-22. CrossRef PubMed
17. Minas TZ, Lord BD, Zhang AL, et al. Circulating trans fatty acids are associated with prostate cancer in Ghanaian and American men. Nat Commun. 2023;14(1):4322. CrossRef PubMed
18. Noriega Landa E, Quaye GE, Su X, et al. Urinary fatty acid biomarkers for prostate cancer detection. PLoS One. 2024;19(2):e0297615. CrossRef PubMed
19. Lieu EL, Nguyen T, Rhyne S, Kim J. Amino acids in cancer. Exp Mol Med. 2020;52(1):15-30. CrossRef PubMed
20. Strmiska V, Michalek P, Eckschlager T, et al. Prostate cancer-specific hallmarks of amino acids metabolism: towards a paradigm of precision medicine. Biochim Biophys Acta Rev Cancer. 2019;1871(2):248-258. CrossRef PubMed
21. Schcolnik-Cabrera A, Juárez-López D. Dual contribution of the mTOR pathway and of the metabolism of amino acids in prostate cancer. Cell Oncol (Dordr). 2022;45(5):831-859. CrossRef PubMed
22. Hinata N, Fujisawa M. Racial differences in prostate cancer characteristics and cancer-specific mortality: an overview. World J Mens Health. 2022;40(2):217-227. CrossRef PubMed
23. Ibrahim ME. Genetic diversity of the Sudanese: insights on origin and implications for health. Hum Mol Genet. 2021;30(R1):R37-R41. CrossRef PubMed
24. Greenberg JH. The languages of Africa. Bloomington, IN: Indiana University Press 1963. Online (Accessed May 2024)
25. Nagana Gowda GA, Raftery D. Analysis of plasma, serum, and whole blood metabolites using ^{1}H NMR spectroscopy. Methods Mol Biol 2019;2037:17-34. CrossRef PubMed
26. Marshall I, Higinbotham J, Bruce S, Freise A. Use of Voigt lineshape for quantification of in vivo 1H spectra. Magn Reson Med. 1997;37(5):651-657. CrossRef PubMed
27. Serkova N, Fuller TF, Klawitter J, Freise CE, Niemann CU. H-NMR-based metabolic signatures of mild and severe ischemia/reperfusion injury in rat kidney transplants. Kidney Int. 2005;67(3):1142-1151. CrossRef PubMed
28. Cacciatore S, Tenori L, Luchinat C, Bennett PR, MacIntyre DA. KODAMA: an R package for knowledge discovery and data mining. Bioinformatics. 2017;33(4):621-623. CrossRef PubMed
29. Zinga MM, Abdel-Shafy E, Melak T, et al. KODAMA exploratory analysis in metabolic phenotyping. Front Mol Biosci. 2023;9:1070394. CrossRef PubMed
30. Reynolds AP, Richards G, de la Iglesia B, Rayward-Smith VJ. Clustering rules: a comparison of partitioning and hierarchical clustering algorithms. J Math Model Algorithms. 2006;5(4):475-504. CrossRef

31. Rousseeuw PJ. Silhouettes: a graphical aid to the interpretation and validation of cluster analysis. J Comput Appl Math. 1987;20:53-65. CrossRef
32. Akbaraly T, Würtz P, Singh-Manoux A, et al. Association of circulating metabolites with healthy diet and risk of cardiovascular disease: analysis of two cohort studies. Sci Rep. 2018;8(1):8620. CrossRef PubMed
33. Cacciatore S, Wium M, Licari C, et al. Inflammatory metabolic profile of South African patients with prostate cancer. Cancer Metab. 2021;9(1):29. CrossRef PubMed
34. Taha SM, Weng HY, Mohammed MEI, Osman YM, Mohammed SI, Abuidris DO (2020). Prostate cancer clinical characteristics and outcomes in Central Sudan. Ecancermedicalscience. 2020;14:1116. CrossRef
35. Scaglia N, Frontini-López YR, Zadra G. Prostate cancer progression: as a matter of fats. Front Oncol. 2021;11:719865. CrossRef PubMed
36. Wu X, Daniels G, Lee P, Monaco ME. Lipid metabolism in prostate cancer. Am J Clin Exp Urol. 2014;2(2):111-120. PubMed
37. Zhang Z, Wang W, Kong P, et al. New insights into lipid metabolism and prostate cancer (Review). Int J Oncol. 2023;62(6):1-13. CrossRef PubMed
38. Siltari A, Syvälä H, Lou YR, Gao Y, Murtola TJ. Role of lipids and lipid metabolism in prostate cancer progression and the tumor's immune environment. Cancers (Basel). 2022;14(17):4293. CrossRef PubMed
39. Wolny-Rokicka E, Tukiendorf A, Wydmański J, Ostrowska M, Zembroń-Łacny A. Lipid status during combined treatment in prostate cancer patients. Am J Mens Health. 2019;13(5):1557988319876488. CrossRef PubMed
40. Zadra G, Loda M. When fat goes down, prostate cancer is on the ropes. Mol Cell Oncol. 2019;6(3):1595308. CrossRef PubMed
41. Xu H, Wang X, Xu X, et al. Association of plasma branched-chain amino acid with multiple cancers: a mendelian randomization analysis. Clin Nutr. 2023;42(12):2493-2502. CrossRef PubMed
42. Dereziński P, Klupczynska A, Sawicki W, Pałka JA, Kokot ZJ. Amino acid profiles of serum and urine in search for prostate cancer biomarkers: a pilot study. Int J Med Sci. 2017;14(1):1-12. CrossRef PubMed
43. Samaržija I, Trošelj KG, Konjevoda P. Prognostic significance of amino acid metabolism-related genes in prostate cancer retrieved by machine learning. Cancers (Basel). 2023;15(4):1309. CrossRef PubMed
44. Pardo-Rodriguez D, Santamaría-Torres M, Salinas A, et al. Unveiling disrupted lipid metabolism in benign prostate hyperplasia, prostate cancer, and metastatic patients: insights from a Colombian nested case-control study. Cancers (Basel). 2023;15(22):5465. CrossRef PubMed
45. Ahmad F, Cherukuri MK, Choyke PL. Metabolic reprogramming in prostate cancer. Br J Cancer. 2021;125(9):1185-1196. CrossRef PubMed
46. Chen L, Xu YX, Wang YS, Zhou JL. Lipid metabolism, amino acid metabolism, and prostate cancer: a crucial metabolic journey. Asian J Androl. 2024;26(2):123-134. CrossRef PubMed
47. Stepka P, Vsiansky V, Raudenska M, Gumulec J, Adam V, Masarik M. Metabolic and amino acid alterations of the tumor microenvironment. Curr Med Chem. 2021;28(7):1270-1289. CrossRef PubMed
48. Lécuyer L, Victor Bala A, Demidem A, et al. NMR metabolomic profiles associated with long-term risk of prostate cancer. Metabolomics. 2021;17(3):32. CrossRef PubMed
49. Pérez-Rambla C, Puchades-Carrasco L, García-Flores M, Rubio-Briones J, López-Guerrero JA, Pineda-Lucena A. Non-invasive urinary metabolomic profiling discriminates prostate cancer from benign prostatic hyperplasia. Metabolomics. 2017;13(5):52. CrossRef PubMed
50. Schröter D, Höhn A. Role of advanced glycation end products in carcinogenesis and their therapeutic implications. Curr Pharm Des. 2018;24(44):5245-5251. CrossRef PubMed
51. Moreno-Vedia J, Rosales R, Ozcariz E, et al. Triglyceride-rich lipoproteins and glycoprotein A and B assessed by 1H-NMR in metabolic-associated fatty liver disease. Front Endocrinol (Lausanne). 2022;12:775677. CrossRef PubMed

Journal of Circulating Biomakers

www.aboutscience.eu

ISSN 1849-4544

ABOUTSCIENCE